UNIVERSIDADE
BEIRA INTERIOR

Weight Estimation of a Twin-body Liquid Hydrogen Airliner "Gondola"
(Versão final pós-defesa)

Leonardo Rodrigo Sousa Ferreira

Dissertação para obtenção do Grau de Mestre em
Engenharia Aeronáutica
(Mestrado Integrado)

Orientadores: Prof. Doutor Leandro Barbosa Magalhães
Prof. Doutor André Rodrigues Resende da Silva
Prof. Doutor Raj Nangia

Covilhã, maio de 2025

Declaração de integridade

Eu, Leonardo Rodrigo Sousa Ferreira, que abaixo assino, estudante com o número de inscrição 43744 do curso de Mestrado Integrado em Engenharia Aeronáutica da Faculdade de Engenharia, declaro ter desenvolvido o presente trabalho e elaborado o presente texto em total concordância com o Código de Integridade da Universidade da Beira Interior.

Mais concretamente afirmo não ter incorrido em qualquer tipo de Fraude Académica, e que aqui declaro conhecer, que em particular atendi à exigida referenciação de conceitos, frases, excertos, dados ou imagens de outros autores, cuja propriedade do trabalho intelectual deve ser (e foi) preservada, atribuindo-lhes na íntegra o mérito e as responsabilidades da autoria.

Universidade da Beira Interior, Covilhã 14/05/2025.

Assinado por: **Leonardo Rodrigo Sousa Ferreira**
Num. de Identificação: 15572930
Data: 2025.05.14 08:06:07+01'00'

“I do not know what I may appear to the world, but to myself, I seem to have been only like a boy playing on the seashore and diverting myself in now and then finding a smoother pebble or a prettier shell than ordinary, whilst the great ocean of truth lay all undiscovered before me.”

Isaac Newton

Acknowledgements

First and foremost, I would like to express my immeasurable gratitude to my parents for the encouragement, support, and efforts taken to provide me with this academic degree. Although I was the family’s pioneer in this educational environment, I only succeeded by following the sobriety of our family values with humility.

I would also like to take this opportunity to thank my supervisors. Professor André Silva for helping me choose the dissertation topic, providing me with a workspace, guidance on the tasks to be performed and motivation for the subsequent assignments. Professor Leandro Magalhães for always being available to provide research materials, reconciling agendas for meetings to present results, suggesting topics conducive to the advancement of the work and giving feedback on the content and formatting of this document. To Professor Raj Nangia, after all these years in the field of aeronautical engineering, he still found the patience for our meetings in recent months, providing valuable insights that only his experience in this area can provide, suggesting lines of work, research materials and data to validate the results obtained throughout this work.

It is usually stated that we are the average of the people that surround us. Well, in my case it is no different. Therefore, I appreciate all the colleagues and friends I made during this academic path in Covilhã, especially the ones with who I shared my personal life aspects, lively convivial moments and the most stressful situations.

My sincere appreciation and thanks to everyone I met on this five-year journey.

Resumo

A seguinte dissertação aborda a utilização do hidrogénio no setor aeronáutico, com a apresentação geral dos objetivos ambientais que se pretendem alcançar e a divulgação do histórico científico relativamente ao surgimento de novos conceitos de aeronaves ou adaptação dos já existentes.

Das configurações propostas, este trabalho dedica-se ao novo conceito de uma aeronave assimétrica comercial de dupla fuselagem movida a hidrogénio líquido – “Gondola” Airliner. Neste documento, efetuou-se o estudo preliminar da estimativa da massa desta nova configuração, da qual se destaca a precisão do método de Torenbeek utilizado na estimativa da massa da fuselagem “Gondola” e a utilização da equação de Breguet para o alcance na estimativa de combustível necessário. Com a massa da nova configuração estimada procedeu-se à comparação da sua distribuição longitudinal de massa com o modelo equivalente da Airbus, o A320, seguindo o método de segmentação longitudinal proposto no manual de peso e centragem do A320. Tendo em conta que o hidrogénio não é transportado nas asas da aeronave e que os seus reservatórios contribuem significativamente para o peso da nova configuração, distribuição longitudinal de massa das duas aeronaves embora tenham um perfil parecido, diferem principalmente nas regiões onde se localizam os tanques de hidrogénio.

Posteriormente, alcançada a estimativa de combustível necessário e tendo em vista a escalabilidade da estrutura da aeronave para outras missões de voo, procedeu-se à concretização da tarefa principal deste trabalho que se prende com o projeto preliminar tridimensional do novo modelo da aeronave, utilizando o software *Catia V5*. A elaboração dos modelos 3D da nova configuração e do A320 têm em vista um estudo de comparação aerodinâmica futura, utilizando uma ferramenta CFD.

Palavras-chave

Hidrogénio, aeronave assimétrica, projeto preliminar.

Abstract

The following dissertation addresses the use of hydrogen in the aeronautical sector, presenting the environmental objectives intended to be achieved and disseminating the scientific history regarding the emergence of new aircraft concepts or the adaptation of existing ones.

Of the proposed configurations, this work is dedicated to the new concept of a double-fuselage asymmetrical aircraft powered by liquid hydrogen—the “Gondola” Airliner. In this document, a preliminary study estimates the mass of this new configuration, highlighting the precision of Torenbeek’s method used to calculate the mass of the “Gondola” fuselage and the application of Breguet’s range equation for the required fuel valuation. Having estimated the mass of the novel configuration, its longitudinal mass distribution was compared with the equivalent Airbus model, the A320, following the longitudinal segmentation method proposed in the A320 weight and balance manual. Considering that hydrogen is not stored in the aircraft’s wings and that its tanks significantly contribute to the weight of the new configuration, the longitudinal mass distribution of the two aircraft, while having a similar profile, primarily differs in the regions where the hydrogen tanks are located.

Posteriorly, once the required fuel estimate was reached and considering the scalability of the aircraft structure for other flight missions, the main task of this work was executed, which is related to the three-dimensional preliminary design of the new aircraft model, using the *Catia V5* software. The creation of 3D models of the new configuration and the A320 aims at a future aerodynamic comparison study, using a CFD tool.

Keywords

Hydrogen, asymmetrical aircraft, preliminary design.

Table of Contents

List of Figures

List of Tables

Nomenclature

a – speed of sound

A_{ap} – wetted area of aperture or opening

A_{fl} – fuselage floor area

A_{ws} – windshield wetted area, frame included

b - width

b_f – maximum width of the fuselage

D_f – fuselage diameter

f – actual hoop stress level

f_{ref} – mean hoop stress level

g – gravitational acceleration

h - height

h_f - maximum depth of the fuselage

H-arm – horizontal arm from station 0 (zero) in length unit

k_{wf} – factor of proportionality for the basic fuselage weight

k_λ – factor that allows the fuselage slenderness ratio to influence the gross skin weight

l_f – fuselage length

l_t – distance between quarter-chord points of wing and horizontal tailplane root

L/D – aerodynamic efficiency

M – mach number

$\dot{m}_f$ – mass flow rate of fuel

$\dot{m}_{ox}$ – mass flow rate of oxidizer

n_{ult} – ultimate load factor corresponding to W_{to}

pkm_e – ton-kilometre equivalent

S_G – gross shell area of the fuselage

V_D – design dive speed of the aircraft

W_{ai} - the additional weight items

W_F – fuselage weight

W_f – basic fuselage weight

W_{fl} – fuselage floor weight

W_{fr} – gross frame weight

W_G - gross shell weight

W_{H_2} – weight of hydrogen the tank can hold

W_{sct} – total weight penalties due to fuselage shell cutouts

W_{sk} - gross skin weight

W_{str} – gross stringer and longeron weight

W_{tank} – empty tank weight

W_{to} – maximum takeoff weight

r – stoichiometric fuel-to-air ratio

pkm_e – passenger-kilometre equivalent

$Y\text{-}arm$ – lateral arm from station 0 (zero) in length unit

Greek symbols

λ_f – fuselage fineness ratio

Δp - maximum operational pressure differential

η_{tank} – gravimetric efficiency (or mass fraction) of the tank

ϕ – equivalence ratio

Acronyms

ACI – Airports Council International

AMC – Acceptable Means of Compliance

APU – Auxiliary Power Unit

ASTM – American Society for Testing and Materials

BAU – “Business-as-usual”

BWB – Blended Wing Body

CAD – Computer-Aided Desing

CG – Centre of Gravity

COP_{21} – 21st Conference of Parties

FE – Finite Element

FLOPS – Floating-point operations per second

FTF - Flap Track Fairings

FW – Fuel weight

GCOL – Ground Collision

GHG – Greenhouse Gas

IATA – International Air Transport Association

ICAO – International Civil Aviation Organisation

IDG – Integrated Drive Generator

IEA – International Energy Agency

IRENA – International Renewable Energy Agency

LDI – Lean Direct Injection

LFL – Lower Flammability Limit

LHV – Lower Heating Value

MEW – Manufacturer’s Empty Weight

MZFW – Maximum Zero Fuel Weight

NASA – National Aeronautics and Space Administration

NDT – Non-Destructive Testing

OEW – Operating Empty Weight

OIW – Operator’s Items Weight

PW – Payload Weight

SAF – Sustainable Aviation Fuel

SDL – Span Distributed Load

SMR – Steam Methane Reforming

TBA – Twin-body Aircraft

TOW – Take-Off Weight

TNT – Trinitrotoluene

TSFC – Thrust-Specific Fuel Consumption

UERF – Uncontained Engine Rotor Failure

ZFW – Zero Fuel Weight

WFR – Weight Fuel Reserves

WFB - Weight of Block Fuel

TSFC – Thrust Specific Fuel Consumption

SFC – Specific Fuel Consumption

1 Introduction

In the modern world, the environmental crisis and the natural resources shortage, namely fossil fuels, have increasingly become key topics on multiple political and social agendas. Therefore, the development and implementation of technologies that promote environmental sustainability and the emergence of a net-zero carbon society have been strengthened.

The transport sector is one of the main drivers of society’s functioning and one of the main ones responsible for the emission of greenhouse gases. Hence, along with other means of transport, many alternatives have been studied in the aviation sector that would allow us to achieve zero carbon emissions in the future. One of the proposed alternatives is using hydrogen as a sustainable green fuel [1].

With successful projects in automobile technology using hydrogen, this sustainable alternative fuel has also been addressed in the aviation sector, from the mid-20th century to the early 21st century [2]. However, due to the peculiar properties of this fuel, the configuration of conventional aircraft must be adapted to make this transition to a hydrogen-powered plane, so that all design parameters comply with the typically strict rules of the aeronautical sector. From the referred adaptations, new aircraft configurations may emerge.

To fully comprehend the forceful effort of introducing an innovative and efficient aircraft configuration, this thesis’s state-of-the-art starts by detailing the environmental goals settled and the current aviation scenario regarding the net-zero emissions mark. Then, hydrogen is presented as a sustainable green fuel, diving into hydrogen production methods and combustion products. Availing these chemical aspects explanation, hydrogen is then presented as aviation fuel which inevitably leads us to the idiosyncrasy of hydrogen’s storage that mostly results in a weight penalty relative to kerosene storage. Thus, the gravimetric efficiency is introduced as a performance figure, representing the fuel fraction of the tank-fuel system [1]. This structural metric will estimate the tank’s weight, knowing the fuel needed for a specific flight mission.

Regarding all the new technology concepts, hydrogen properties and desirable goals settled as a target for the aviation sector, replacing kerosene with hydrogen as a power source will surely change the current certification. So, the strict intricacies of Certification and Crashworthiness issues will be addressed, as they also influence the

aircraft’s design. The literature review ends with presenting publicised aircraft concepts that result from adapting the existing configurations or the emergence of a new idea.

LH_2 tanks must have a lower surface area-to-volume ratio to minimise the boil-off rate. Thus, using a conventional wing box structure to house hydrogen fuel tanks is not feasible. In addition, liquid hydrogen is kept at -253° C, so a fuel tank leak leads to a cryogenic spill. The rapid boiling of the fuel can condense and freeze oxygen, nitrogen, and any other trace elements in the atmosphere around. The excess of LH_2 and the solid oxygen produce an explosive mixture that can be detonated by the impact velocity of a turbine disc fragment [3]. Of the proposed configurations, a double-fuselage concept seems to be one of the most safe concepts.

This work is dedicated to the new concept of a double-fuselage commercial aircraft, powered by liquid hydrogen, the “Gondola” Airliner [4], presented in Figure 1.1. This concept seems to be one of the safest to prevent passengers and crew from hydrogen hazards once the fuel storage and the power system are well separated from the main fuselage.

Figure 1.1 - "Gondola" Airliner concept [4].

As shown in Figure 1.1, the two fuselages are of different lengths, and this overall asymmetry allows an opportunity to apply other design ideas, such as wing twists and new platform designs. The starboard tank fuselage has a similar diameter to the passenger fuselage but is shorter. This allows fuel tanks with a lower surface area-to-volume ratio to be used, reducing heat leaks mentioned above. These and other features will be discussed throughout this document.

1.1 Motivation

In Chapter 2, the global passenger traffic projection shows that the demand values in aviation broke successively the records settled in the previous years. This uptrend only ceased in 2019 due to the COVID-19 pandemic. However, according to IATA, in 2023, global passenger traffic recovered 94.1% of the pre-pandemic levels (2019), corroborating ACI’s medium-term global passenger traffic projection [5]. Furthermore, following the ‘Current projection’, the aviation industry is expected to recover the 2019 levels in 2024 (and maybe surpass that level by 3%). Thus, the developmental effort of aviation technology has a prominent role in achieving zero carbon emission goals.

Considering this preamble about the aviation demand scenario and its conciliation with the environment, two motives drove me through this work: the urge to be part of this scientific path towards net-zero emissions and my network expansion.

Using hydrogen as aviation fuel is one promising solution to accomplish environmental goals. However, as mentioned in the introduction chapter, transitioning from a kerosene-fuelled aircraft to a hydrogen-powered aircraft requires several adaptations in the existing configurations or the suggestion of new aircraft models, aiming for a deeper set of modifications. Both cases imply the project submission to extensive engineering processes and certification work.

The novel configuration of the LH_2 gondola airliner is an auspicious solution for hydrogen use as aviation fuel once it minimises the inherent hazards compared to other layout proposals that include fuel storage inside the passenger’s fuselage. However, the gondola concept has an unusual layout, so it is like an embryonic project compared to an adaptation of a conventional aircraft’s kerosene to hydrogen transition. Thus, it is a huge motivation to be part of this scientific work aiming at the development and certification of this novel configuration.

1.2 Objectives

This work aims for several goals ranging from the state-of-the-art, where the work of original authors devoted to hydrogen usage as aviation fuel is presented, to my contribution to developing a new concept.

For a clearer understanding, this document presents a preliminary study to estimate the mass of this new configuration, comparing its longitudinal mass distribution with the equivalent Airbus model, the A320. As this Airbus model is used as a work base, only the weight of the gondola fuselage, central wing, LH_2 and tanks must be estimated.

Once the required fuel estimate was reached and considering the scalability of the aircraft structure for other flight missions, i.e., the aircraft’s adaptation for greater ranges or longer endurance, the main task of this work is the three-dimensional representation of the novel aircraft model using the *Catia V5* software. The creation of new configuration 3D models and the A320 also aims at a future aerodynamic comparison study using a CFD tool.

In a concluding remark, the present work also included modelling several 3D designs that should be useful in the developmental effort of the novel LH_2-powered aircraft that is presented as a feasible solution to pursue the net-zero emission scenario in aviation.

1.3 Methodology

In Chapter 2, the cadence of the bibliographic review follows the cause-effect link. For example, the state-of-art begins with presenting aviation demand data and forecast and then correlates with the carbon intensity scenario (“cause”). Then, hydrogen is suggested as a sustainable green fuel (“effect”). Considering this proposal (that is the next “cause”), we dive into hydrogen properties, advantages and disadvantages, which condition the storage layouts and requirements (“effect”). Thus, bearing in mind the influence of the hydrogen storage tanks in the aircraft design (the new “cause”), the certification and crashworthiness considerations are then addressed (“effect”). Finally, some hydrogen-powered aircraft concepts published in the open literature are exhibited (“effect”) due to the rules imposed by the Aviation Authority (“cause”).

The practical part of this thesis can be divided into three major parts: preliminary weight estimation of the gondola aircraft, longitudinal weight distribution, and 3D models exhibition. For the weight estimation, Breguet’s Range equation was used to estimate the amount of fuel needed for a given flight mission. Then, the tank weight was defined using the gravimetric efficiency figure that correlates the storage tank weight and fuel weight. Also, the fuel tank dimension and gondola fuselage dimension can be given by knowing the necessary fuel capacity. Finally, Torenbeek’s method is applied to estimate gondola fuselage weight. The central wing weight was evaluated using a simplistic method that

relates the wing weight to the area. The estimation of A320’s MTOW was supported by A320’s weight and balance manual [6], which provides the component’s location and mass. Besides, this Airbus manual also provides the CG position for each design weight, i.e., for the Manufacturer’s Empty Weight, Operational Empty Weight and Take-Off Weight (MTOW at the design point). These values from A320’s manual helped corroborate the results that were obtained. With the estimated weights of the A320 and the gondola airliner, we proceeded to the longitudinal weight distribution that, using Excel, consisted of a longitudinal discretisation of the aircraft length into small intervals (compared to the total length) and then distributing every component’s weight by the intervals where they were positioned.

The A320 was 3D modelled using its blueprints, whereas the gondola airliner 3D modelling was made considering the amount of fuel needed for a given flight mission and the insights provided by the supervisors of this work. As it is a new concept, the Gondola 3D models also permitted some creativity on the tail design as shown in sub-Chapter 3.3.

1.4 Overview

This section presents a brief explanation of each chapter’s subject. Although the motivation, objectives and methodology that guide this work are already clear, the structure and division of sub-themes must be presented.

Chapter 2 is where all the bibliographic reviews about hydrogen background in aviation are made. This section presents aviation demand data and forecast and then correlates with the carbon intensity scenario. Then the climate impact of hydrogen use is introduced by briefly presenting its production methods and combustion products. Knowing the positive role of hydrogen usage in the environment, hydrogen is then suggested as aviation fuel, exposing its properties, advantages and disadvantages. As mentioned, using hydrogen as a power supply entails several storage requirements that influence the aircraft’s design, which is also addressed by showing different layouts for hydrogen tank integration in aircraft structural frames (integral and non-integral tanks) and then signalising the main qualitative pros and cons. These fuel storage configurations lead to aircraft modifications. Thus, the safety measures, certification and crashworthiness considerations are also a topic in this work’s state-of-art. Chapter 2 concludes with a presentation of various hydrogen-powered aircraft concepts from the open literature.

Chapter 3 initiates with the exhibition of the LH_2 gondola airliner concept, which is included in the twin-fuselage aircraft type. Thus, this section also counts with a brief twin-fuselage analysis of weight and bending moments. This chapter also has the preliminary estimation of the gondola airliner’s weight, the longitudinal weight distribution of the A320 and the gondola airliner and their comparison. Chapter 3 concludes with the proposal of several 3D models for future work involving the novel configuration.

Chapter 4 includes the main conclusions about the work done, some final remarks about the improvements to be made and future studies that might be interesting for developing the gondola airliner configuration.

2 H_2 powered aircraft: towards net zero emissions

2.1 Hydrogen Study Background in Aviation

2.1.1 Achieving Net-Zero Emissions in Aviation

Aviation has an essential role in society and its activities, such as developing tourism routes, market integration or cargo transport. Ground transport may be suitable for a short-range journey, less than 300 miles [7], or a ship might be used for transcontinental heavy cargo transport. However, from a saving time and security promotion point of view, air transportation has no direct competitors for 400-plus miles trips [7], neglecting harmful factors such as pollutant emissions or the (possible) higher monetary cost. The commodity, safety and security offered by air transport are reflected in its demand growth throughout aviation history. The year 2020 was a breaking point due to the COVID-19 pandemic, however, the aviation sector is gradually recovering the previous demand values. According to IATA, in 2023, global passenger traffic recovered 94.1% of the pre-pandemic levels (2019), corroborating the medium-term global passenger traffic projection made by ACI [5] (Figure 2.1).

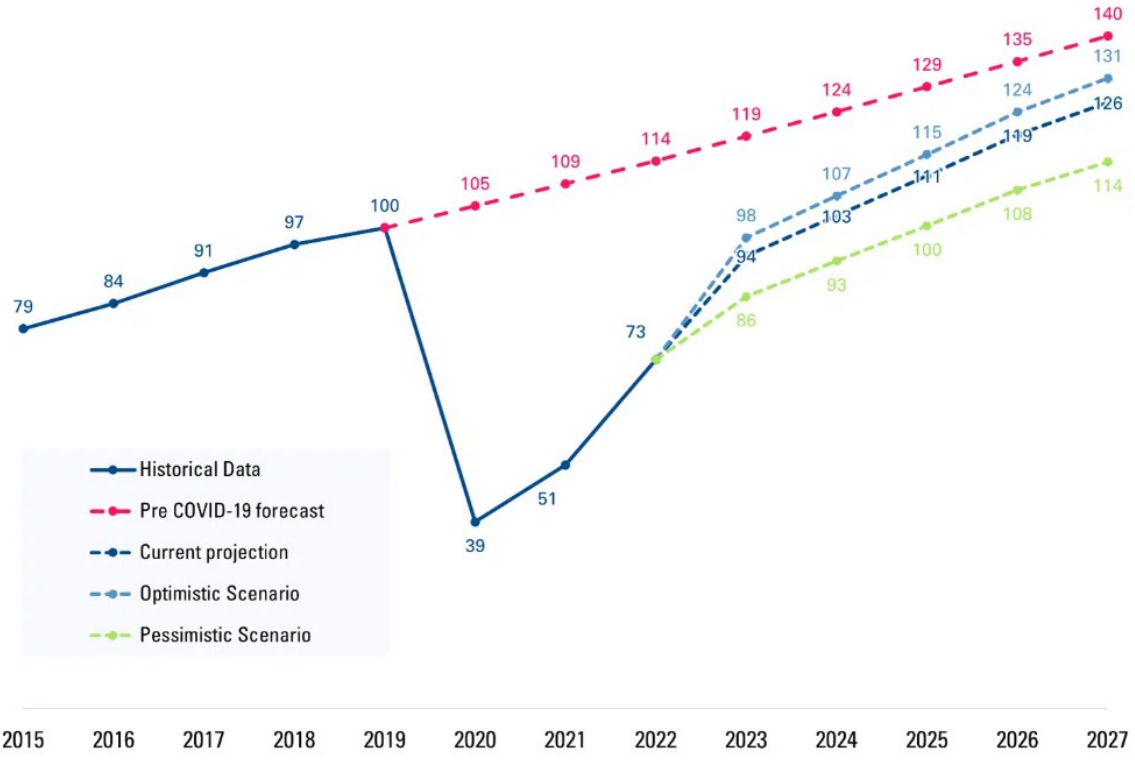

Figure 2.1 - Global passenger traffic projection indexed, 2019 level is considered 100% [5].

Thus, by following the 'Current projection', the aviation industry is expected to recover the 2019 levels in 2024 (and maybe surpass that level by 3%). If that happens, it means a total aviation demand of around 1 trillion ton-kilometre equivalent (*tkm*$_e$ or 11.1 trillion passenger-kilometre equivalent, *pkm*$_e$), with around 80% representing passenger flights and about 20% freight, which recovered its pre-pandemic levels in 2021 already. Despite the uncertainty about other future cataclysms, the past few years' recoveries performed by the aviation industry and its historical data show the feasible projections of consistent and continued growth [8] in demand for air transport in the coming periods. The demand trajectories in the aviation sector [8] can be projected according to the previous values, the industry forecasts or the goals desired. Then, the demand scenario comprehends multiple trajectories (Figure 2.1): 'BAU' raises 4% a year (to 2.9 trillion tkm$_e$ or 32.1 trillion *pkm*$_e$ in 2050), 'Industry' projections of 2.8% augmentation per year (2.1 trillion *tkm*$_e$ or 23.7 trillion *pkm*$_e$) and 'Ambitious' demand swaps keeping 1% growth per year (1.1 trillion *tkm*$_e$ or 12.4 trillion *pkm*$_e$). It is worth mentioning that this last scenario implies an abrupt divergence in the historical relationship between aviation demand, economic growth and expected population.

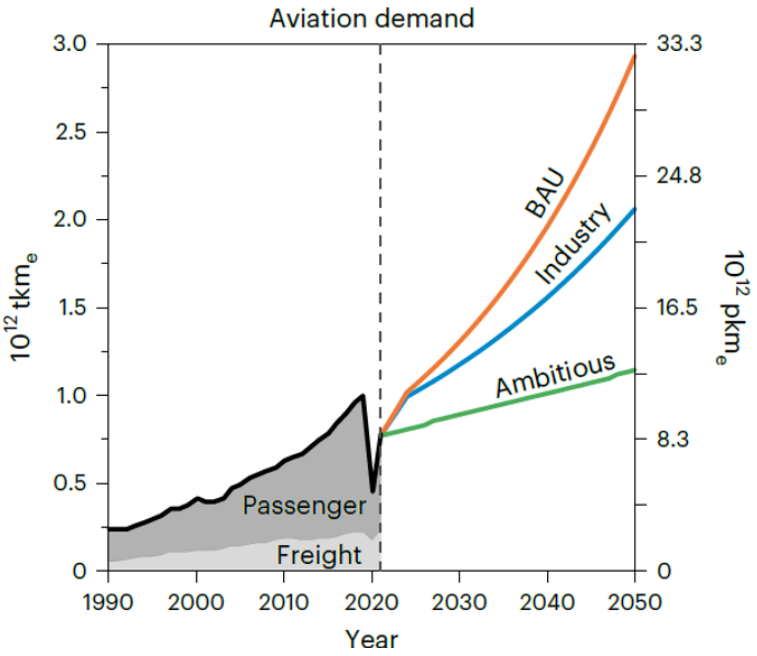

Figure 2.2 - Total aviation demand for 'BAU', 'Industry' forecasts and 'Ambitious' scenarios [8].

In 2019, the IEA forecasts indicate that aviation carbon emissions were 1.03 $GtCO_2$, of which 36% were related to domestic flights and 64% came from international flights. Therefore, it is likely that this year, aviation carbon emissions will probe around these values due to the demand recovery projection for aviation to the 2019 levels, as mentioned before.

Jet fuel has been the perennial energy source for most commercial aircraft, leading to an almost constant carbon intensity of 73.5 $gCO_2\,MJ^{-1}$. In the past few years, some airlines have begun using other alternative bio-base jet fuels, pursuing the carbon intensity decrease of aviation energy. However, these biofuel production efforts cannot fill the market demand. As a reference, in 2019, 140 million litres of bio-based jet fuel were produced and was largely blended with fossil fuels, bearing the standard D7566 from the ASTM[1], which permits a maximum 50% blend. This production volume was less than 1% of the aviation fuel used in that year [8]. So, to tackle the growing tendency of CO_2 and non-CO_2 emissions to the atmosphere due to the global aviation industry development, it is necessary to modify the carbon intensity of aviation energy. Once the global aviation sector is responsible for a notorious percentage of anthropogenic carbon dioxide, which has been proven to be the major contributor to climate change, IATA has set a 50% reduction of global aviation emissions until 2050 as a target. Also, an international treaty on climate change, The Paris Agreement, was presented at COP21, proposing the reduction of global warming to 1.5 degrees Celsius compared to pre-industrial levels, which would assuredly bring several environmental benefits. Following this projected scenario, IRENA assumes that, by the year 2050, 70% of aviation's energy demand will be bridged by SAFs and around 14% will come from electricity and hydrogen. IATA has also made some assumptions regarding its net-zero commitment, projecting that 65% of the estimated 2050 emissions (about 1.8 $GtCO_2$) will be reduced using SAFs, with electricity and hydrogen-powered aircraft decreasing by 13%.

Regarding the proposed reduction of global aviation emissions, three carbon-intensity scenarios (Figure 2.3) must be considered: a 'Carbon intensive' option where the aviation sector keeps relying on fossil jet fuel, maintaining the near-constant carbon intensity of 73.5 $gCO_2\,MJ^{-1}$; a 'Reduced fossil' alternative in which 57% of energy demand by short-haul aviation in 2050 is met by SAFs, 30% by fossil jet fuel and 13% by non-emitting propulsion systems and to medium- and long-haul aviation energy demand about 65% is assured by SAFs (the remaining 35% is still met by fossil jet fuel), thus leading to 23.9 $gCO_2\,MJ^{-1}$; a 'Net-zero' scenario in which the total medium- and long-haul aviation energy in 2050 are met by SAFs as well as 50% of short-haul aviation (other non-emitting propulsion systems supply the remaining 50%), resulting in dreamlike null carbon intensity.

[1] ASTM D7566 is a standard specification developed by ASTM International that covers the manufacture of aviation turbine fuel containing synthesized hydrocarbons. This specification defines the minimum property requirements for such fuels and lists acceptable additives for use in civil-operated engines and aircraft. Once fuel is certified to meet D7566 requirements, it is considered equivalent to conventional aviation turbine fuel specified under ASTM D1655.

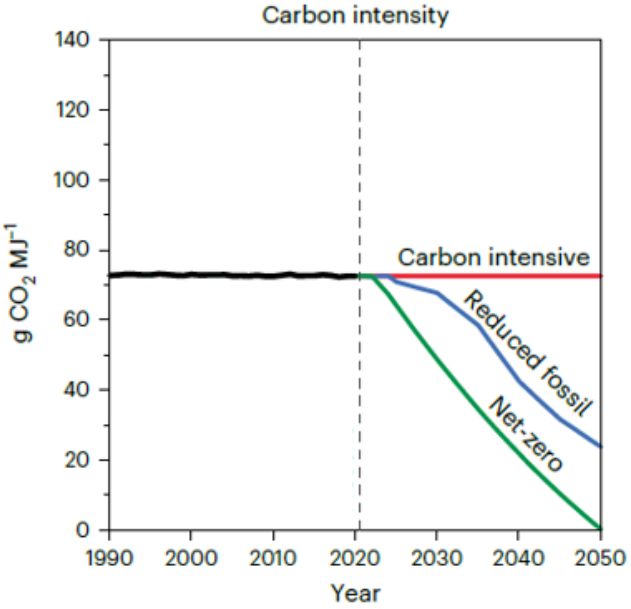

Figure 2.3 - Carbon intensity of aviation energy for ‘Carbon Intensive’, ‘Reduced fossil’ and ‘Net-zero’ scenarios [8].

Combining the three carbon intensity pathways with the three demand scenarios, the carbon dioxide emissions from fossil jet fuel burning can be represented (based on the previous data) and projected for the next decades (Figure 2.4). The coloured areas represent the emissions ranges for each group of demand and carbon intensity scenarios.

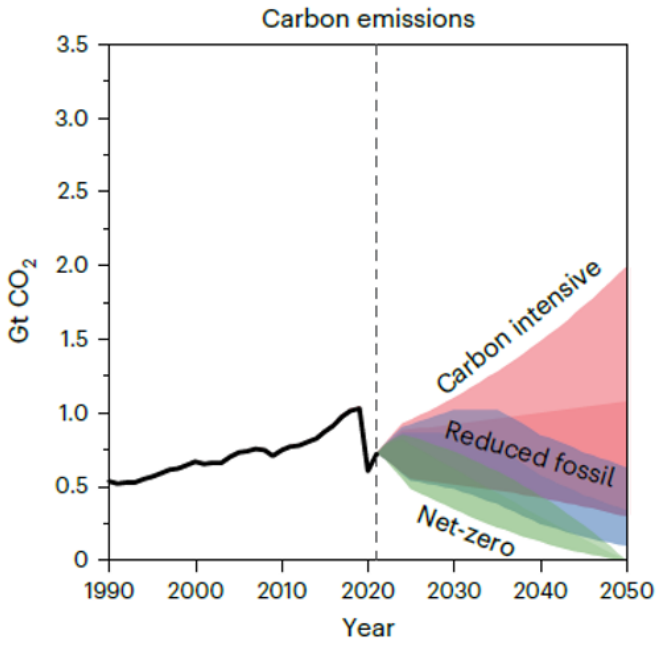

Figure 2.4 - CO2 emissions from jet fuel consumption by combining the three carbon and energy intensity scenarios with the three demand scenarios [8].

Once the aviation sector projections regarding demand and emissions are known, the environmental goals aiming for net-zero direct emissions from aviation in 2050 might be achieved simultaneously through several pathways, including changes and trade-offs in demand, propulsion systems, energy efficiency, compensatory carbon removals, and alternative fuels for both freight and passenger transport [9], [10].

Since carbon-based fuel is burnt, CO_2 will always appear as a by-product. Thus, disregarding the SAFs alternative, the key to reducing the emittance of kerosene-powered aircraft CO_2 (and non-CO_2 gases) is to burn less fuel. That is done by improving aircraft efficiency, whether in the aerodynamic performance or the propulsion system functioning. Today's aircraft are around 80% more fuel efficient than 60 years ago due to technological enhancements [11]. However, as we move to more sophisticated and efficient systems, further reductions in fuel burning are becoming increasingly challenging, as noticeable in Figure 2.5.

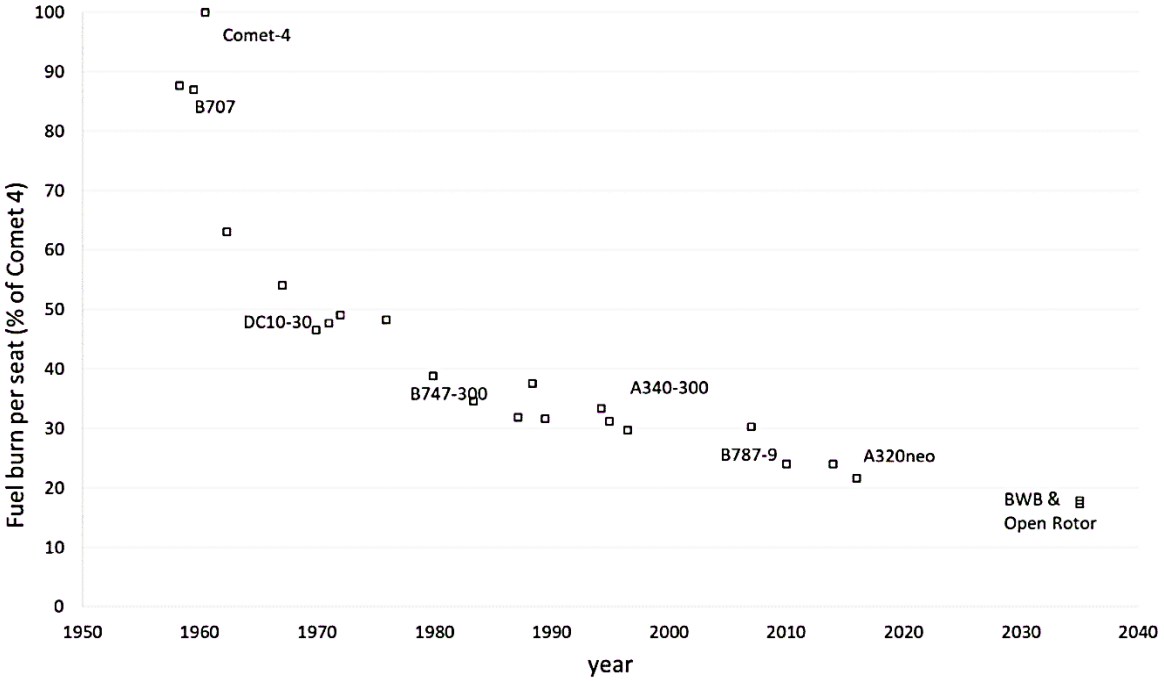

Figure 2.5 - Aircraft fuel efficiency over the years [11].

Regarding the aircraft fuel efficiency over time plotted in the figure above, it is expected that after 2035 future novel technologies provide up to 40% fuel-burning reduction. Nevertheless, it becomes clear that the margin for improvement is getting successively lower. So, significant future enhancements must come from new aircraft concepts and technologies [10], which can arguably create new challenges in the aviation sector. Also, environmental commitments such as alternative fuel usage can trigger some of those challenges and considerations. Those alternative power sources embrace SAFs,

electricity or hydrogen. The first one includes biofuels and synthetic fuels [10] that are a prompt alternative to jet fuel replacement, fulfilling ICAO’s sustainability criteria that impose a net greenhouse gas emission of at least 10% compared to fossil jet fuel. Some SAFs enable an offset of 80% in emissions. Although this solution can help reduce emissions, it will be difficult to fully replace fossil jet fuel until SAF production doesn’t meet the aviation sector’s demand. Besides, SAFs still emit some CO_2.

Most commercial aviation emissions are caused by wide and narrowbody aircraft (Figure 2.6). In the next decade, short-haul regional routes could be serviced by fully electric-powered aircraft, thus reducing emissions. However, the low specific energy of the batteries prevents this power solution from being applied to most commercial flights. For example, for a 1-hour flight on a Boeing 737, its entire fuselage would have to be filled with batteries, just because the specific energy of the current batteries is about fifty times lower than that of kerosene [1]. While some technological advancements in lithium-air batteries propose a potential increase in specific energy by an order of magnitude, some crucial issues still need to be addressed. These include increasing the battery’s power density and improving its cycle life. For all these reasons, hydrogen is a strong ‘green’ alternative fuel to kerosene-based ones, as presented in the next subsection.

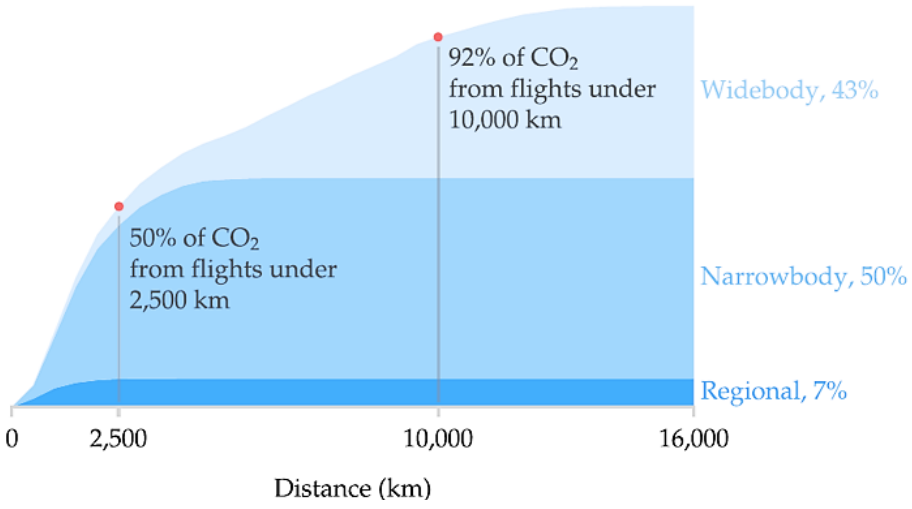

Figure 2.6 - Cumulative CO2 emissions from passenger flights [1].

2.1.2 Climate Impact of Hydrogen Usage

Hydrogen is the most abundant element in the universe, and, unlike kerosene fuel, its combustion only produces water vapour (H_2O) and some nitrous oxides (NO_x) as by-products. When burning, kerosene-based fuel emits several chemical species such as H2O, NO_x, CO_2, CO (carbon monoxide), SO_x (sulphur oxides), unburned hydrocarbons and soot. The emittance of these GHG and other polluting substances hinders accomplishing the environmental goals to slow down global warming. Despite NO_x emissions in both fuel combustion, hydrogen burning offers 90% less nitrogen oxide emissions (and 50% to 70% less than SAF-powered turbines [12]).

To fully comprehend the potential environmental impact reduction due to hydrogen use, some of the so-called *well-to-wake* emissions aspects, such as hydrogen production and transportation, should also be considered. Hydrogen production can be done using several methods, listed in Table 2.1.

Table 2.1 - Hydrogen production methods, ordered from least to most environmentally harmful [1].

Colour	Source
Green	Electrolysis powered by renewable energy sources
Pink	Electrolysis powered by nuclear energy
Blue	SMR with carbon capture and storage
Gray	SMR
Brown	Coal gasification

The first and second listed hydrogen production methods have a near-zero climate impact, whereas the fifth option surpasses the harmful impact of continued fossil fuel use. Thus, the source of hydrogen matters to the environmental impact analysis. Green hydrogen production (the first method) may have a low climate impact, but never zero. For example, some renewable energy sources still emit GHGs when produced (like photovoltaic solar panels). Besides, using these sustainable methods is not yet profitable due to electricity consumption, making them unacceptably expensive compared to other production options. Nevertheless, green hydrogen costs become an advantage as the electrolysis process becomes used on a larger scale and the renewable energy cost decreases. Currently, electrolysers convert 70% of the electric energy into the equivalent hydrogen energy [13] and it is expected to increase that value up to 80%, with further developments.

The fourth hydrogen production method is known as a low-carbon hydrogen source. This production option relies on methane (natural gas) dependence as a power source, which is a downside. Furthermore, intentional methane venting or pipeline leaks might be an additional safety concern once methane is a mighty GHG. These fugitive emissions may neglect the climate impact reduction of the carbon capture application (85% to 90% reduction of CO2 emissions, compared to the SMR without carbon capture).

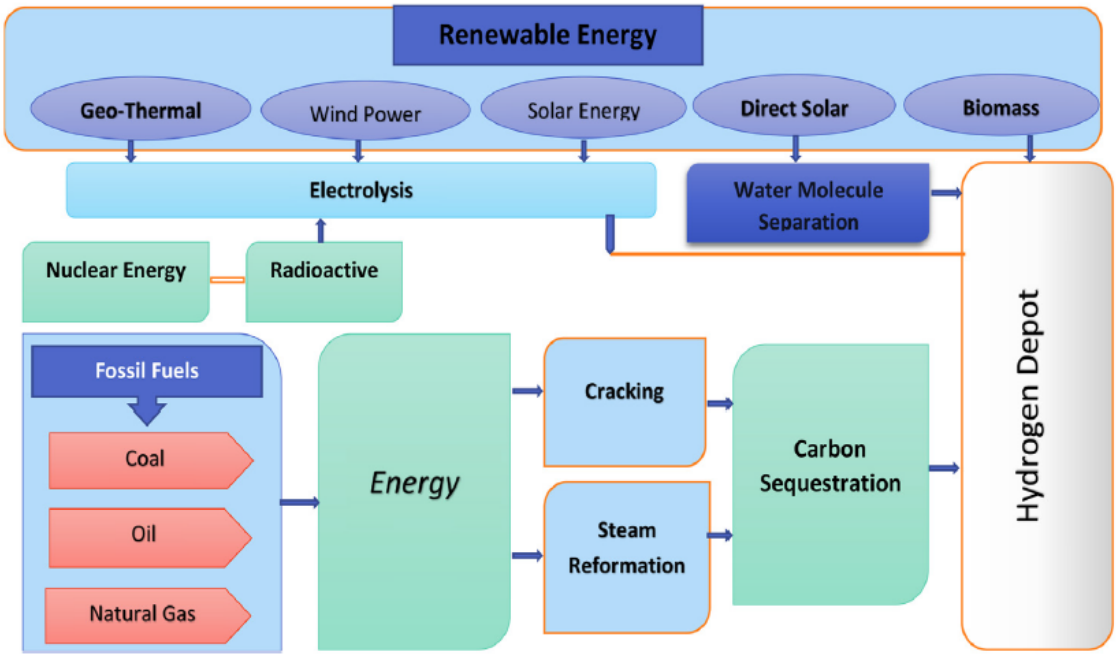

Figure 2.7 - Diagram of the hydrogen production methods [2].

Moving to the hydrogen transportation issue, the main concern lies in its tendency to leak and the need to vent to avoid exceeding tank pressure limits, particularly for LH_2 transportation due to its boiling off. Besides, some greenhouse gas behaviour, such as the lifetime of methane, is affected by hydrogen atmospheric presence. The climate impact of hydrogen transportation, with a low leakage rate, is minimal compared to the impact caused by its production and application. However, it is estimated that 1-10% of the produced hydrogen is leaked so, the climate impact of a leakage rate around the upper limit of the estimated range may not be negligible. In practice, a 10% leakage rate is unlikely, but if it occurs it would be reversed as soon as possible to minimise economic and safety problems. Fossil fuel burning also uses hydrogen as a by-product thus, reducing its consumption makes up some of the hydrogen venting and leakage emissions.

The efforts applied in the hydrogen aircraft development aim to reduce aviation's climate impact forcefully. However, this is seldom airframers' goal. Their main concern usually tends to be the search for an ideal combination of aircraft purchase and operating costs,

bearing the customer’s requirements [1]. Proesmans and Vos [6] designed a medium-range narrowbody aircraft for each concept to comprehend the difference between a climate- and a cost-optimised aircraft. It was concluded that kerosene-powered aircraft optimised for minimal climate impact caused a 7% rise in the cash operating cost compared to the cost-optimized model. This value reaches 15% for hydrogen-powered aircraft, mostly because of the lower cruise altitude to mitigate contrail formation. Regarding cost optimisation, the hydrogen-powered design reduces the climate impact by 71% compared to the kerosene aircraft.

2.1.3 Hydrogen as Aviation Fuel

Since hydrogen presents itself as a strong option to reduce aviation emissions, its study becomes more and more relevant to achieving climate goals. Nonetheless, using hydrogen as a fuel presents challenges regarding safety enforcement due to its high specific energy and unique storage requirements because of its lower energy density.

Table 2.2 lists some properties of jet fuel, cryogenic liquid hydrogen (LH_2) and gaseous hydrogen (GH_2) at two different pressures.

Table 2.2 - Properties of Jet A-1, LH_2 and GH_2, where the specific energies are given as LHV [1].

Property	Jet A-1	LH_2	GH_2 (350 bar)	GH_2 (700 bar)
Specific energy (MJ/kg)	43.2	120	120	120
Energy density (MJ/L)	34.9	8.5	2.9	4.8
Density (kg/m^3)	808	71	24	40
Storage temperature (K)	Ambient	20	Ambient	Ambient
Storage pressure (bar)	Ambient	1.5 - 2	350	700

To achieve desired energy densities, hydrogen must be stored as a cryogenic liquid or as a compressed gas. As shown in Table 2.2, LH_2 has the highest energy density compared to GH_2. However, that value is about 4.1 times lower than kerosene fuel (Jet A-1) and, on an equal energy basis, the cryogenic LH_2 is about 2.8 times lighter than kerosene. Hydrogen being less dense results in more volume space needed than kerosene, for the same energy content.

The highly compressed hydrogen, particularly the GH_2, requires specialised pressure vessel tanks, usually cylindrical, to support the pressure loads. On the other hand, LH_2

needs a heat management system to control its boil-off. This process occurs because of the environmental heat entering the LH_2 (also known as heat leak), causing a pressure augmentation inside the tank. Therefore, tanks can be designed to withstand greater pressures and insulate better because once the pressure reaches the tank’s structural limit, the hydrogen must be vented, which wastes fuel. Cryogenic tanks are a great option to reduce heat leaks and they are most efficient when they have a low surface area-to-volume ratio. The closer a cryogenic tank shape is to a sphere, the better. Some more details about hydrogen tank design will be provided in Section 2.1.4.

Hydrogen can be turned into thrust using mostly hydrogen fuel cells or the combustion process in turbomachinery (Figure 2.8).

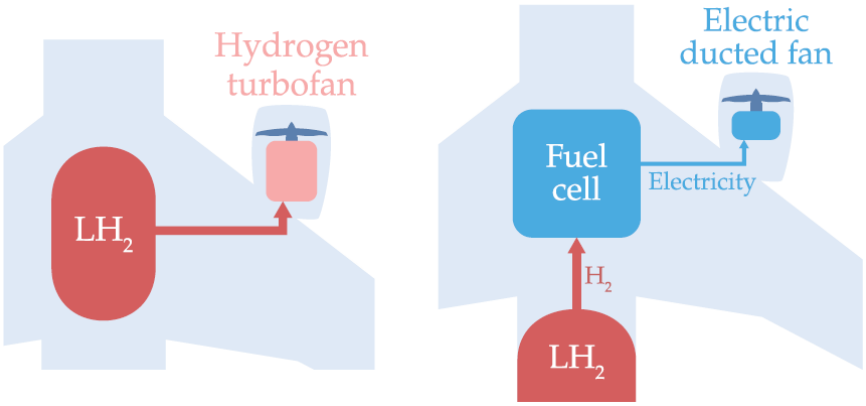

Figure 2.8 – The power plant of the most common systems used to turn hydrogen into thrust [1].

As shown in Figure 2.8, a propeller or a ducted fan can be powered using a fuel cell to convert hydrogen to electricity. Fuel cells operate at efficiencies of around 50% to 60%, having only water vapour as a by-product, which is an environmental upside. However, their sizing to high-power propulsion systems is challenging because of thermal and specific power constraints. So, hydrogen turbofans may be more suitable for higher specific power required and fewer thermal management issues than hydrogen fuel cells. For example, a turbofan propulsion system for a 737-sized aircraft would be three times lighter than a fuel cell propulsion system for the same aircraft.

Currently, most of the demand for aviation is met by using gas turbine-powered turboprops and turbofans. Despite its capability to produce thrust using hydrogen burning, there is still the need for new engines optimised specifically for hydrogen due to its combustion properties compared to kerosene. However, the existing turbomachinery conformation, modifying the fuel supply system and combustor, might be a faster short-term solution, instead of designing new power plants. Furthermore,

adapting the current gas turbines leverages existing knowledge, manufacturing techniques and design tools, thus saving resources. The existing gas turbines operate at efficiencies of around 40%, and the thrust-specific energy consumption of hydrogen turbofans is expected to meet the same as that of kerosene turbofans. As mentioned, the only substantial change to the current turbomachinery is the combustor's design for hydrogen's combustion and thermal properties. It is worth noting that some hydrogen's properties, such as those of cryogenic LH_2, can be used as a heat sink to transfer heat to more beneficial locations in the engine [1]. The water vapour in the exhaust can be condensed and injected into the engine cycle again, also providing some operating benefits. The downside of combustion compared to fuel cells is its higher environmental impact because it produces NO_x aside from water vapour. Regarding fuel combustion, there are also some relevant properties listed in Table 2.3.

Table 2.3 - Safety properties of fuels for aviation [14].

Property	SynJet	Methane	Hydrogen
Flammability in the air (vol%)	0.8 - 6.0	5.3 - 15.0	4.0- 75.0
Detonation in the air (vol%)	1.1 – 3.3	6.3 – 13.5	13 – 65
Minimum ignition energy in the air (mJ)	0.25	0.29	0.02
Burning velocity (m/s)	43	40	265
Autoignition temperature (°C)	440	40	585
Thermal energy radiated by surroundings (%)	33 - 43	23 - 33	17 - 25
Theoretical explosion energy (kg TNT/m^3 gas)	44.42	7.03	2.02
Diffusion coefficient in air (cm^2/s)	0.05	0.16	0.61
Buoyancy in air (m/s)	———	0.8 – 6.0	1.2 – 9.0

To continue the hydrogen's properties presentation, it is worth recalling that when the amount of oxidant in a reactive mixture is theoretically necessary and sufficient to burn all the fuel completely, that mixture is called stoichiometric, in an ideal combustion process. Besides, an ideal combustion process presupposes the formation of completely oxidised chemical species in the combustion by-products. Following this, the ratio of fuel mass flow to air mass flow, when all the oxygen in the air is consumed and all the fuel is burned, is called the stoichiometric fuel-to-air ratio. The quotient between the actual fuel-to-air ratio and the stoichiometric fuel-to-air ratio yields the fuel-air equivalence ratio (Equation 1). This is a convenient parameter to quantify how much air is present in the combustion process. Also, lean combustion occurs when $\phi < 1$, which means that the air supplied is more than necessary to burn the fuel fully. An equivalence ratio $\phi > 1$ implies a fuel-rich mixture. The equivalence ratio [15] is determined using

$$\phi = \left(\frac{\dot{m}_f}{\dot{m}_{ox}}\right)/r \quad (1)$$

where the stoichiometric fuel-to-air ratio [15], r, is given by

$$r = \left(\frac{\dot{m}_f}{\dot{m}_{ox}}\right)_{stoic} \quad (2)$$

Returning to the main topic, kerosene- and hydrogen-powered gas turbines work both the same way and thus require minimal design adjustments, except for the combustor. In this component, and applying the thermodynamic terms previously defined, the kerosene's stoichiometric fuel-to-air ratio is 1:15 which is more than double hydrogen's 1:34. Besides, hydrogen has a wide flammability range permitting it to be burned much leaner than kerosene (Figure 2.9) and this is also a warning about the hazard of premixing the hydrogen-air mixture before injection into the combustor since flashback may occur, where combustion flames can go back from the combustor into the premixing zone.

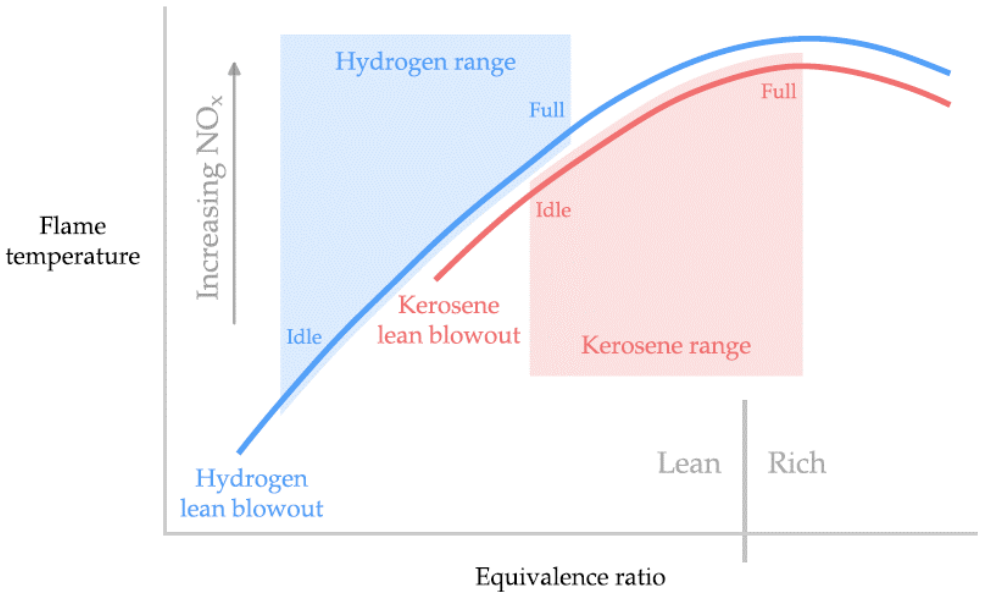

Figure 2.9 - Flame temperature variation with the equivalence ratio [1].

As mentioned, hydrogen combustion has water vapour and nitrogen oxide as by-products. The combustion temperature and the residence time influence the amount of NO_x produced by fuel burning. Hydrogen has a higher flame speed and thus faster combustion than other fuels, such as kerosene, SynJet or Methane (Table 2.3), yielding lower NO_x emissions (Figure 2.9). At a unitary equivalence ratio, kerosene's flame temperature is greater than hydrogen's. Nevertheless, as hydrogen can be burned much leaner than kerosene, its flame temperature can be lowered. Therefore, assuming the

hydrogen-air mixture is completely mixed, the hydrogen burning at the lower flame temperature of lean combustion produces less NO_x. The nitrogen oxide produced comes from combustor regions where air and fuel are at stoichiometric conditions due to insufficient mixing. So, one of the options to lower the NO_x emissions arising from hydrogen usage might be the mechanisms enhancements to increase the mixing intensity [1].

Khandelwal *et al* [16] propose LDI and micro-mix combustion as both solutions to increase the mixing intensity of the hydrogen-air mixture. These approaches involve deploying several gaseous hydrogen injectors at a certain angle to the airflow direction to boost turbulent mixing between the hydrogen and air streams. These mechanisms have already been experimentally tested with satisfactory results. For example, Marek *et al* [17] tested the LDI combustion, which was revealed to be stable, and produced low NO_x emissions. Furthermore, no flashback phenomenon was observed, which could be caused by hydrogen lean combustion. The micro-mix mechanism was tested by Dahl *et al* [18] by converting an Airbus A320 APU from kerosene to hydrogen with a micro-mix combustor that decreased the NO_x emissions by a factor of four. Without the micro-mix approach, the kerosene-to-hydrogen APU conversion only enables slight modifications to nitrogen oxide emissions.

Hydrogen can be burned much leaner than kerosene, allowing for a lower flame temperature and thus reducing the hot gas temperature entering the turbine after combustion, increasing the turbine's lifetime and reducing the maintenance inspection frequency. According to Montañés and Corchero [19], for a hydrogen engine, it is possible to reach a 37 K decrease in the turbine inlet temperature compared to a similar kerosene engine. This temperature reduction allows for almost doubling the turbine's lifetime.

Storing hydrogen as a liquid can serve as a heat sink, enhancing engine performance. To investigate potential improvements, Boggia and Jackson [9] explored various modifications for a hydrogen-burning version of the IAEV2527-A5 engine applied in the Airbus A320. At the first approach, they analysed precooling air to ease compression, achieving a 5.7% TSFC reduction. Secondly, they proceeded by cooling bleed air around the combustor and mixing it before the turbine, which yielded a 2.1% TSFC reduction by increasing the turbine inlet temperature. The latest modifications involved vaporising the fuel, which is preheated using the engine's hot exhaust to decrease fuel consumption. In this last modification, Montañés and Corchero [19] foresee a TSFC reduction of around 1%-3%, by preheating hydrogen from 25 K to 250 K.

Beyond hydrogen-specific changes, future engine advancements apply to both kerosene and hydrogen engines. These include increasing the bypass ratio for better propulsive efficiency, enhancing the overall pressure ratio for improved thermal efficiency, and employing advanced materials and manufacturing to reduce engine weight.

The aviation sector has quite strict safety standards. Therefore, the transition from kerosene to hydrogen is the focus of several studies of hydrogen properties that make it safer or more dangerous than kerosene, depending on the property being considered. IATA [11] provides a summarised comparison of safety parameters between kerosene and hydrogen, listed in Table 2.4.

Table 2.4 - Safety parameters comparison between hydrogen and kerosene [11].

	Hydrogen	Kerosene
Auto-ignition temperature	+	-
Buoyancy	+	-
Diffusivity	+	-
Spill Hazard	+	-
Burning time	+	-
Lower Flammability limit	+	-
Flammability range	-	+
Leakage detection	-	+
Leakage Avoidance	-	+
Flame detection	-	+
Minimum ignition energy	-	+

Just to clarify, in the table above, the plus signal means a beneficial feature of one fuel over the other, whereas the minus signal means the opposite. For example, the hydrogen flame is invisible, and the gas is odourless, so this is a downside (minus signal) in hydrogen leakage detection. Regarding buoyancy, hydrogen is about 14 times lighter than air, so if spilt it would quickly disperse, preventing its accumulation on the ground level. As mentioned, hydrogen’s flammability range is wider than kerosene’s, so to have a fire it will be needed higher hydrogen concentrations (4% to 76%) than kerosene (1.4% to 7.6%) [11]. Also, the flammability limit is lower for kerosene (1.4%) than hydrogen (4%), which means that the hydrogen concentration must be around 3 times greater for a fire to occur. Furthermore, the minimum ignition energy of hydrogen is lower than kerosene, so a weaker spark can trigger the ignition. Besides all the hydrogen combustion advantages over kerosene and the future engine improvements awaited, some issues regarding hydrogen storage might also introduce challenges to aircraft design.

2.1.4 Aircraft Design: Storage Tanks Overview

For all the aspects mentioned before, hydrogen storage demands specialised tanks with a large volume (bulky) to store a useful amount of energy and a higher dry weight, since these tanks are pressurised. So, hydrogen storage incurs a weight penalty relative to kerosene storage and the low surface area-to-volume ratio tank shape does not adjust well into aircraft wings (where the kerosene is often reserved). Instead, hydrogen tanks are usually placed in fuel pods or fuselage compartments. This extra fuselage space and the external fuel pods cause the aircraft’s wetted area incrementation, increasing aerodynamic drag. The wing’s structural weight may also increase because the structural load alleviation benefits no longer exist due to the fuel being removed from the wings. So far, hydrogen storage introduces drag and weight penalties to the aircraft design.

Comparing the same energy quantities required for a flight mission, it takes about one-third of the weight of hydrogen as compared to kerosene [4]. Therefore, if the hydrogen storage particularities caused no drag or weight sanctions, this would mean a lower TOW and, thereby, a smaller wing, especially for an aircraft with an elevated fuel fraction (defined by the quotient between the fuel weight at the mission start and the TOW). Due to the iterative quality of the aircraft design procedure, a smaller wing allows the aircraft drag reduction and its structural weight, reducing the TOW, and so on. However, those storage penalties exist and taking the hydrogen’s energy per unit mass benefits into account, it is important to know the net effect in the energy used for a given flight. Verstraete [20] says that for a large-haul aircraft fuelled by hydrogen, the TOW is reduced by 25% and the total energy required is reduced by 15% compared to a kerosene-powered aircraft. Verstraete [21] also predicts that, for a long-haul aircraft and assuming hydrogen has a cost parity with kerosene per unit of energy, a hydrogen aircraft provides a net decrease in direct operating cost, despite the hydrogen storage complexity and the drag and weight penalties caused whether using fuel pods or fuselage compartments.

For a similar design mission, the Cryoplane technical report [22] reveals a TOW decrease of 14.8% and a 9% increase in the total energy required for flight. This Cryoplane study reveals that to match the operating costs of kerosene aircraft, the cost of hydrogen per unit of energy would need to decrease. The difference between the previous studies’ conclusions can be explained by the fact that the Cryoplane project used an existing aircraft design instead of creating a new one.

The constraints in the aircraft’s design can be influenced by the fuel weight reduction due to hydrogen’s specific energy. In practical terms, to climb to the cruise altitude, the

hydrogen required to provide the amount of energy needed is around a third of the mass of the required kerosene. Well, this implies that a hydrogen aircraft loses less fuel weight during the climb than a kerosene aircraft [1]. Thus, at the end of the climb, it is expected that the hydrogen aircraft may require more thrust relative to the takeoff thrust, which is a constraint on the engine design. Furthermore, the weight loss during the cruise phase is also lower compared to a similar kerosene-powered aircraft so, in terms of flight motion, the ideal cruising altitude to the hydrogen aircraft can be reached without or with small altitude step climbs due to slow increase.

As presented by Adler and Martins [1], to quantify the weight penalties introduced by the specialised tanks to store hydrogen, a performance figure is used, called gravimetric efficiency or mass fraction defined by

$$\eta_{tank} = \frac{W_{H_2}}{W_{H_2} + W_{tank}} \quad (3)$$

For a tank full of fuel, this performance metric represents the fuel weight fraction of the tank-fuel system. Thus, comparing two different tanks, the one with the higher gravimetric efficiency value has a higher fuel weight fraction (using the respective tank weight for each one), which also means a lower weight penalty introduced by the storage tank used. In Kerosene aircraft the fuel tanks are usually integrated into the wingbox structure which permits considerable weight-saving and thus gravimetric efficiency values around 100% [1].

Regarding energy usage, for high gravimetric efficiencies, hydrogen aircraft performance tends to be better than kerosene aircraft as the range increases. In Figure 2.10, this is represented by the lower right region of the diagram, where the hydrogen aircraft energy usage relative to kerosene aircraft is increasingly lower as the tank gravimetric efficiency tends to be 100% and as the flight range increases from ‘Regional’ to ‘Transcontinental’ and finally to ‘Intercontinental’.

However, for low gravimetric efficiencies, the tendency is reversed which means that, as the range increases the hydrogen aircraft energy usage relative to kerosene aircraft is higher, as represented in the upper left region of the diagram. For all these considerations, a hydrogen aircraft with a lower tank gravimetric efficiency might be more appropriate for short- and medium-range flights whereas a higher tank gravimetric efficiency might be more desirable for a long-range flight. For tank gravimetric efficiency

of 55%, there is a tipping point between these scenarios where, regardless of the flight range, hydrogen aircraft energy usage matches the kerosene aircraft.

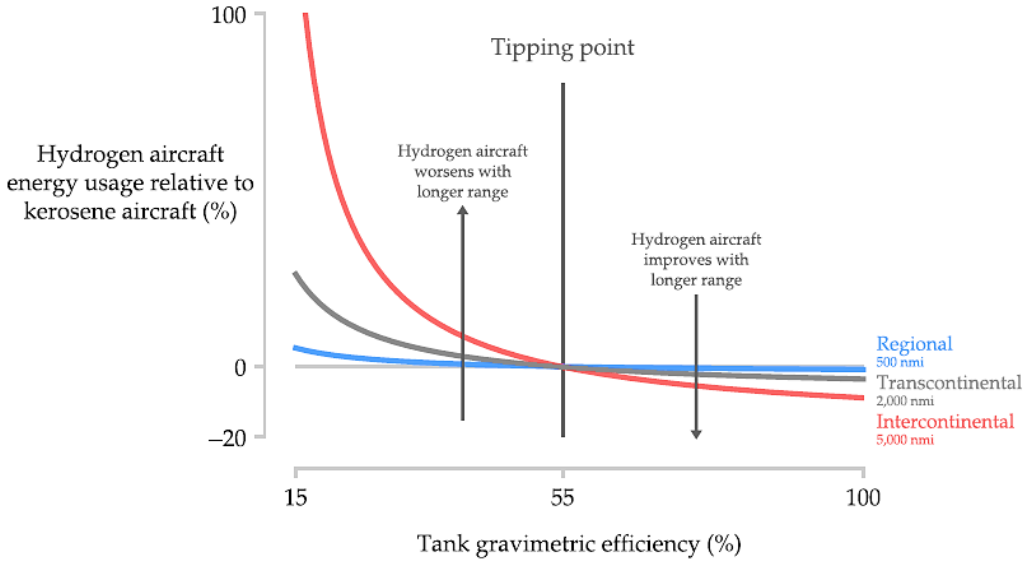

Figure 2.10 - Hydrogen aircraft performance relative to kerosene aircraft, varying tank gravimetric efficiency [1].

Another aspect that should be considered is hydrogen’s physical state which leads to the comparison between GH_2 and LH_2. Increasing GH_2 density by compressing it to high pressures is one of the solutions to obtain some different onboard storage capabilities. As listed in Table 2.2 shows that compressed GH_2 tanks add more simplicity to the aircraft fuel system than LH_2 tanks because they can be managed at ambient temperature without needing to be refilled or vented for a long time. However, GH_2 requires pressurised tanks which usually are heavy to resist the high internal pressure safely. Thus, most compressed hydrogen tanks have low gravimetric efficiencies, from 1% to 15% [1]. Exceptionally, this value could go up to around 20% using advanced manufacturing and design techniques along with composite materials.

The LH_2 tank gravimetric efficiency can reach values between 30% and 90% and the storage density is almost twice that of compressed hydrogen. So, LH_2 presents itself as a good option for medium- and long-range missions. However, the complexity added to the fuel system is still a challenging topic.

The way that the hydrogen tank is fitted on the aircraft can introduce some beneficial features that are worthy to be mentioned. There are two different tank mounting configurations: integral and non-integral (Figure 2.11).

Integral tanks, as the term indicates, are an integral part of the aircraft’s structure and thus it is expected that the tank walls resist multiple loads such as bending, axial and

shear stresses. Like the conventional kerosene aircraft tanks that are integral to the wingbox structure and thus enable aircraft weight savings, the hydrogen tanks can be an integral part of the fuselage providing similar weight advantages. However, to support the airframe loads, integral tanks must be more resistant compared to non-integral ones, which is achieved with thicker walls, worsening the tank’s gravimetric efficiency.

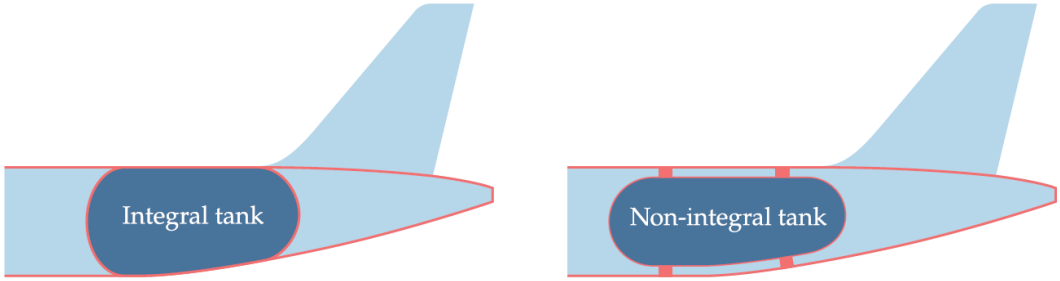

Figure 2.11 - Integral and non-integral tank’s structure [1].

The hydrogen tank shape must be as close to a sphere as possible to minimise the boil-off rate. So, in tube-and-wing aircraft designs, the integral tank might be a better option over the non-integral because it can use the whole fuselage cross-section, shorten its longitudinal length and thus be closer to a spherical shape, as shown in Figure 2.12. Furthermore, Onorato *et al* [23] concluded that the mass savings due to integral tank use over non-integral tank are increasingly greater as the aircraft is larger.

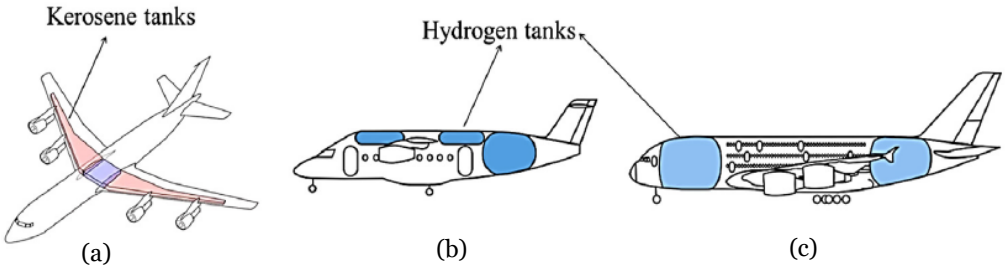

Figure 2.12 - Fuel tank position in (a) conventional kerosene aircraft, (b) medium-range and (c) long-range hydrogen-powered aircraft [41].

In turn, non-integral tanks are not an integral part of the aircraft’s airframe. Instead, they are usually mounted inside a conventional fuselage or in fuel pods on the wings. As a result, these tanks support thermal loads, aerodynamic loads and fuel dynamic loads [24]. Therefore, unlike the integral tanks, the non-integral tanks are easier to design and can be placed anywhere in the aircraft using the appropriate fixing brackets.

Verstraete [21] uses the simulation tool FLOPS, which is a multidisciplinary aircraft design and analysis package developed by the NASA Langley Research Center, to propose

the LH_2 powered-aircraft design shown in Figure 2.13 (a). Once the LH_2 tanks are an integral part of the aircraft's airframe, the fuselage length is a function of the fuel required for the flight. Thus, FLOPS is run iteratively until fuel weight and fuselage length converge. Verstraete [21] presents this configuration for a long-range aircraft, acknowledging that for larger aircraft an integral tank might be a better option over the non-integral due to the weight savings [23]. Besides, the integral tank uses the whole fuselage cross-section and thus has a near-spherical shape, preventing a higher heat leakage rate. This storage arrangement also provides some safety benefits over the wing tanks option, since the tanks have a lower frontal impact [21].

In the 70s, Brewer *et al* [25], by the Lockheed Aircraft Corporation's remit, studied the hydrogen fuel application to long-range subsonic transport aircraft and proposed a design (Figure 2.13 (b)) very similar to Verstraete's [21] posterior solution. The front tank is positioned between the cockpit and the passenger cabin and there is a sidewalk passage to allow cockpit access. Gomez and Smith [26] proved that this passage causes a nearly 10% gravimetric efficiency decrease. Furthermore, this forward tank might be inappropriate for a narrowbody aircraft, if the pilot's access to the passenger cabin is desirable because its fuselage diameter is not large enough for sidewalk passage inclusion.

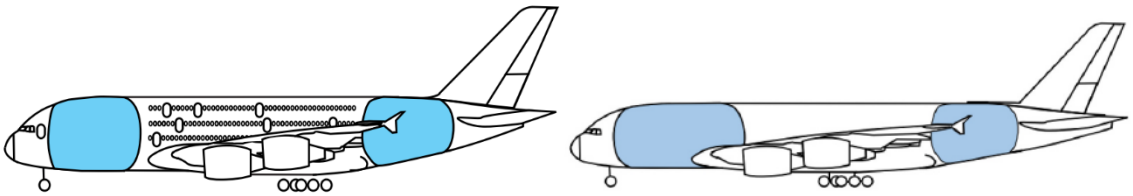

(a) (b)

Figure 2.13 - (a) Long-range aircraft [16] and (b) Forward and aft tank configuration [20].

All studies indicate that the most gravimetric efficient configuration for fuel tanks is a single tank located behind the rear pressure bulkhead [27], using the full cross-section of the fuselage as an integral tank (Figure 2.14 (a)). Once more, this configuration minimises the heat leak because it provides the lowest tank area-to-volume ratio and if the tank's outer surface conforms to the fuselage's outer surface (integral tank) there are also weight savings, as previously mentioned. This configuration is suitable for smaller aircraft with shorter ranges, which usually translates to a low fuel fraction. For a larger aircraft with a tube-and-wing configuration, the forward and aft tank layout might be crucial to constrain the CG movement and so stay within trim and stability limits. As Druot *et al* [28] denote, an aircraft with a rear fuselage tank has a bipolar functional

segmentation (tank-cabin) which may bring a forward move of CG during the flight mission due to fuel weight loss. This CG forward move may increase trim drag, despite it does not imperil the longitudinal stability.

The FlyZero research project developed three aircraft concepts using LH_2 as a fuel. The regional concept (Figure 2.14 (b)) range was set at 800 nautical miles and 325 knots cruise speed [29], using a fuel cell system to generate thrust.

The short-range narrowbody concept is like the baseline and reference aircraft (Airbus A320neo) but with a three-lifting surface, regarding the centre-of-gravity movement. As the hydrogen tank is aft, the canard helps in longitudinal trim authority, allowing a netter pitch control for rotation and a wider CG range [29]. For more efficient hydrogen storage, it would be desirable to have a wider fuselage at the rear so, this short-range concept has an alternative approach to the conventional narrowbody concept. Instead of having a constant section fuselage, the cross-section has a variable width favouring natural laminar flow hoping to reduce the drag.

Finally, the last concept (Figure 2.14 (c)) is a medium-range aircraft. Besides a larger range compared to the previous narrowbody aircraft, this FlyZero midsize concept has its engines placed under the wings, a larger LH_2 tank in the rear of the fuselage and two additional delta tanks ahead of the wing in an unpressurized zone to ensure reasonable limits of weight and balance [29].

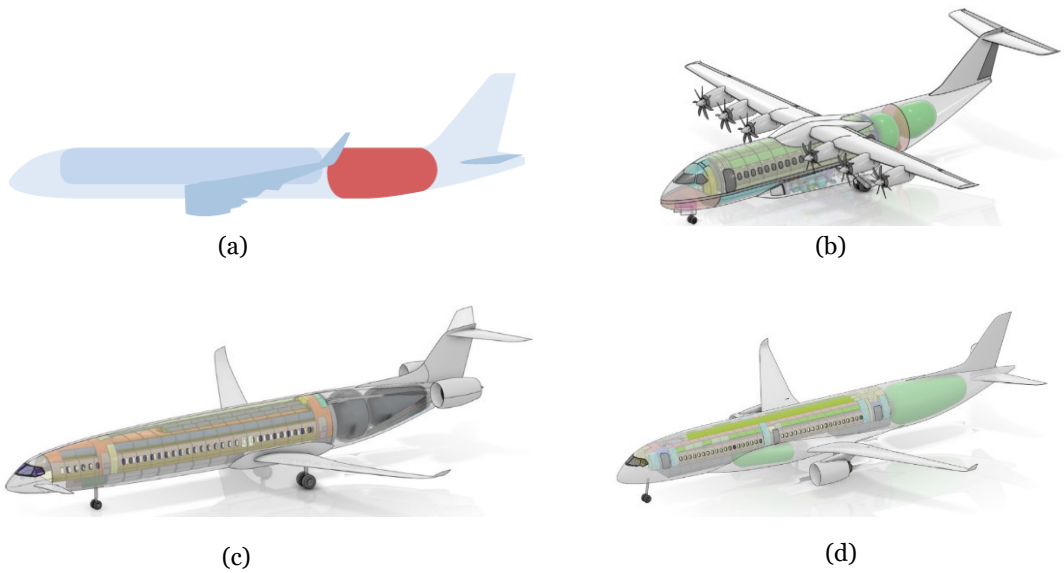

(a) (b) (c) (d)

Figure 2.14 - (a) Aft tank configuration [1]; FlyZero (b) Regional, (c) Short and (d) Medium-Range [29].

The upper tank configuration, shown in Figure 2.15 (a), has several safety features. Positioning the tanks above the fuselage along its length prevents damage caused by

debris projection during the takeoff or landing manoeuvre. Or, considering a hypothetical landing gear fail, this layout also avoids the tank destruction during the belly landing. Furthermore, likely, that leaks vent upward and away from the passenger cabin [1] due to their location outside of the pressure vessel if the tank puncture occurs.

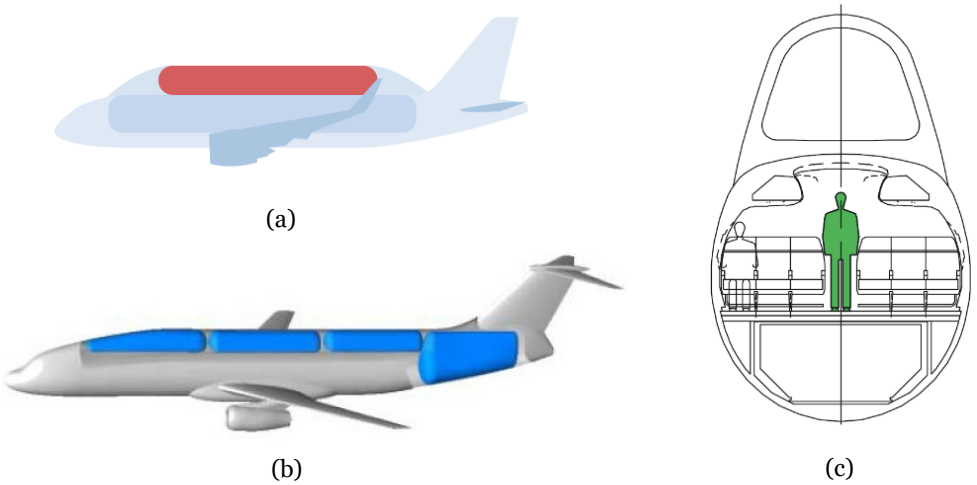

(a) (b) (c)

Figure 2.15 - (a) Upper tank configuration [1]; (b) Cryoplane project and (c) cross-section of a fuselage with over-cabin tank configuration [48].

Once these upper tanks are longer and thinner, they require more insulation to prevent heat leaking and, besides that, they cannot be integral to the fuselage. Thus, this tank layout introduces a weight penalty compared to other tank arrangements previously discussed. Verstraete [30] made the fuel efficiency comparison between an aircraft with a forward and aft integral tank configuration (analogous to the design proposed by Brewer *et al* [25], shown in Figure 2.13) and similar aircraft where two upper tanks substitute the forward integral tank, as shown in Figure 2.16. When the top tanks’ fuel is not enough for the whole flight mission, a tail tank is added. Verstraete [31], in a previous study about hydrogen fuel tanks for subsonic transport aircraft, verified that the tank weight is very sensitive to the tank diameter. Thus, besides the weight penalties, as the top tanks have a smaller diameter and a higher longitudinal length (high surface area-to-volume ratio), they could also lead to a CG control issue, often related to the excessive centre-of-gravity dislocation to the aircraft aft, therefore requiring a larger tail section [30].

In the comparative study, Verstraete [30] concluded that for a medium-range aircraft, the top tanks are 50% heavier than the equivalent integral tanks, despite the rear tank containing 63% of the required fuel. This increase in the fuel tank weight leads to an operating empty weight of 23.4% higher and an energy use augmentation of 19% compared to the forward and aft integral tank configuration (Figure 2.16 (b)).

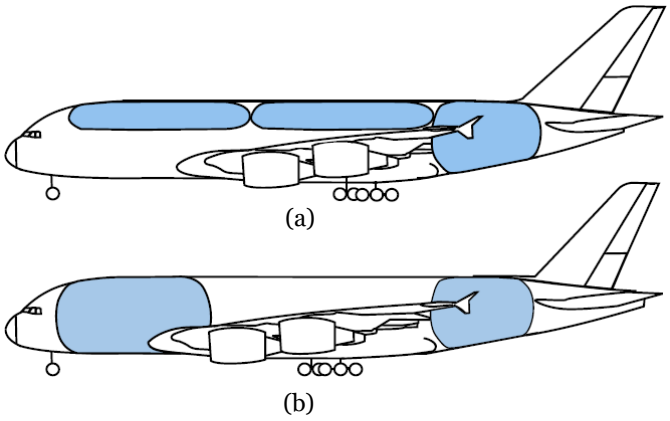

Figure 2.16 - Aircraft model sized to use (a) top tanks and (b) forward and aft integral tanks [30].

Unlike the previous fuel tank configurations, the under-wing tank pod layout provides the wing root bending moment decrease, which is an advantage from the structural point of view. Besides, this solution also brings some safety aspects because it permits positioning the tanks as far as possible from the passenger cabin. Regarding the ground handling, tank accessibility is very similar to the engine and its configuration allows different tank size installation depending on the mission range requirements.

A twin under-wing engine-mounted aircraft permits two different pod positions. The first one is between the cabin and the nacelle, which would generate aerodynamic overspeed and a lot of extra drag. Besides, this internal tank position endangers even more the fuselage regarding potential fire situations. The second position option is on the outer wing. However, Druot *et al* [28] suggest some aspects study such as:

- the disk burst trajectories in the case of an under-wing engine-mounted aircraft
- the pitch attitude during the takeoff and landing
- the aerodynamic interactions between the pods and the wings
- the aero-structural interactions and flexible modes
- the ground clearances in case of banking attitude.

As shown in Figure 2.17, the high-wing configuration mitigates ground clearance issues. Therefore, the T-tail configuration is adopted to ensure the right operation of the horizontal stabilizer elevator, out of the wing wake. This structural arrangement introduces some weight penalties.

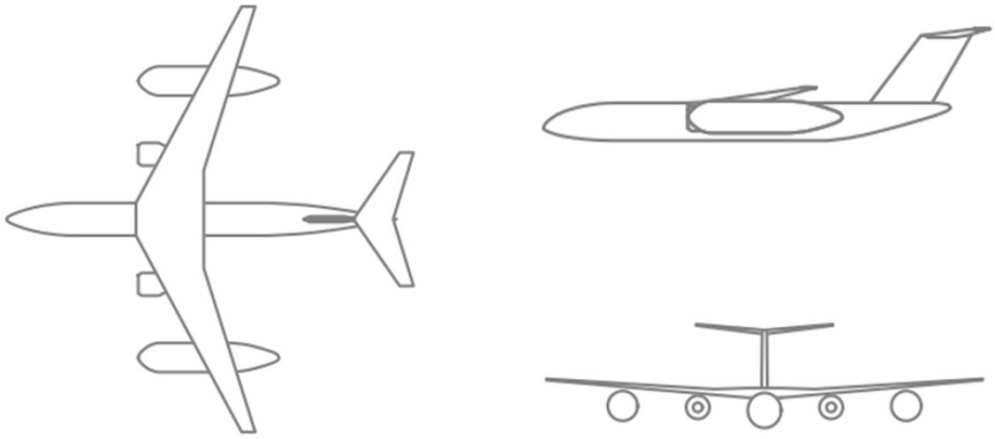

Figure 2.17 - Under-wing fuel tank pod configuration [28].

During the Cryoplane project development [22], some hydrogen storage proposals were associated with unconventional aircraft configurations such as the BWB (Figure 2.18) and the twin-boom concept (Figure 2.19). It was concluded that the BWB was not appropriate to fit pressure vessel tanks due to its profile shape. Besides, for smaller shorter-range aircraft where the overall dimensions are often small compared to human beings, there is a large unused volume [22]. Thus, the BWB concept might be better when applied to very large long-range aircraft. There, the large irregularly shaped volume created by the blending region between the cabin and the wings may be appropriated for storing hydrogen with a low drag penalty [1]. This concept also requires further studies in many other operational fields, such as an emergency evacuation plan.

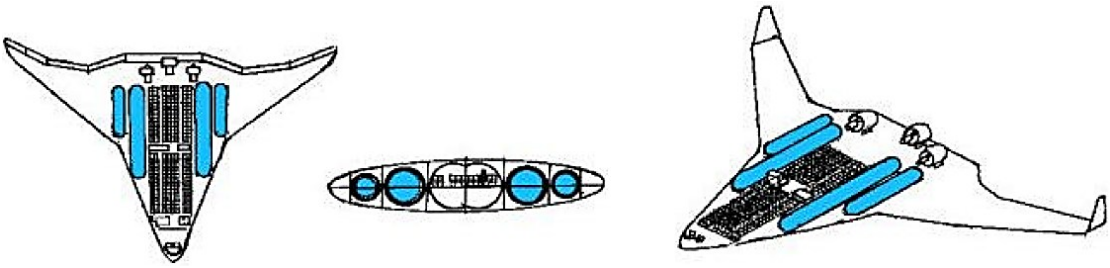

Figure 2.18 - Blended Wing Body configuration [22].

Like the BWB, the twin-boom configuration does not appear to be superior compared to the conventional tube-and-wing configuration. Moreover, its external tanks increase the interference and profile drag.

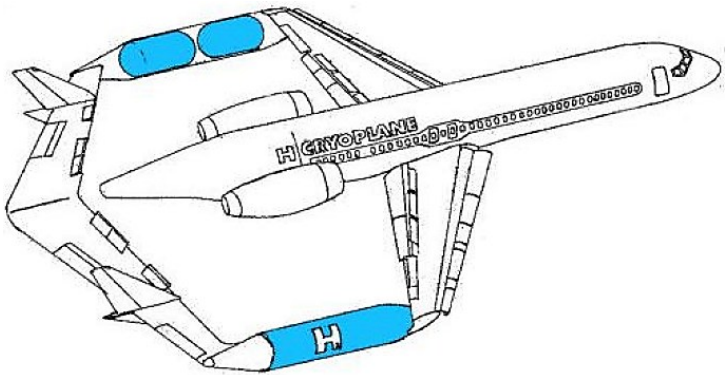

Figure 2.19 - Twin Boom configuration [22].

The piggyback tank configuration resembles historical projects such as the Buran shuttle on top of an Antonov-225 or the space shuttle on top of the modified Boeing 747. This arrangement has an intermediate safety level between the under-wing tank pod layout and the rear fuselage tank configuration. Like the under-wing pod tank, the piggyback tank [28] also has several issues that must be addressed in-depth such as:

- The aerodynamic interaction between the fuselage and the tank
- The aircraft’s lateral stability
- The disk burst trajectories for an under-wing engine-mounted aircraft
- The structural connection between the fuselage and the tank body.

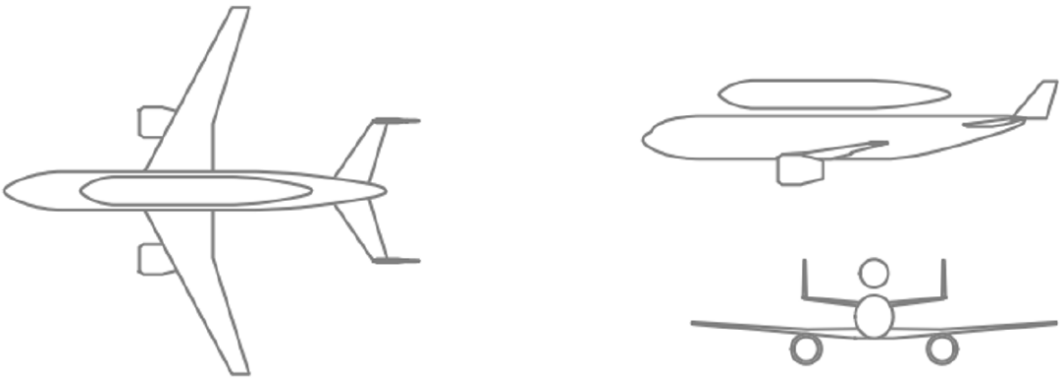

Figure 2.20 - Piggyback fuel tank configuration [28].

Druot *et al* [28] provide a summary of the qualitative features of three H_2 tank configurations (Table 2.5), pointing out their advantages (green cells) and disadvantages (yellow and red cells, where the red ones are critical points).

Table 2.5 - Qualitative pros and cons of three tank layouts [28].

		Rear fuselage tank	Under-wing pods	Piggyback tank
Design	Structural complexity	Low	Medium	High
	Aerodynamic	Low impact	High impact due to tank external wing interaction	Medium impact due to tank fuselage interaction
	Engine disc burst	No impact	Requires suitable positioning	It may require a dry bay
	Ground clearance	Max pitch on the ground	Pitch and bank angle	No impact
Operation	Safety	Good	Maximal	Good
	CG management	To be checked	Easy	Easy
	Operability	Good	Easy	Difficult
	Maintenance	Good	Easy	Difficult

2.1.5 Certification and Crashworthiness Considerations

Regarding all the new technology concepts, hydrogen properties and the desirable goals settled as a target for the aviation sector, replacing kerosene with hydrogen as a power source will surely bring some changes to the current certification. On the other hand, the strict intricacies of Certification & Crashworthiness issues will also influence the aircraft's design.

As shown in Table 2.2, LH_2 maximises volumetric energy density over its gaseous forms (compressed hydrogen at 350 bar and supercritical hydrogen at 700 bar). However, it still has a low density compared to Jet A-1, which has roughly a quarter of LH_2-specific energy. As mentioned before, although compressed hydrogen (at 350 bar) and supercritical hydrogen (at 700 bar) do not require cryogenic storage conditions, they still incur weight penalties because their pressure tank vessels would be much heavier [3]. Besides, maximising volumetric energy density means that will be needed less fuel volume to obtain a certain amount of energy. Thus, the tanks can be less bulky, with a smaller wetted and/or frontal area, which provides an additional drag reduction. This being said a CS 25 [32] certified hydrogen-powered aircraft would resort to low-pressure LH_2 as a fuel. So, from now on, this work will focus on an LH_2 aircraft concept.

Until now, in terms of safety, the only conclusion is that fuel tanks and their inherent systems should be placed as far as possible from the passenger cabin and out of the rotor disc burst impact area. However, LH_2 use as fuel surely requires more safety precautions.

LH_2 requires pressurization, ideally, its tanks must have a lower surface area-to-volume ratio and might require as well to be removed for NDT [3]. Thus, the use of a conventional wing box structure to house hydrogen fuel tanks is not a feasible option. Therefore, one of the configurations previously presented might be a potential concept solution.

Liquid hydrogen is kept at -253° C. So, a fuel tank leak leads to a cryogenic spill and thus, the rapid boiling of the fuel can condense and freeze oxygen, nitrogen, and any other trace elements in the atmosphere around. The excess of LH_2 and the solid oxygen produce an explosive mixture that can be detonated by the impact velocity of a turbine disc fragment [3]. Like the inert ullage of a kerosene fuel tank, the pressurisation of hydrogen tanks seals them from the atmosphere, preventing oxygen inflow. Then, an LH_2 fuel system could include several pressure vessels connected by pipes, pumps, heat exchangers and valves, which becomes the CS 25.981 *Fuel tank explosion prevention* [32] applicable to the pressurized fuel system, as mentioned by Spencer [3].

According to CS 25.1309 [32], LH_2 system failures causing air inflow and oxygen freezing must be very improbable. Such failures occurrence would probably be an outcome of proceeding mistakes during fuelling or post-maintenance. To prevent fuel contamination and potential failures, the hydrogen must be purged from the fuel system before its opening for repair or maintenance procedures. Afterwards, the air in the system must be also purged before hydrogen insertion in the system. Furthermore, it would be beneficial to allocate the LH_2 storage outside of UERF trajectories to remove a detonation source. However, some fuel systems components, such as pipes, pumps, or valves, cannot be placed outside of the rotor burst zone and thus will need particular care to avoid hazards to the aircraft's integrity and passenger safety. Once again it is concluded that the rotor burst requirements influence the aircraft's architecture because the hydrogen containment, pumps, pipes, and valves must be well separated from passengers.

Spencer [3], in his paper about certification considerations for the configuration of a hydrogen-powered aircraft, denotes that the certification requirements [32] for an emergency landing on land or water are similar whether a kerosene system or a hydrogen's. The equally applicable certification requirements are:

- CS 25.561 *Emergency landing conditions*
- CS 25.562 *Emergency landing dynamic conditions*
- CS 25.563 *Structural ditching provisions*
- CS 25.721 *Landing gear*
- CS 25.801 *Emergency provisions – ditching*
- CS 25.963(d) *Fuel tanks – emergency landing conditions*

- CS 25.994 *Fuel system components in a nacelle – wheels-up landing*

CS 25.963(d) must also include additional information regarding the LH_2 leak hazards near the cabin or the engines, such as its cryogenic temperature, risk of asphyxiation, and fire likelihood.

The over-arching constraint regarding crashworthiness directives is that the structure should survive a rotor disk burst, a tail scrape, or a crash landing, protecting the LH_2 fuel system and thus avoiding an ignition source. Therefore, the aircraft's airframe must be appropriately designed for tank load distribution and protection against such hazards. For example, in a wing-mounted tank aircraft, the fire likelihood and trajectory of a potentially released tank from its default position during a crash landing must be addressed in the crashworthiness requirements, considering the hazard to the aircraft and its passengers.

Besides the emergency landing regulations about the undercarriage collapse or GCOL, the certification process must also feature an emergency evacuation plan, whose feasibility depends on many situational constraints, such as the passenger safety exit obstruction. Thus, crashworthiness requirements are also expected to influence the aircraft's configuration.

Lastly, in cooperation with the airport code of practice, to ensure a quick turnaround, the LH_2-fuelled aircraft concept must facilitate ground handling procedures, such as refuelling and baggage handling.

2.1.6 Publicised Aircraft Concepts

In 1955, Silverstein and Hall [27] of the NACA-Lewis Flight Propulsion Laboratory explored liquid hydrogen's potential as fuel for subsonic and supersonic aircraft, noting its significant range improvement. This led to the so-called Project Bee which included a flight test of a modified Martin B-57 Canberra bomber (Figure 2.21) to burn hydrogen in a turbojet engine, first flown in 1956. Liquid hydrogen was stored under the left wing, with a pressurised gaseous helium tank under the right-wing tip. The hydrogen tank and plumbing system were purged using gaseous helium, avoiding oxygen contamination.

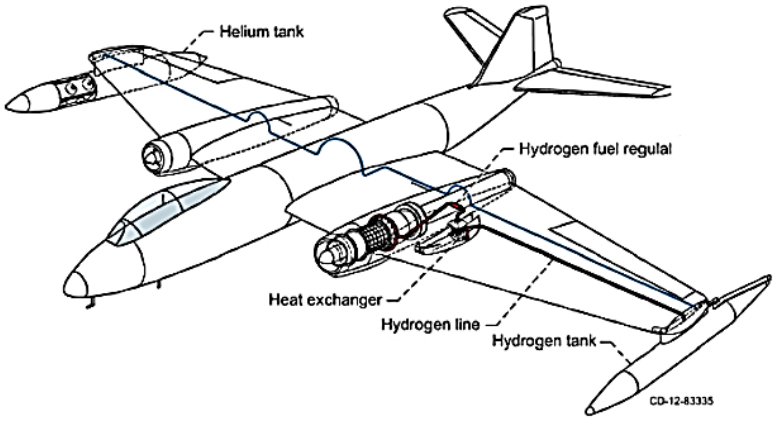

Figure 2.21 - Modified Martin B-57 Canberra bomber [12].

On the flight, the converted B-57 operated normally, climbing to the altitude and speed specified using conventional JP4 fuel in both engines. Upon reaching the cruise altitude, the flow of JP4 on the left wing to the convertible J-65 turbojet engine was reduced and recirculated back to its tank [27], while the hydrogen flow was increased to the required rate. The JP4 flow to the left engine was restored when the LH_2 supply ran out.

The NACA hydrogen flight test program demonstrated a reliable and smooth engine performance with no operational safety issues with the hydrogen fuel system.

From 1954 to 1955, Lockheed Aircraft Corporation in cooperation with Rex Division of AiResearch Corporation and Pratt & Whitney Aircraft made several conceptual design studies of hydrogen-powered aircraft. In 1956, the U.S. Air Force contracted Lockheed’s Advanced Development Projects organisation to build a reconnaissance aircraft, capable of cruising at Mach 2.5 at 30.48 km altitude [27].

The concept presented was the CL-400 aircraft, whose three-view sketch is shown in Figure 2.22. The wing tips nacelles house stabilising outriggers that assisted the aircraft’s stability on ground manoeuvres, once the nose and main gears were centreline mounted. Besides, the CL-400 had a retractable ventral fin to improve directional stability.

The hydrogen fuel tanks were segmented into three parts within the fuselage: one sump tank and two main tanks [27]. To favour the fuel transfer, the two main tank pressures were maintained at 2 psi higher than the sump tank pressure.

The engines were mounted at the wing tips and thus the LH_2 was pumped through the wing structure which would reach around 162 °C during the cruise phase. Therefore, to minimise heat transfer to the hydrogen, the fuel pipes were vacuum jacketed.

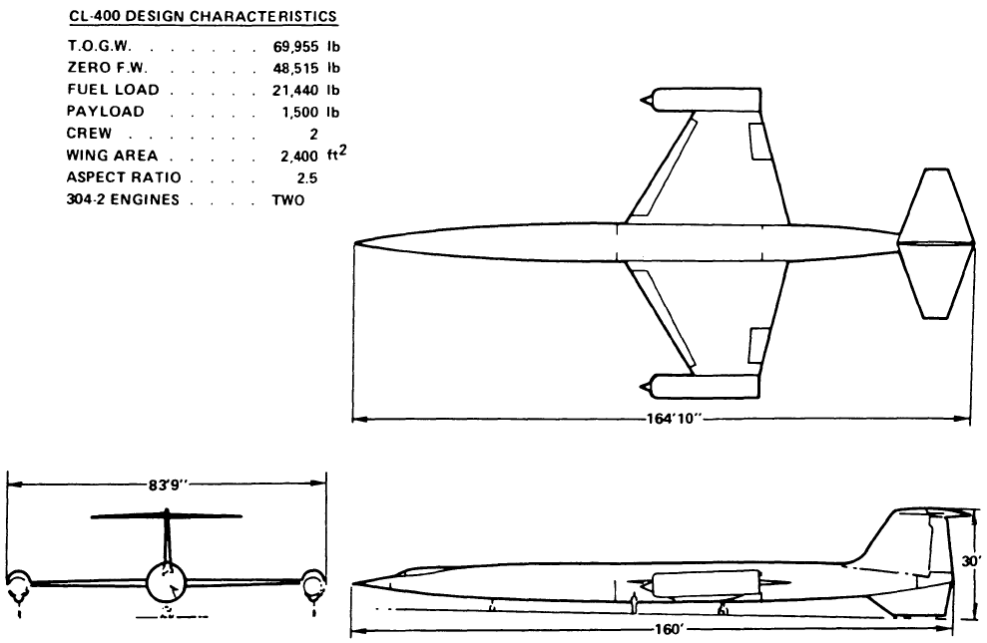

Figure 2.22 - Three-view drawing of the Lockheed CL-400 hydrogen-powered aircraft project [27].

In the late 80s, the Soviet Union presented a modified version of the Tupolev Tu-154 (Figure 2.23). It was the Tupolev Tu-155 that was used as an alternative fuel testbed such as hydrogen and liquid natural gas. The aircraft has a trijet configuration, with two conventional Kuznetsov NK-8s engines and one modified version, the experimental NK-88 engine, that could burn hydrogen or natural gas. At the time, the engineers have already opted for cryogenic storage to increase hydrogen density. The LH_2 containment was a large aft tank, reducing the aircraft's passenger capacity. Once the fuel storage was close to the turbomachinery, there were operational challenges, including boil-off due to ambient heat, despite the thermal insulation. To mitigate boil-off, it was installed a suitable venting system to maintain the fuel tank pressure near-constant. One of the venting system parts that stands out in the exterior view of the aircraft is the small fin mounted on top of the tail (Figure 2.23). Besides, the nacelle intake of the NK-88, which is mounted on the starboard side, is also different.

The project was meant to evolve into the Tu-156, but the program was diverted towards using liquid natural gas and it was scrapped before any prototype was built. Dismissed at the fall of the Soviet Union, the only existing Tu-155 is now displayed at Ramenskoye Airport, near Moscow.

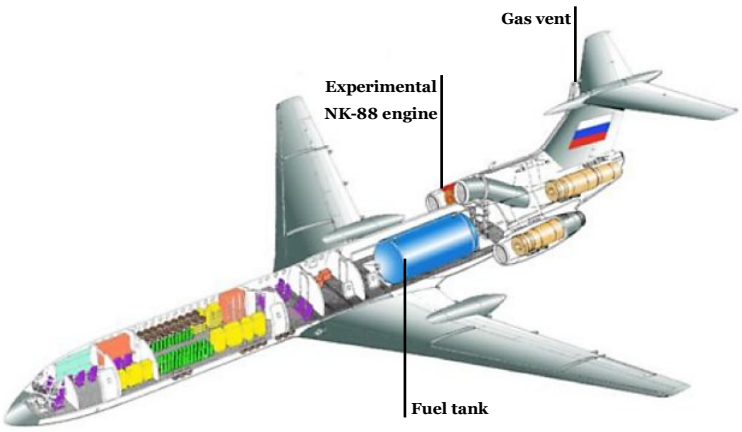

Figure 2.23 - Tupolev TU-155 [49].

Scholz [33] proposes LH_2 layouts based on the Airbus A320 concept (Figure 2.24). In new configurations nomenclature, the red capital letter *H* stands for ‘LH_2-powered aircraft’, the green *W* means that is an A321 with additional under-wing hydrogen tanks, the pink *S* indicates that is an A321 with additional stretch (more volume to store LH_2), and the blue *19* means that is A321 filled with only 156 one-class passengers, instead of 180, which provides more room left for LH_2 tanks, with the same payload and range.

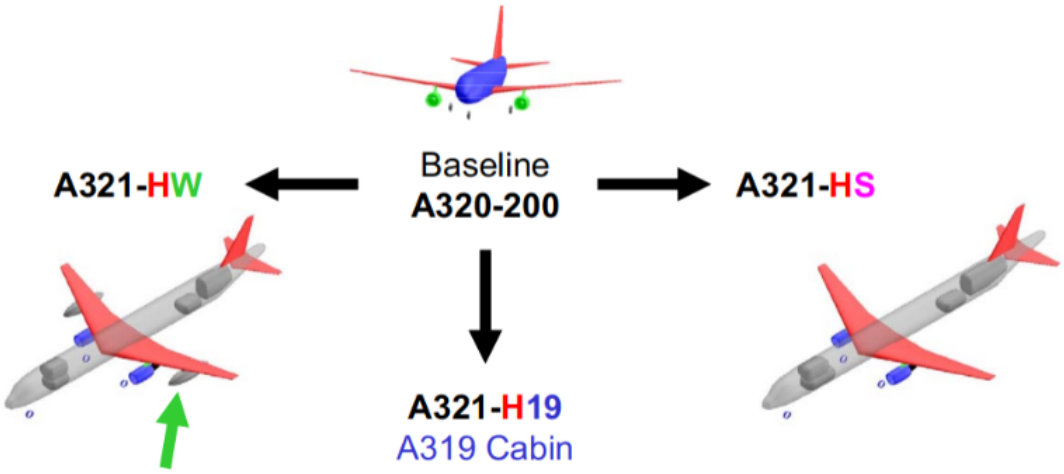

Figure 2.24 - LH_2-powered aircraft layouts proposed by Scholz [33], with forward and aft tanks.

During the Green Freighter project that ran from December 2006 until April 2010, Seeckt *et al* [34] presented some hydrogen-powered freighter aircraft concepts as shown in Figure 2.25. The design analyses demonstrated great technical advantages of the hydrogen aircraft. It indicated a 6.5% to 8.5% lower take-off mass relative to the kerosene reference aircraft. These results relate to the 63.8% to 66.4% lower fuel masses that offset the weight penalties of the hydrogen tanks. Thus, the take-off distance was shortened by 14% to 28%. As referenced before, this study also concluded that the hydrogen-powered

BWB does not show a substantial superiority compared to a conventional tube-and-wing aircraft design. However, the BWB cruise glide is 8% higher than the tube-and-wing aircraft's and, despite a 50% larger inner wing wetted area, the BWB structural mass is only 21% larger [34].

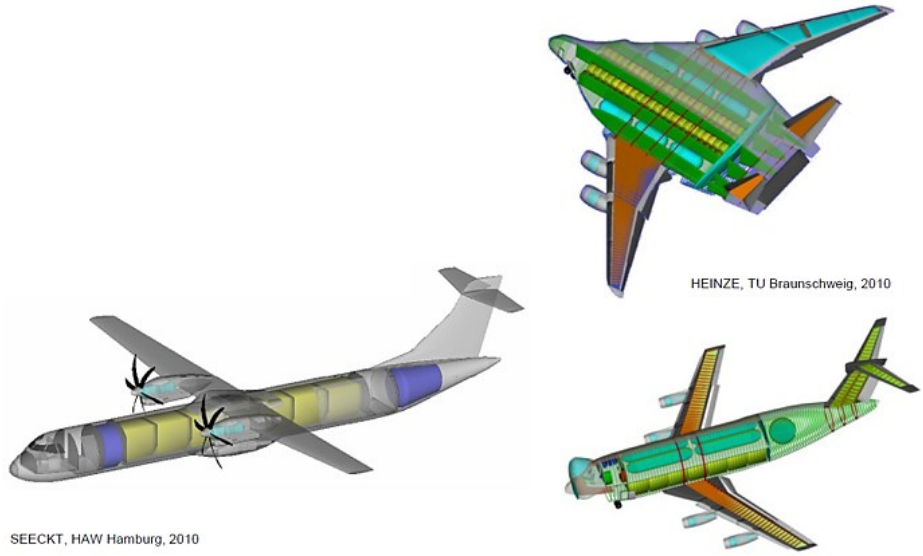

Figure 2.25 - Configurations from the "Green Freighter" Project [34].

On January 1975, Brewer *et al* [25] published a summary report about the application of hydrogen fuel to long-range subsonic aircraft, where it is also discussed the aircraft configuration, as shown in Figure 2.26. Due to their feasibility, the only layouts retained for evaluation were the twin-podded fuel tank configuration and the well-known forward and aft tank layout. The forward canard/wing aircraft configuration has also been studied as a potential solution. However, positioning the power plant and the fuel storage at the rear requires a lengthened forward cabin fuselage, which brings a high technical risk, and the canard size severely limits the CG travel and load capacity [25].

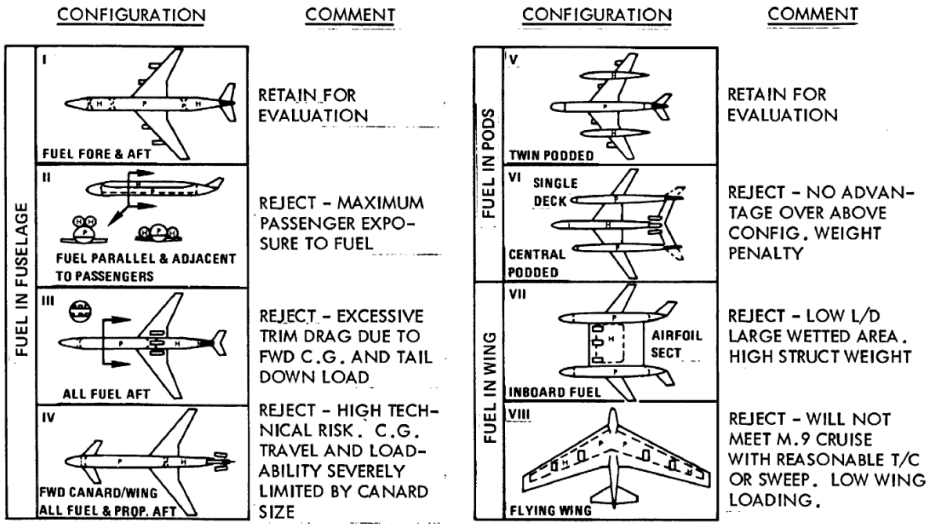

Figure 2.26 - Configurations of LH_2 passenger aircraft, proposed by Brewer *et al* [25].

Brewer *et al* [25] in that same report also present an LH_2 passenger aircraft concept where the liquid hydrogen is housed in external tanks mounted on pylons above the wings (Figure 2.27). This layout's primary goals were to evaluate the potential advantages over an internal fuel tank configuration concerning safety, maintenance, and operations. It was recognised that the accessibility of the tanks for inspection and repair would be easier. Moreover, externally mounted tanks allowed a crucial separation of the passengers from the fuel storage, minimising the hazards from cryogenic leak effects. However, Brewer *et al* [25] also note that these potential advantages may not compensate for the performance penalty associated with carrying that large external tank. Thus, comparing several key design and performance parameters between this concept and an equivalent internal tank design showed a substantial performance superiority of the internal tank approach. For smaller tank fuel pods the internal tank configuration benefits may not stand out as much.

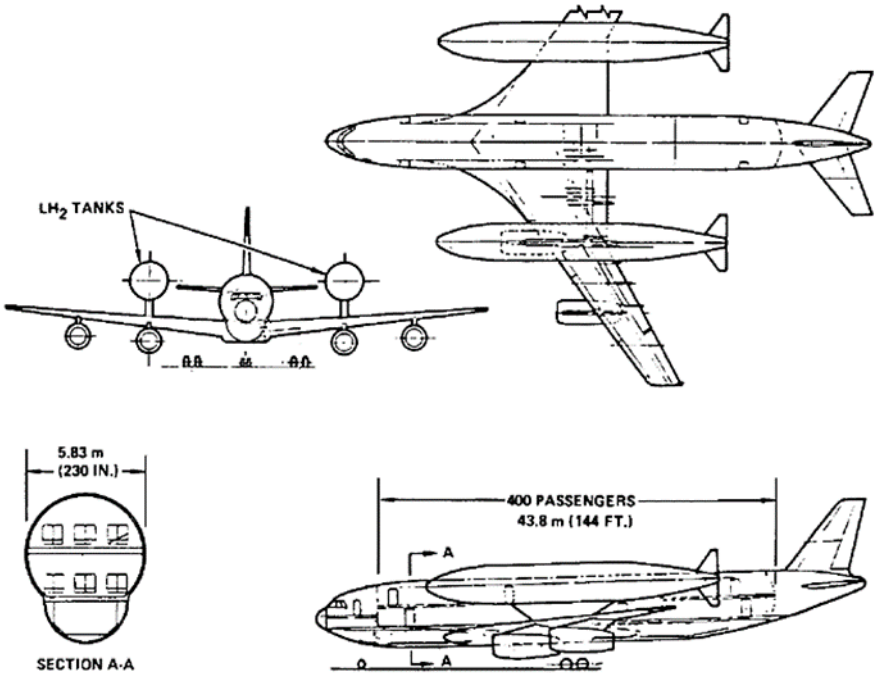

Figure 2.27 - LH_2 passenger aircraft with an external tank configuration [15].

As Nangia *et al* [4] indicate, most of the previous aircraft concepts presented have fuel tanks positioned ahead, alongside, above or behind the cabin. Except for the fuel tank pod configuration, such concepts have the fuel storage too near to passengers, and therefore, do not meet the certification requirements, such as crashworthiness criteria or emergency access of passengers. Besides, regarding CG position, there are still significant issues in preserving a safe static margin for several passenger or fuel loadings circumstances.

In summary form, the Certification and Crashworthiness (C&C) considerations, which primarily involve ensuring LH_2 containment and associated fuel equipment remain consistently separate from passengers and crew, address other related issues such as the unobstructed nature of evacuation exits, the aircraft structure’s ability to withstand events like engine disc-failure or tail scrapes, and adherence to emergency landing regulations, including scenarios like undercarriage collapse, or encountering objects on the runway.

For all the current barriers presented, the ramifications for the existing certification basis and the necessary AMC it is acceptable to affirm that a certifiable LH_2-powered aircraft will look different from a conventional aircraft concept. This work discussion will focus on an unconventional concept Nangia *et al* [26] presented that broadly corresponds to the Airbus A320 in performance and payload capacity. The unusual concept is referenced as the LH_2 Gondola airliner.

3 LH_2 Gondola Airliner

The gondola concept is a twin-fuselage aircraft. The starboard fuselage houses the fuel in two separate tanks, ahead and behind the centre-section wing box, providing an alternative arrangement for ensuring that the neutral point is always behind the CG aft limit [3]. Each tank supplies one engine to mitigate the fuel contamination hazard resulting in all-engine failure. On the other hand, the port fuselage transports the passengers and the crew and has similar access to galley servicing and passenger doors as an Airbus A320.

As shown in Figure 3.1, the two fuselages are of different lengths, and this overall asymmetry allows an opportunity to apply other design ideas, such as wing twists and new platform designs. The starboard tank fuselage has a similar diameter to the passenger fuselage but is shorter. This allows fuel tanks with a lower surface area-to-volume ratio to be used, reducing heat leaks. To prevent heat entrance to the LH_2, the tanks have a thick layer of heat insulation including a double wall structure. This structural composition also permits sealing and pressurising the fuel tanks, preventing the ingress of unwanted substances such as oxygen that would freeze solid at cryogenic temperature and create an explosive mixture. The starboard fuselage design allows it to be detachable and thus the fuel tanks can be replaced (their structural life may be low) with pre-fuelled tanks on the landing apron, speeding up the turnaround. The refuelling operation can be executed at a specialised facility away from the apron thus reducing the risk of cryogenic spillage. The fin and tailplane are mounted on the passenger fuselage to simplify this ground operation.

Figure 3.1 - LH_2 Gondola Airliner [4].

The passenger fuselage is longer, providing a better space for passenger accommodation and, beyond that, positioning the cockpit ahead of the fuel tank fuselage gives the pilots a good all-around view, especially sideways (the starboard outer wing monitoring can be done using a remote camera). The passenger can access the aircraft’s interior by stairs or the loading bridge on the port side and the baggage loading is done on the starboard side of the passenger fuselage. Therefore, a special baggage loading ramp may be required once the baggage bay access is slightly constrained by operating between the two fuselages. However, this loading plan prevents passenger exposition to potential hazards during fuel-related ground operations, such as the detachable fuel tanks exchange for the pre-fuelled tank on the landing apron.

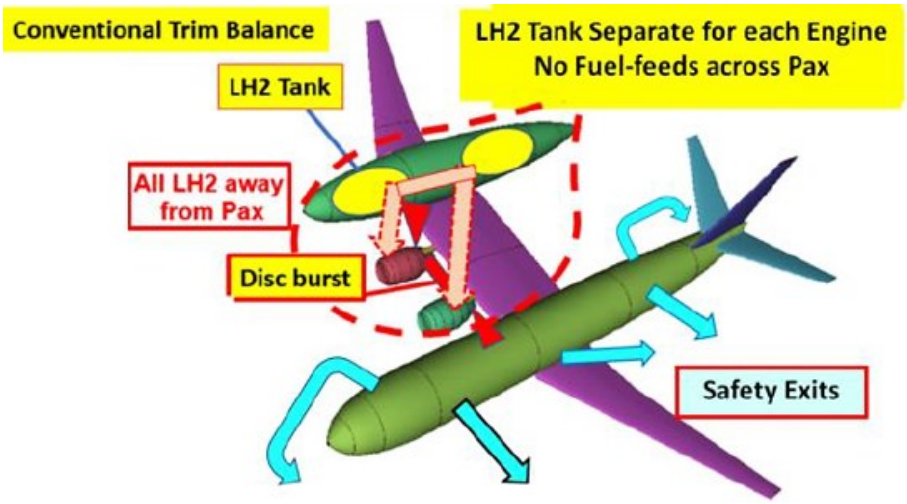

Figure 3.2 - Twin-fuselage "Gondola" concept using LH_2, by Nangia *et al* [4].

Two engines, with an assumed propulsive efficiency of 35% [4], are mounted in the central section of the wing connecting the two fuselages. Moreover, the total wingspan is about 50m which meets better the ICAO Type D loading bay regulation (span limit of 52m). The folding wing tips technology can also be applied to fit in the smaller airport C-type bays (<36m) and Nangia *et al* [4] note that such features provide a good cruise L/D comparable with an equivalent single fuselage aircraft. In any case, the fuel system components are well separated from the passenger accommodation, overcoming one of the problems of the previous configuration. Furthermore, this arrangement avoids positioning the (majority) of the fuel system in the UERF trajectories, fulfilling the requirements of the CS25.903(d) [32], and the part of the fuel tank fuselage above the wing box does not house fuel as it lies in the debris zone from a virtual engine turbine disc burst.

This positive aspect and the LH_2 tank installation within the gondola allows the wing structure and the starboard fuselage to act as secondary barriers under crash conditions. Besides, the incorporation of a crushable structure (CS25.965 [32]), e.g. on the nose cap of the tank fuselage, will also aid in the LH_2 tank protection in an accident scenario (CS25.561 [32]), absorption of bird strikes, and a heater mat for de-icing on the ground or in the air. However, the asymmetric concept introduces beneficial features if the crashworthiness precautions fail. Any deflagration after a tank rupture would be far enough from the passengers' cabin, allowing a reasonable margin of distance to execute the emergency egress safely. The two over-wing exits, and the four-door exits can be used as emergency exits, during the emergency evacuation execution. The emergency egress (CS25.803 [32]), especially from the starboard fuselage exits, must consider the cryogenic temperature and asphyxiation hazards, besides the fire likelihood. Spencer [3] denotes that this layout also favours the compliance of LFL avoidance measures (e.g., ventilation) and the application of ignition prevention settled in CS25.981(a) [32]. The Gondola design also offers the possibility for deflagration instead of detonation of accumulated hydrogen, reducing potential damage and higher hazards. Moreover, the dry wing structure gives space for design innovation, such as the fire-retardant material application in its interior, restraining the fire towards the passenger fuselage.

The landing gear configuration consists of a main landing gear, mounted in the passenger fuselage and gondola, which will retract sideways into the fuselages, and a nose wheel placed behind the cockpit on the inner side of the main fuselage, which will retract sideways into the belly [35]. The landing gear needs a track of about 9 to 10m, depending on the separation of the fuselages. Thus, a wider track may be more suitable as it would be for larger aircraft.

Spencer [3] also alerts that the landing gear system would demand guidance through an AMC for CS25.495 *Turning*, CS25.499 *Nose-wheel yaw and steering*, and CS25.503 *Pivoting* [32]. Regarding ground handling, the LH_2 tanks and the fuel system’s entirety should be assured by cautiously applying tyre and wheel failure models (AMC 25.734).

In a conventional tube-and-wing aircraft, a pitching motion does not produce a rolling or yawing motion due to the symmetry along the fuselage [3]. However, considering side elevation, a conventional aircraft is not symmetrical, and a yawing motion induces a rolling motion (the opposite also occurs). In this flight situation, a small pitching motion is induced and thus the lateral stability is more elaborated than longitudinal stability. Regarding the unconventional concept presented in Figure 3.2, longitudinal stability becomes a complex issue because there is no symmetry plane. Therefore, this asymmetry in shape causes cross-coupling between longitudinal and lateral motions, which requires

a fly-by-wire solution to integrate the lateral and longitudinal responses [4]. For instance, a pitch command will combine rudder, tailplane and aileron deflections to produce the proper motion [35]. The design of the main fuselage empennage needs to be size-optimized, and so the control parameters, to offset the shape asymmetry and engine failure case. The trim ailerons will help to balance the aircraft during the flight as the fuel is consumed. As Spencer [3] alerts, guidance through an AMC for CS25.143 *Control & Manoeuvrability* will be required, although there is no CS-25 [32] demand for an aircraft to be laterally symmetric. It is worth noting that the gondola configuration would also require an analysis of ditching qualities (CS25.563 and CS25.801 [32]).

3.1 Twin-fuselage Analysis: Weight and Bending Moments

Torenbeek [36] demonstrated that a twin-fuselage aircraft provides a beneficial structural effect of span-distributed load to reduce wing bending. Lockheed’s concept presented in Figure 3.3, highlights this advantage by carrying its payload in two fuselages at equal distances outboard from the symmetry plane. The SDL permits a substantially lower wing structural weight for a given span, as shown in Figure 3.4, deriving a larger optimum aspect ratio in contrast to a conventional layout. Although a tri-body aircraft with two outboard fuselages and one central is feasible, it is not likely to offer outstanding advantages that make it a strong candidate for civil aircraft design [36]. Lockheed’s multibody aircraft study supports that statement [37] because they found approximately 10% and 30% drag increases for two-body and three-body aircraft fuselages, respectively, relative to the single-body reference aircraft. So, a two-body concept may be more feasible.

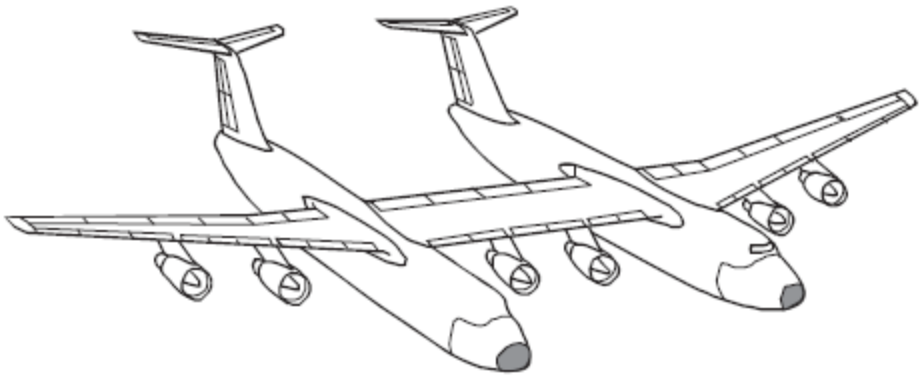

Figure 3.3 - Lockheed twin-fuselage configuration of a very large cargo aircraft [37].

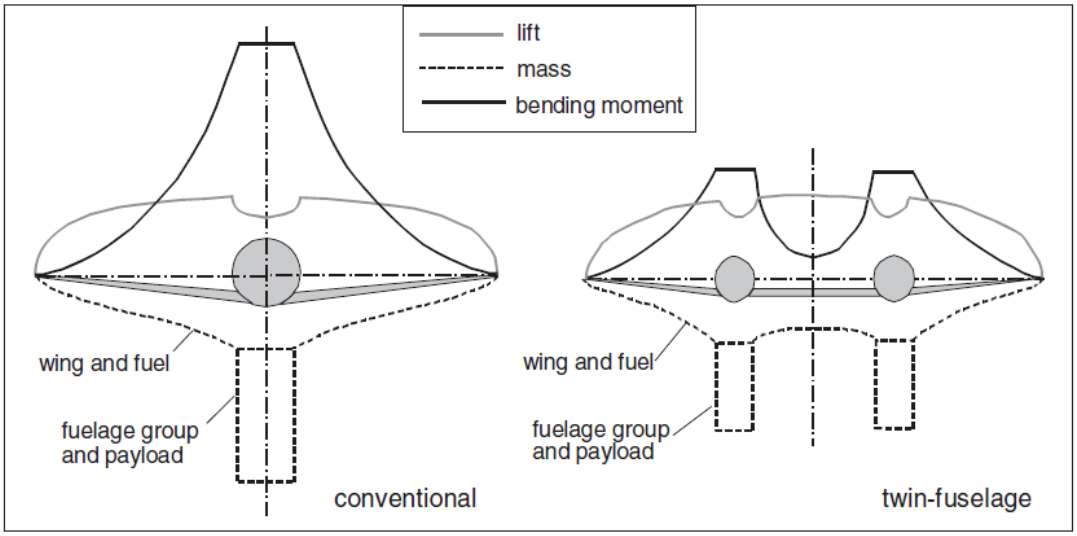

Figure 3.4 - Lift, mass and bending moment distribution along the span of a conventional airliner and an equivalent twin-fuselage aircraft [37].

By comparing the lift, mass and bending moment distribution along the span between a twin-body aircraft and a conventional one with the same range/payload faculties in Figure 3.4, it is verifiable that both configurations have a similar lift distribution along the span (neglecting the local lift losses due to the fuselage(s) presence). However, that similarity does not apply to the mass distribution, which is quite different. Thus, the bending moment distribution is also substantially different. As Torenbeek [36] refers, although both aircraft's wings resist the maximum bending moment where the wing is attached to the fuselage(s), the maximum bending moment is at least 50% lower on the twin-body aircraft. In addition, the bending moment caused by the lift is null in the plane of symmetry when the components are suspended in the centre of pressure of each semi-span so, the bending load between the fuselages tends to decrease quickly towards the plane of symmetry. Therefore, the central wing is mainly dominated by torsion loads.

Considering that the area under the bending moment distribution diagram usually consists of an indicator of the material required to support the bending loads, a substantial weight reduction can be expected for a given span. This also means the central wing has a lower weight per unit span than the carry-through structure and conventional inboard wing.

This comparison between a TBA and the equivalent airliner justifies the empty weight reductions introduced by the novel layout.

3.2 Longitudinal weight distribution overview

The main goal of the current section is to briefly compare the weight penalties introduced to a conventional A320 by adding a fuselage (the 'gondola' concept) and the LH_2 tanks (and the fuel itself) for an equivalent mission. Then that weight penalty is graphically illustrated by the longitudinal weight distribution of both aircraft. Therefore, the A320 weight and balance manual provides most components' weight and longitudinal distance from a fixed referential (the later designated *H-arm*).

For the calculations made in this subchapter, the referential adopted from the A320 weight and balance manual [6], is shown in Figure 3.5.

The reference trihedral is defined by the following planes:

- Horizontal plane (*xoy*) placed 7 m below the fuselage datum line;
- Vertical plane (xoz) being the aircraft's longitudinal plane of symmetry;
- Forward plane *H-arm=0* (*yoz*) located 2.54 m forward of the aircraft nose section.

Using the referential above, every distance from a determined point at the plane *xoz* to the forward plane (*yoz*) is named *H-arm*.

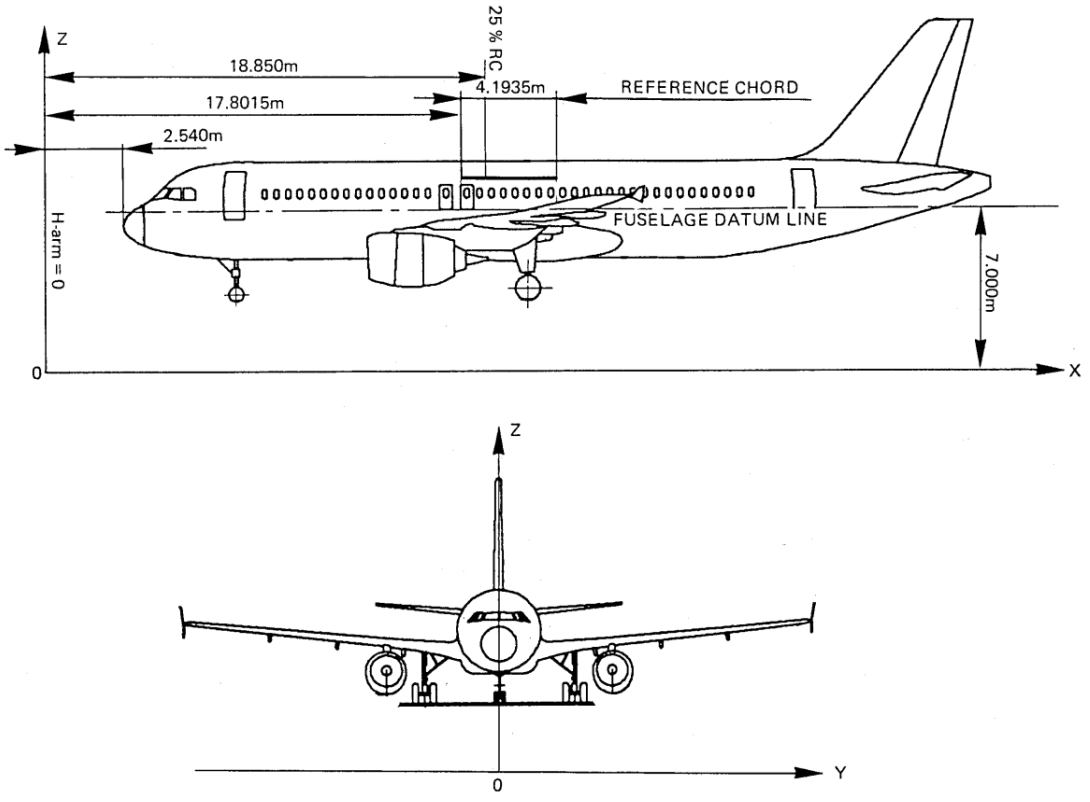

Figure 3.5 – A320 reference axis [6].

The general procedure consisted of collecting the component mass and the *H-arm* of its centre of mass from the referred weight and balance manual [6]. Then, using those values, calculate the moment around the *y-axis*, relative to the *H-arm* origin (2.54 m ahead of the aircraft nose, where *H-arm=0 m*). The moment, in (Nm) is given by:

$$M = W \cdot H\text{-}arm = m \cdot g \cdot H\text{-}arm \qquad (4)$$

Where the weight (W) is in [N], the mass (m) is in [kg], the gravitational acceleration $g \cong 9.807\ m/s^2$ and the moment arm (*H-arm*) is in [m].

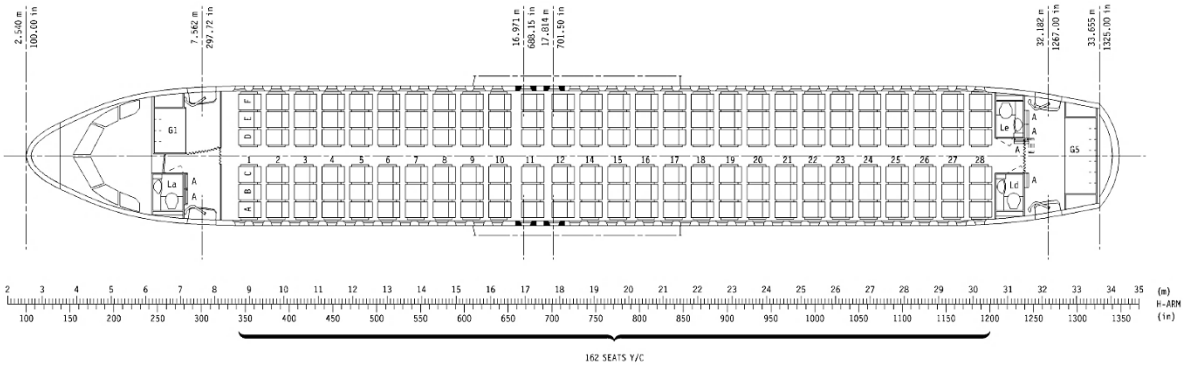

Figure 3.6 - Generic plant of the cabin arrangement [6].

For example, the cockpit and cabin crew results are shown in the tables below, considering the attendants' weight of about 70 kg each.

Table 3.1 - cabin crew location, mass and consequent moment.

Number of seats	Cabin Crew Location	*H-Arm* [m]	Mass [kg]	Moment [Nm]
2	Rear wall of toilet L_a	7.327	140	10063
1	Side wall of toilet L_e	31.678	70	21753
2	Rear wall of toilet L_e	31.852	140	43746
1	Rear wall of toilet L_d	31.926	70	21924
Total			420	97485

Table 3.2 - cockpit crew location, mass and consequent moment.

Number of seats	Cockpit Crew Location	*H-Arm* [m]	Mass [kg]	Moment [Nm]
1	Captain	5.085	70	3492
1	First officer	5.085	70	3492
1	Third occupant (rear of the pedestal)	5.722	70	3929
1	Fourth occupant (left rear flight compartment)	5.867	70	4029
Total			280	14942

The tables for the general structural groups (fuselage, wings, landing gear, engines, vertical and horizontal tails) followed the same methodology. For example, the next tables exemplify the vertical and horizontal tails procedures, illustrated by their schematic drawings [6] in Figure 3.7.

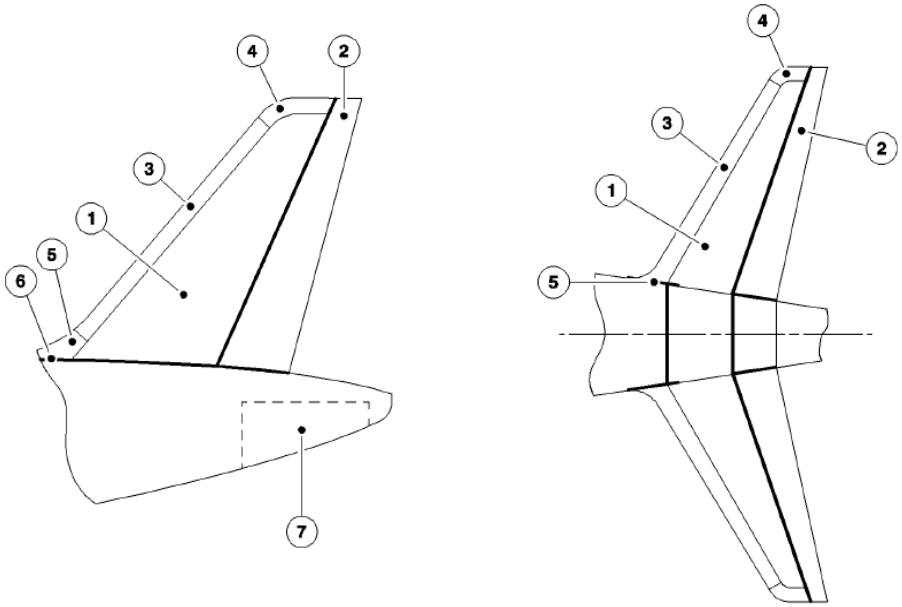

Figure 3.7 - Schematic drawings of the vertical (left) and horizontal (right) tails [6].

Table 3.3 - Vertical tail components' location, mass and moment

Ref nº	Component	*H-Arm* [m]	Mass [kg]	Moment [Nm]
1	Box	36.0	364.6	128773
2	Rudder	37.7	88.4	32695
3	Removable Leading Edge	35.3	47.5	16464
4	Tip	37.9	8.6	3198
5	Dorsal Fin	33.1	25.5	8272
6	Fuselage Fairings	35.2	15.4	5314
7	Airborne Auxiliary Power	38.2	136	50905
Total			686	245621

Table 3.4 - Horizontal tail components' location, mass and moment

Ref nº	Component	*H-Arm* [m]	Mass [kg]	Moment [Nm]
1	Box	36.5	417.5	149631
2	Elevator	38.0	96.6	36039
3	Removable Leading Edge	36.3	84.2	30017
4	Tip	38.5	6.3	2378
5	Fuselage Fairing	37.3	7.3	2668
Total			1224	220733

Beyond these tables above, there are also similar tables for passengers, flight compartment stowage (briefcase, document and baggage stowage), cabin hatracks, galleys, toilets, cargo holds, wings, fuselage, landing gear, propulsion group (pylons, pods, engines), and many others (usable fuel, unusable fuel, hydraulic fluid, potable water, waste tank, and so on).

Using all the tables of structure, power plant, systems, furnishings and equipment items that are integral parts of the aircraft configuration, including fluids in closed systems, we can obtain the MEW by summing all the respective mass values. Repeating the same operation to the moment, a total moment is obtained. Then dividing the total moment by the total weight results in the *H-arm* of the MEW. The formula is:

$$H\text{-}arm = \frac{\Sigma M}{g \cdot \Sigma m} \quad (5)$$

Table 3.5 – MEW value, moment and *H-arm*.

$\sum m$ – Total Mass or MEW [kg]	$\sum M$ - Total Moment [Nm]	*H-arm* [m]	%RC
38254	7053367	18.8	23.7

An *H-arm* dimension can be converted into percentage of the reference chord through:

$$\%RC = \frac{H\text{-}arm - 17.8015}{0.041935} \quad (6)$$

Applying the previous formula to the *H-arm* of the MEW, we conclude that the centre of mass is around 23.7% of the reference chord (represented in Figure 3.5). According to the A320 weight and balance manual [6], the weight of the operator's items should also be addressed. These items include the following:

- Unusable fuel;
- Oil for engines, IDG and APU;
- Water for galleys and toilets;
- Chemical fluid for toilets;
- Tables and baby bassinets;
- Galley structure and fixed equipment;
- Catering;
- Pallets and baggage containers;
- Crew and their baggage;
- Aircraft documents and tool kits;
- Passenger seats and passenger life jackets;

- Emergency equipment (including evacuation aids, portable O_2 bottles and boxes, extinguishers, megaphones, flashlights, axes, first aid kits, emergency radio beacons, asbestos gloves and smoke goggles, demonstration kits, and life jackets for crew and children).

The operator's items list, provided in the cited manual, was adopted for a given mission, as shown in the next table.

Table 3.6 – Operator's items list, mass, moment and H-arm.

Operator's Items	Mass [kg]	Moment [Nm]	*H-Arm* [m]
Potable Water	200	30501	15.5
Waste tank pre-charge	10	3144	32.1
Documents and tool kits	12	839	7.1
Galley structure and fixed equipment	530	125979	24.2
Catering and removable equipment	834	192422	23.5
Flight crew	560	104469	19.0
Unusable fuel	77	13785	18.3
Oil for engines and APU	75	12249	16.6
Emergency equipment	285	57818	20.7
Passengers' seats and life jackets	2527	486675	19.63
Total	5110	1027881	20.5

In the table above, the last cell of the *H-arm* collum is determined using Equation 5, where the total mass and the total moment are the values shown in the last line of the table (*5110 kg* and *1027881 Nm*, respectively). Thus $H\text{-}arm = 20.5\,m$ is H-arm of the operator's items group.

$$OEW = MEW + OIW \quad (7)$$

Equation 7 gives the Operational Empty Weight as a sum of the Manufacturer's Empty Weight and the Operator's Items Weight. Thus, using the data from the previous tables (total mass and total moment) and applying Equation 5, the *H-arm* of the OEW can be calculated and presented in the next table.

Table 3.7 – OEW value, moment and *H-arm*.

OEW	Mass [kg]	Moment [Nm]	*H-Arm* [m]	%RC
	43364	8081248	19.00	28.51

The %RC of the OEW is quite close to the value shown in the weighing report included in the A320 weight and balance manual [6], which indicates $\%RC = 28.60$. Thus, the values calculated are valid.

It is also important to consider the payload requirements regarding baggage, cargo, and passenger transport. The following table values result from adding the total mass and total moment values of tables similar to Table 3.1, but for cargo, baggage, and passengers. Equation 5 is used to obtain the H-arm of the payload.

Table 3.8 - Payload mass, moment and H-arm.

Payload (Cargo, Baggage, Passengers)	Mass [kg]	Moment [Nm]	*H-Arm* [m]
	14286	2753874	19.65

The Equation 8, gives the Zero Fuel Weight as a sum of Operational Empty Weight and the Payload Weight:

$$ZFW = OEW + PW \quad (8)$$

Thus, using the data of the previous tables (total mass and total moment of OEW and Payload) and applying Equation 5, the *H-arm* of the ZFW can be calculated and presented in the next table.

Table 3.9 - ZFW value, moment and *H-arm*

ZFW	Mass [kg]	Moment [Nm]	*H-Arm* [m]
	57650	10835122	19.16

The ZFW obtained seems plausible, once the A320 weight and balance manual indicates *61000 kg* as the Maximum Design Zero Fuel Weight (MZFW). For the Take-Off Weight, the Zero Fuel Weight (ZFW) and the Fuel Weight (FW) must be summed:

$$TOW = ZFW + FW \quad (9)$$

Using the data of Table 3.9 (total mass and total moment of ZFW) and values of tables for the fuel tanks (central tank, inner right cell, outer right cell, inner left cell and outer left cell) similar to Table 3.1, the total mass (or TOW) and the total moment can be determined. Then, applying Equation 5, the *H-arm* of the TOW can be calculated and presented in the next table.

Table 3.10 - TOW value, moment and H-arm.

	Mass [kg]	Moment [Nm]	*H-Arm* [m]	%RC
TOW	76737.8	14253431	18.93	27.0

The first remark about the previous table is that the TOW is below the Maximum Design Take-Off Weight (MTOW), fixed at *77000 kg* in the weight and balance manual [6]. Equation 6 can be applied to convert the *H-arm* of the TOW into the percentage of the reference chord, also indicated in the table above. The TOW's *H-arm* (or the %RC) is the longitudinal location of the aircraft's centre of mass. The value obtained, $\%RC = 27.0$, meets the CG limits for an A320 operating around the MTOW (%RC between *26.0* and *39.5*), as shown in the A320 CG envelope (Appendix 1), validating the result obtained.

Once the A320 weighing and balance values are according to its weight and balance manual [6], the mass of the aircraft's components and its location can be utilised to calculate the longitudinal weight distribution.

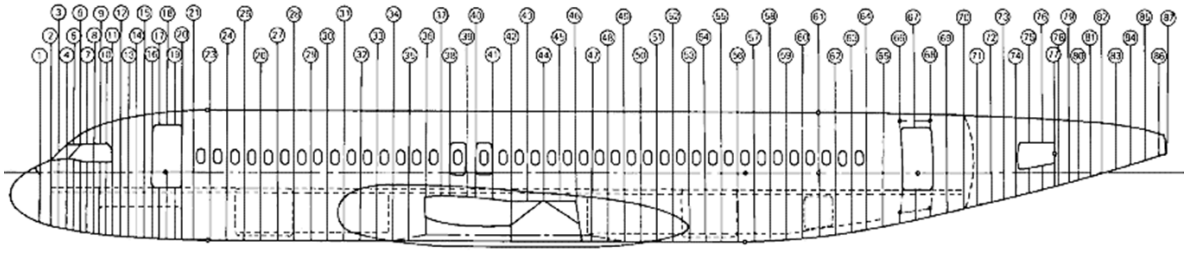

Figure 3.8 - Fuselage segmentation used in A320 weighing and balance [6].

The A320 length was discretised into *0.2 m* intervals using the fuselage segmentation principle above. Then, each component length along the *x-axis* was also discretised into *0.2 m* intervals and their mass was divided by the number of intervals resulting from the component segmentation. The next table gives the thrust reverser example, indicating where the component is located (from *15.93 m* to *17.13 m*), its division in *0.2 m* intervals {15.93; 16.13; 16.33; 16.53; 16.73; 16.93; 17.13}, and the total mass distributions by those locations.

Table 3.11 - Thrust reverser segmentation

Thrust Reverser			
From [m]	To [m]	delta [m]	Total Mass [kg]
15.93	17.13	0.20	1036
x [m]	Mass repartition [kg]		
15.93	148.0		
16.13	148.0		
16.33	148.0		
16.53	148.0		
16.73	148.0		
16.93	148.0		
17.13	148.0		
Total	1036		

Table 3.12 - Rear (bulk) cargo hold segmentation.

Rear (Bulk) Cargo Hold			
From [m]	To [m]	delta [m]	Total Mass [kg]
27.8	30.2	0.20	1497
x [m]	Mass repartition [kg]		
27.8	115.2		
28.0	115.2		
28.2	115.2		
28.4	115.2		
28.6	115.2		
28.8	115.2		
29.0	115.2		
29.2	115.2		
29.4	115.2		
29.6	115.2		
29.8	115.2		
30.0	115.2		
30.2	115.2		
Total	1497.0		

The methodology for the fuel was slightly different. Each wing has an inner fuel cell and an outer fuel cell, and between the right and left inner cells, there is a central tank. With the wing station diagram (Figure 3.9), the geometry of the fuel tanks was replicated using straight segments connecting the vertices, since the coordinates of which are known (Table 3.13).

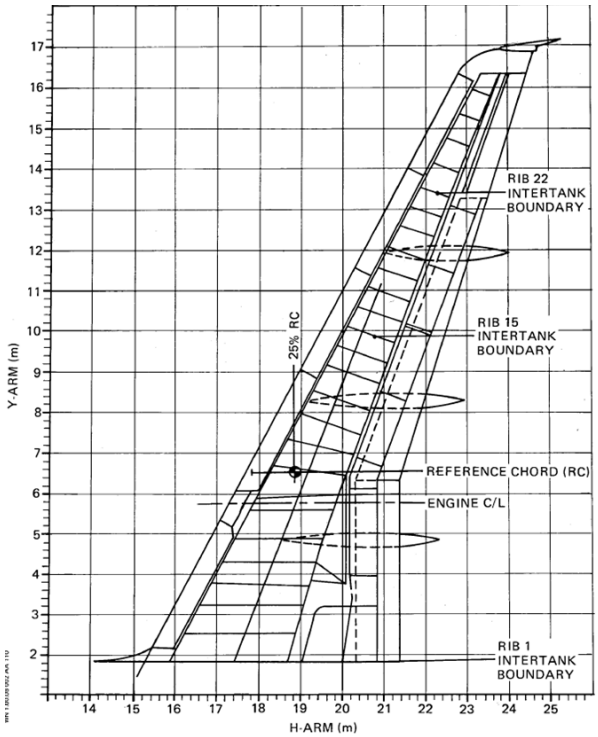

Figure 3.9 - Wing station diagram for the wing [6].

Table 3.13 - Coordinates of the fuel tank vertices.

	H-arm	Y-arm
Inner cell	15.8	1.8
	18.6	1.8
	20.0	9.8
	21.4	9.8
Outer cell	20.0	9.8
	21.4	9.8
	21.8	13.4
	22.4	13.4
Central tank	15.8	1.8
	18.6	1.8
	15.8	-1.8
	18.6	-1.8

The inner cell geometry (Figure 3.10) was replicated using straight segments connecting the vertices coordinates shown in the first four rows of the previous table.

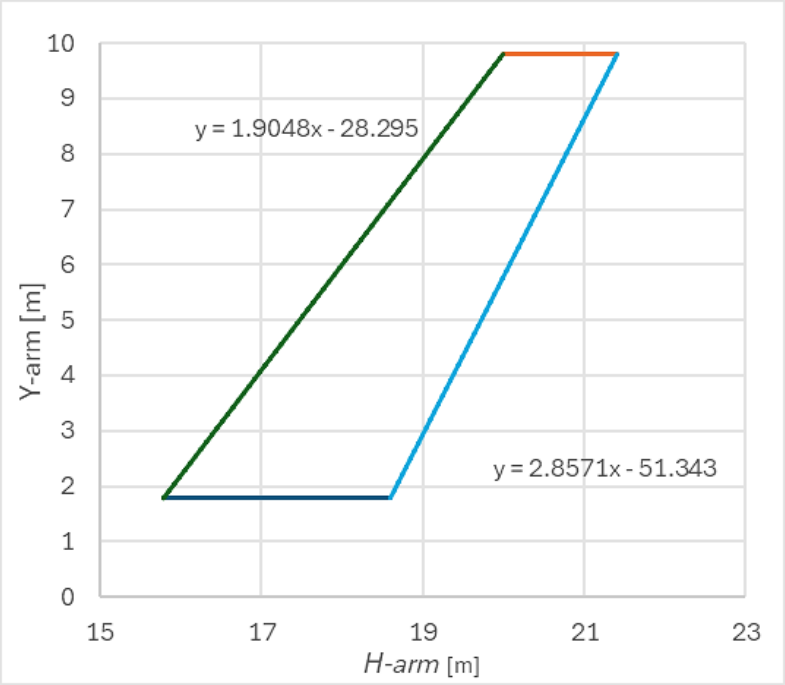

Figure 3.10 - Inner cell geometry.

Then, as done for the other components, the *H-arm* was discretised in *0.2 m* intervals. From leftmost vertex, (*H-arm, Y-arm*) = (15.8, 1.8), to rightmost vertex, (*H-arm, Y-arm*) = (21.4, 9.8), the Y-arm was determined. For the green line points, if $H\text{-}arm \leq 20.0$ then $Y\text{-}arm = 1.9048 \cdot H\text{-}arm - 28.295$, else $Y\text{-}arm = 9.8$ (orange line). For the light blue line points, if $H\text{-}arm \geq 18.6$ then $Y\text{-}arm = 2.8571 \cdot H\text{-}arm - 51.343$, else $Y\text{-}arm = 1.8$ (dark blue line). Then, the goal was to compute the area inside the polygon in each *0.2 m* interval. The area below the green and dark blue lines was approximated to a rectangle area, where the width is equal to the discretization step (*0.2 m*) and the height is the mean value of the previous point *Y-arm* and the next point *Y-arm*. To exemplify, let us consider the first interval, where the first point has the coordinates (*H-arm, Y-arm*) = (15.8, 1.8) and the second point (over the green line) has the coordinates (*H-arm, Y-arm*) = (16.0, 2.2). The second point's first coordinate results from adding the discretization step to the first point's first coordinate. The second point's *Y-arm* coordinate results from applying the equation $Y\text{-}arm = 1.9048 \cdot H\text{-}arm - 28.295$. The area inside the polygon for that interval, is given approximately by multiplying the discretization step (*0.2 m*) by the mean value of the *Y-arm* (that is *2*) and subtracting the rectangle area below the dark blue line, which is given by multiplying the discretization step (*0.2 m*) by the first point's *Y-arm* (*1.8 m*). Seen this example, with $H\text{-}arm \in [15.8,21.4]$ and considering the discretization step $h = 0.2\,m$, the area (A_n), in [m^2], inside of the polygon limited between $a = 15.8+(n-1)\cdot h$ and $b = 15.8 + n\cdot h$ is given by

$$A_n = \begin{cases} \left(\frac{f(a)+f(b)}{2} - 1.8\right) \cdot h & if\ 15.8 \leq H\text{-}arm \leq 18.6 \\ \left(\frac{f(a)+f(b)}{2} - \frac{g(a)+g(b)}{2}\right) \cdot h & if\ 18.6 < H\text{-}arm \leq 20.0 \\ \left(9.8 - \frac{g(a)+g(b)}{2}\right) \cdot h & if\ 20.0 < H\text{-}arm \leq 21.4 \end{cases} \quad (10)$$

Where $f(x) = 1.9048 \cdot x - 28.295$, $g(x) = 2.8571 \cdot x - 51.343$, i.e., the equations of the green and dark blue lines, and n is the interval number which the area is being calculated given by $(21.4 - 15.8)/h = 28$.

The tank projected area is calculated with the inner cell vertices coordinates (Table 3.13), resulting in *16.8 m²*. The A320 manual [6] indicates that the inner cell capacity is about *6925 l*, which is *6.925 m³*. Dividing this value by tank projected area, we obtain a mean tank depth of *0.41 m*. For each interval *n*, if we multiply the area A_n by mean tank depth and correct the units (using the factor *1000*), the capacity of that discretised section is known. Then using the fuel density of *0.8 kg/l*, indicated in the A320 manual [6], we determined the mass of that same section that can be doubled due to the aircraft symmetry (the inner right cell is similar to the inner left cell). This methodology explains the Table 3.14 build-up.

Similarly, two more tables were elaborated, one regarding the central tank longitudinal weight distribution and the other addressing the outer cells (on the right and left side of the aircraft).

The total capacity obtained in Table 3.14 is *6927.68 l*, about *0.04%* higher than the inner cell capacity indicated in the A320 manual [6], fixed at *6925 l*. Once this difference has a minute magnitude, the methodology adopted for the fuel tank segmentation seems reliable and accurate.

Table 3.14 -Inner cell segmentation.

Delta [m]						
0.2	Green and orange line	Blue lines			Mass [kg]	
H-arm [m]	Y_1 [m]	Y_2 [m]	Area [m²]	Capacity [l]	Single wing	Both wings
15.8	1.8	1.8	0.00	0.00	0.0	0.0
16.0	2.2	1.8	0.04	15.74	12.6	25.2
16.2	2.6	1.8	0.11	47.18	37.7	75.5
16.4	2.9	1.8	0.19	78.59	62.9	125.7
16.6	3.3	1.8	0.27	109.99	88.0	176.0
16.8	3.7	1.8	0.34	141.40	113.1	226.2
17.0	4.1	1.8	0.42	172.81	138.2	276.5
17.2	4.5	1.8	0.50	204.21	163.4	326.7
17.4	4.8	1.8	0.57	235.62	188.5	377.0
17.6	5.2	1.8	0.65	267.02	213.6	427.2
17.8	5.6	1.8	0.72	298.43	238.7	477.5
18.0	6.0	1.8	0.80	329.84	263.9	527.7
18.2	6.4	1.8	0.88	361.24	289.0	578.0
18.4	6.8	1.8	0.95	392.65	314.1	628.2
18.6	7.1	1.8	1.03	424.06	339.2	678.5
18.8	7.5	2.4	1.05	431.95	345.6	691.1
19.0	7.9	2.9	1.01	416.29	333.0	666.1
19.2	8.3	3.5	0.97	400.58	320.5	640.9
19.4	8.7	4.1	0.93	384.88	307.9	615.8
19.6	9.0	4.7	0.90	369.18	295.3	590.7
19.8	9.4	5.2	0.86	353.48	282.8	565.6
20.0	9.8	5.8	0.82	337.74	270.2	540.4
20.2	9.8	6.4	0.74	306.29	245.0	490.1
20.4	9.8	6.9	0.63	259.18	207.3	414.7
20.6	9.8	7.5	0.51	212.07	169.7	339.3
20.8	9.8	8.1	0.40	164.97	132.0	263.9
21.0	9.8	8.7	0.29	117.86	94.3	188.6
21.2	9.8	9.2	0.17	70.75	56.6	113.2
21.4	9.8	9.8	0.06	23.64	18.9	37.8
21.6	9.8	9.8	0.00	0.04	0.0	0.1
			Total	6927.68	5542.1	11084.3

Like the previous tables, many others were utilised for the components' length and mass segmentation. Having completed those tables, everything was compiled in a final table where the components' mass segmentation was summed for each x location (for each *H-arm*, *0.2 m* apart from the previous and the next *H-arm*, starting in the main fuselage nose section, *H-arm = 2.54 m*). Thus, we have a mass distribution [kg/m] value for each interval, which led to the A320 longitudinal weight distribution (Figure 3.11).

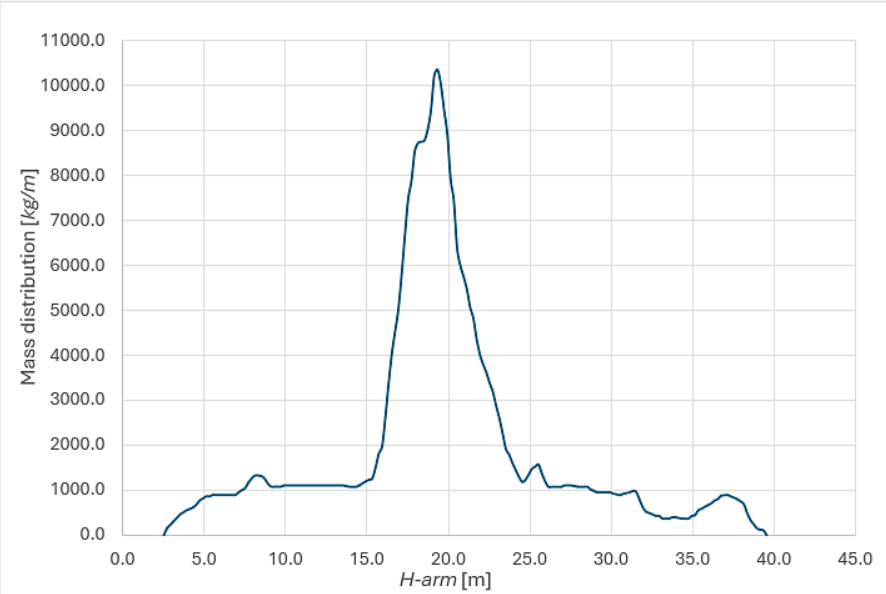

Figure 3.11 - A320 longitudinal weight distribution.

By multiplying the mass distribution value [kg/m] in a determined x position by the interval length (*0.2 m*), the mass of that segment is obtained. Applying this to the mass distribution values calculated, the total mass of the aircraft is around *73 tonnes*, which is plausible, given that the MTOW is *77 tonnes*. The difference between the aircraft mass obtained with this method and the mass calculated in the aircraft weighing and balance process (*76.74 tonnes*) is explained by the fact that some operators' items do not have their x location indicated in the A320 weight and balance manual [6], i.e., it is unknown where they start and where they finish along the *x-axis*. Instead, they only have the *H-arm* indicated concerning their centre of mass. However, the longitudinal mass distribution graph reliability is endorsed by Liu [38] who, based on established FE models of A320 and using the program *HyperMesh*, measured the longitudinal mass distribution section by section, resulting in mass per unit length quite similar to Figure 3.11. As expected, 'the mass per unit length of aircraft nose and tail is small, while the mass per unit length of the medial fuselage was relatively large since the fuselage, wing, engine, landing gear and fuel are concentrated' [38].

Having completed the A320 longitudinal weight distribution, we move forward into the gondola's one. Once the detailed weight analysis is not the main goal of this work, the gondola longitudinal weight distribution is mightily based on the A320. This means that every component's weight and location were availed from the previous calculations, except the new components added to the conventional aircraft (the central wing and the gondola fuselage that houses the LH_2). Thus, for the gondola aircraft weight distribution, it is necessary to estimate the central wing, gondola, tanks and LH_2 weights for an equivalent mission of A320.

Ajaj [39] presents a conceptual wing-box weight estimation model for transport aircraft, the quasi-analytical WWES model. This model is a linearised thin-walled structural analysis code based on linear beam theory. As the WWES model belongs to the family of quasi-analytical methods it combines some advantages of high-fidelity and low-fidelity methods.

Figure 3.12 shows the validation of the model, where the A320 wing-box actual weight is around *6300 kg,* and the model estimation has a *1.5%* error. Considering that the A320 wing area is about *122.6 m²*, an aluminium skin (*2800kg/m³*) with *3.5 mm* of thickness would weigh around *2402.96 kg* for both wings. Therefore, summing the wing-box actual weight and the skin weight, the total wings weight is about *8702.96 kg*. This value is quite close to the one indicated as a reference by Yiyuan [40], about *8750 kg*, during a twin-fuselage weight estimation study. The slight difference might be explained by the wing leading-edge area neglected in the skin weight calculation.

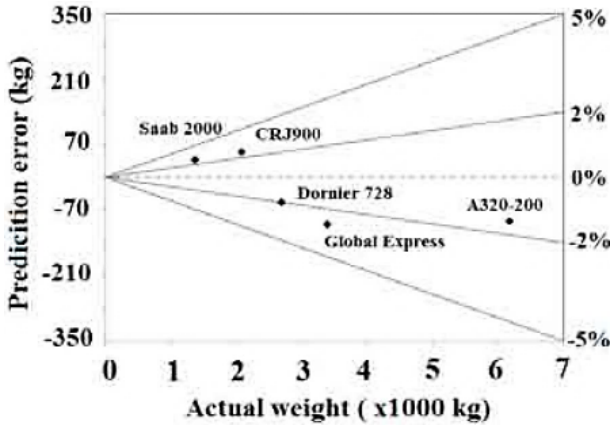

Figure 3.12 - Model validation using different transport aircraft [39].

The A320 wing root chord is around *6.0 m*. This value was maintained for the central wing, which has a constant chord value. Regarding the safety issues addressed in the Gondola Airliner concept explanation, the central wing-mounted engines are as far from both fuselages as in the conventional layout (around *3.8 m*), and that distance between them was also ensured. Thus, the central wing must have a minimum span of 11.4 m. The

central wing area is then *68.4 m²*. The area ratio between the A320 and the novel configuration is *0.56*. Multiplying this factor with the A320 wing-box actual weight and the skin weight previously obtained, the total weight of the central wing is approximately *4855.49 kg*. It could be roughly said that the gondola aircraft has a third wing.

The gravimetric efficiency figure can be utilised to calculate the LH_2 tank weight. However, to proceed that way it is also necessary to find or impose the amount of fuel needed for the mission.

To see the LH_2 aircraft comparison against conventional aircraft regarding efficiency parameters, Nangia *et al* [41] consider an A320 with a *150* passengers capacity over a *2950 nm* range (*5463 km*), MTOW of *78 tonnes*, *L/D* of about 18, cruise velocity and altitude at *Mach 0.78* at 35,000 ft, respectively, and specific fuel consumption (SFC) of *0.584 h⁻¹*. It was assumed that $L/D = 18$ for both aircrafts (the twin-fuselage airliner and the conventional A320). The amount of LH_2 to be stored inside the fuel tanks is estimated using Breguet's Range equation [42]:

$$R = \frac{a \cdot M}{g \cdot TSFC} \cdot \frac{L}{D} \cdot ln\left(\frac{W_{inicial}}{W_{final}}\right) \quad (11)$$

For a given flight condition, it is known that

$$V = a \cdot M \quad (12)$$

The A320 cruise velocity is around *840 km/h* [6].The specific fuel consumption in h^{-1} is given by

$$SFC = g \cdot TSFC \quad (13)$$

The initial weight is assumed to be the Maximum Take-Off Weight ($W_{inicial} = MTOW$) and the final weight is determined by

$$W_{final} = W_{initial} - WFB \quad (14)$$

Where WFB is the Weight of Block Fuel, i.e., is the amount of fuel needed for a given flight mission. Thus, Breguet's Range Equation can be rewritten as it follows

$$R = \frac{V}{SFC} \cdot \frac{L}{D} \cdot ln\left(\frac{MTOW}{MTOW - WFB}\right) \quad (15)$$

In this case, the WFB does not consider the weight fuel reserves (WFR), as the next equation shows WFB and WFR being different portions of TOW [43]:

$$TOW = OEW + PW + WFB + WFR \quad (16)$$

This equation gives the MTOW at the design point [43]. Therefore, after Equation 15 determines the WFB value, we should add WFR to determine the necessary amount of LH_2. The WFR is near *4.5%* of MTOW, but it may reduce to 3.5% MTOW for new generations [44]. Thus, the total fuel weight is given by

$$FW = WFB + 0.045 \cdot MTOW \quad (17)$$

To proceed with the LH_2 estimation it is also necessary to have an estimated value for the gondola airliner MTOW. Nangia *et al* [41] presented a plot that portrays the relationship between the aircraft's MTOW and the range (Figure 3.13). For the determined range (*2950 nm*) the LH_2 twin-airliner has an MTOW around 15% higher than the conventional configuration. Thus, for the WFB calculations it was adopted the $MTOW = 1.15 \cdot 78 = 89.7$ *tonnes*.

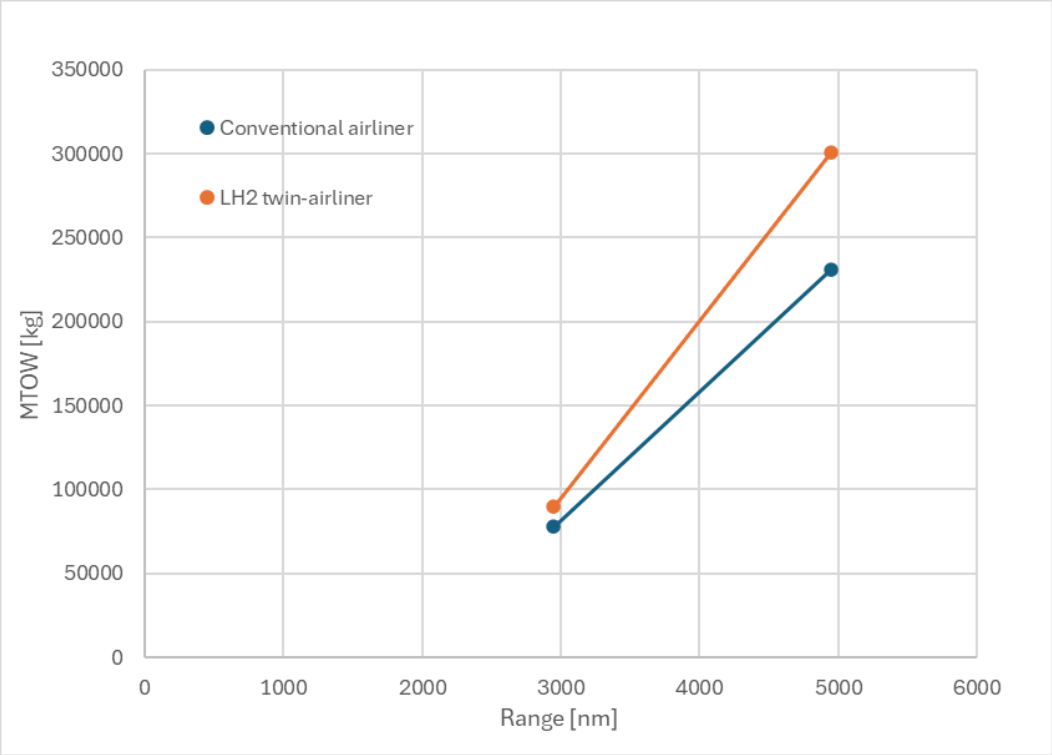

Figure 3.13 - MTOW [kg] variation with the range [nm] for the two types of aircraft, adapted from [41].

Having all the necessary parameters for Breguet's Range equation, the WFB can be found. Thus, solving Equation 15 for the Weight Fuel Block we obtain $WFB = 17.06$ *tonnes*. Adding the Weight Fuel reserve, the total fuel weight needed is *21.1 tonnes*. However, this fuel weight corresponds to a kerosene-powered twin-airliner. Then, using the specific energy of this fuel (Table 2.2) the energy needed is calculated. Doing the reverse calculation, i.e., given the energy and using the LH_2 specific energy we conclude that the estimated LH_2 weight is $FW_{LH_2} = 7.6$ *tonnes*. Using LH_2 density (Table 2.2), this

value amounts to a volume of around *107 m³*. However, instead of doing these conversions and approximations by calculating the values for a kerosene-powered twin-airliner and then adjusting them for the equivalent hydrogen-powered twin-airliner, we can use the typical SFC with hydrogen in Breguet’s Range equation. During the final technical report of Cryoplane [22], it is stated that the SFC, with liquid hydrogen turbofan engines, is about one-third of the SFC using kerosene. Therefore, using $SFC = 0.195\ h^{-1}$, and solving Equations 34 and 35, the estimated LH_2 weight is $FW_{LH_2} = 10$ *tonnes*, which corresponds to *140 m³*.

In fact, Nangia *et al* [41] also point out that the A320-twin requires *130 m³* to *140 m³* of LH_2. For the calculation, the upper limit was adopted, i.e., *140 m³* of LH_2. The LH_2 density is 71 kg/m³, so the fuel mass is *9940 kg*. In sub-chapter 2.1.4, the LH_2 tanks' gravimetric efficiency ranges from 90% to 30% in the worst-case scenario. Using a *50%* efficiency, the tank weighs as much as the LH_2 (Equation 5), i.e., *9940 kg*.

Following the tank layout proposed by Nangia *et al* [4] in Figure 3.14, the fuel is housed in two separated tanks, which introduce a redundancy to the power supply system and provides an easiest structural connection of the central wing, gondola fuselage and right wing, once the gap separating the tanks permits the wing main spar and other structural elements passing through the gondola. Thus, the initial *140 m³* is divided into two tanks of *70 m³* each. From the sections regarding the LH_2 storage, was settled that a spherical tank minimises the boil-off rate. As the gondola fuselage has the same diameter as the main fuselage, *3.95 m*, the tank width must be as close as possible to that value. However, maintenance activities must be considered thus leaving some space margin between the tank walls and the gondola shell structure. The fuel tanks' diameter was then settled at *3.5 m*. Given the tanks' volume and diameter, their length can be determined in view of the later longitudinal segmentation. The tanks' length is *7.3 m*.

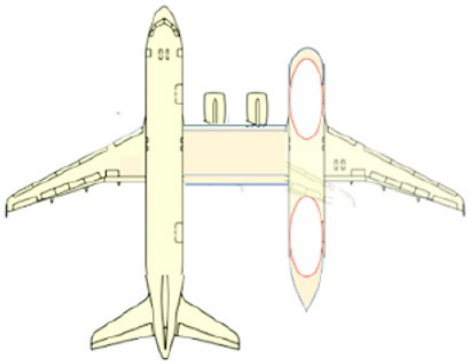

Figure 3.14 - Top view drawing of the gondola airliner [4].

By the values presented (fuel capacity and tank dimensions), there is no reason the gondola to be as long as the main fuselage. Therefore, the gondola fuselage length is about *75%* of the main fuselage length, i.e., around *28 m*. To match the middle region of the gondola with the central wing right root, the gondola nose section is placed at *H-arm* = 5.8 *m*. The forward tank is at *H-arm* = 8.3 *m* and the aft tank is at *H-arm* = 23.6 *m*. The methodology for the tanks' longitudinal segmentation follows the same line of thought as applied to the A320 longitudinal weight distribution: dividing the components' length into *0.2m* intervals and dividing the total weight by the number of intervals. The forward and aft tanks have the same total weight but different locations along the *x-axis*, as shown in Table 3.15. The wing segmentation executed for the A320 fuel storage is removed from the gondola weight distribution, since the fuel is now housed in a separate fuselage, instead of being located inside the wing-box structure.

For the gondola fuselage weight estimation, Torenbeek's method will be applied, once Schmidt *et al* [45] during a semi-analytical weight estimation work conducted a comparison of the estimated weight using their method and the methods from open literature versus the actual fuselage weight. For the A320, the Torenbeek method has around zero per cent error (Figure 3.15).

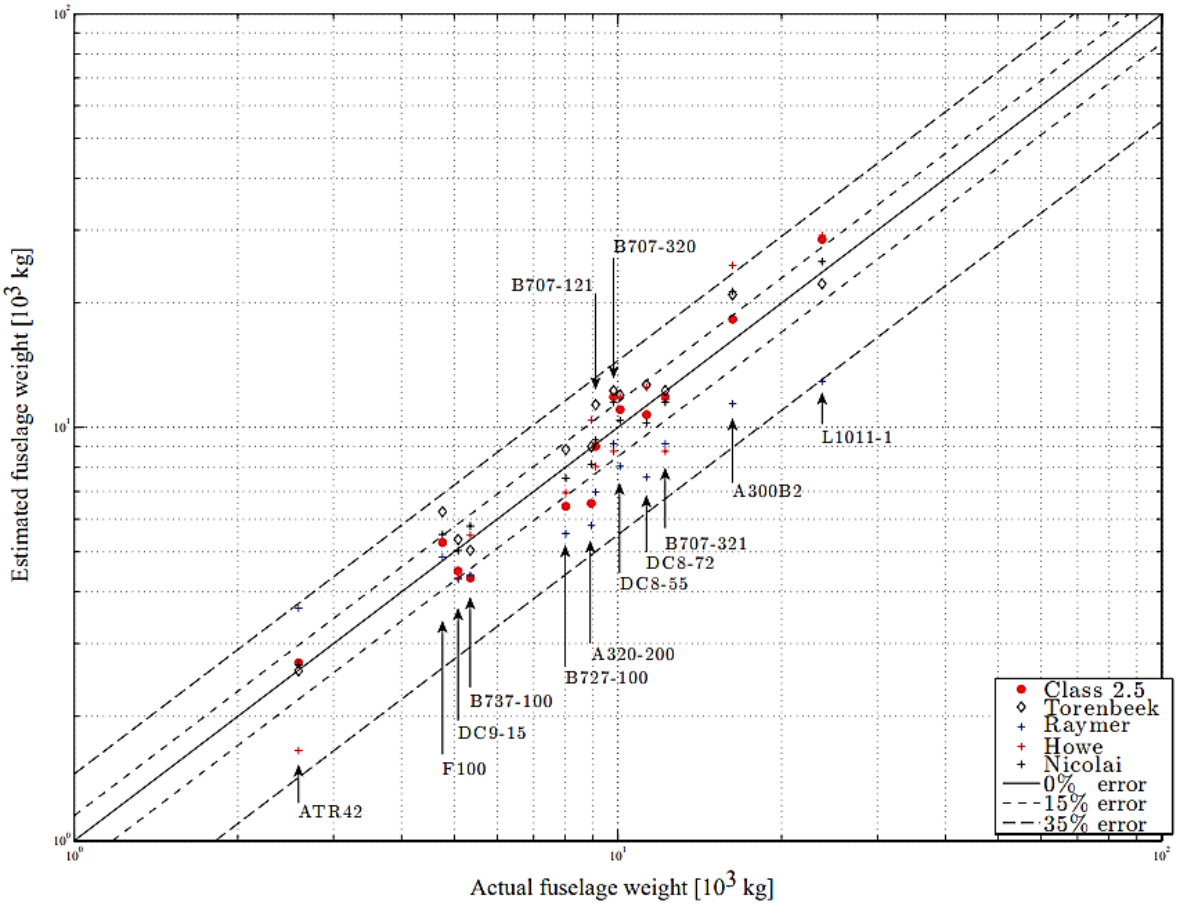

Figure 3.15 - The estimated weight of the fuselage using the described method by Schmidt and methods from open literature [45].

Table 3.15 - LH_2 tanks segmentation

Forward tank and LH_2		Aft tank and LH_2	
From [m]	To [m]	From [m]	To [m]
8.3	15.6	23.6	30.9
x [m]	Mass repartition [kg]	x [m]	Mass repartition [kg]
8.3	268.6	23.6	268.6
8.5	268.6	23.8	268.6
8.7	268.6	24.0	268.6
8.9	268.6	24.2	268.6
9.1	268.6	24.4	268.6
9.3	268.6	24.6	268.6
9.5	268.6	24.8	268.6
9.7	268.6	25.0	268.6
9.9	268.6	25.2	268.6
10.1	268.6	25.4	268.6
10.4	268.6	25.6	268.6
10.6	268.6	25.8	268.6
10.8	268.6	26.0	268.6
11.0	268.6	26.2	268.6
11.2	268.6	26.4	268.6
11.4	268.6	26.6	268.6
11.6	268.6	26.8	268.6
11.8	268.6	27.0	268.6
12.0	268.6	27.2	268.6
12.2	268.6	27.4	268.6
12.4	268.6	27.6	268.6
12.6	268.6	27.9	268.6
12.8	268.6	28.1	268.6
13.0	268.6	28.3	268.6
13.2	268.6	28.5	268.6
13.4	268.6	28.7	268.6
13.6	268.6	28.9	268.6
13.8	268.6	29.1	268.6
14.0	268.6	29.3	268.6
14.2	268.6	29.5	268.6
14.4	268.6	29.7	268.6
14.6	268.6	29.9	268.6
14.8	268.6	30.1	268.6
15.0	268.6	30.3	268.6
15.2	268.6	30.5	268.6
15.4	268.6	30.7	268.6
15.6	268.6	30.9	268.6
Total	9940.0	Total	9940.0

Before applying Torenbeek's method to the gondola fuselage, it will be tested in the main fuselage (the A320 fuselage).

The fuselage has a large contribution to the structural weight of the aircraft due to its dimension and the massive number of local weight penalties caused by cutouts, floors, bulkheads, doors, windows, attachment and support structures, as well as other special structural features. These typical fuselage weight penalties included in Torenbeek's method were shown as simple relationships between weight, size and position. Torenbeek [46] states that the fuselage weight is mostly affected by the gross shell area (S_G), defined as the area of the entire outer surface of the fuselage. All the local excrescences like wheel well fairings, canopies and blisters are removed and faired over and the holes for windows, doors, cutouts, etc. are assumed to be also faired over. The result fuselage from this simplification process seems like the top fuselage of Figure 3.16.

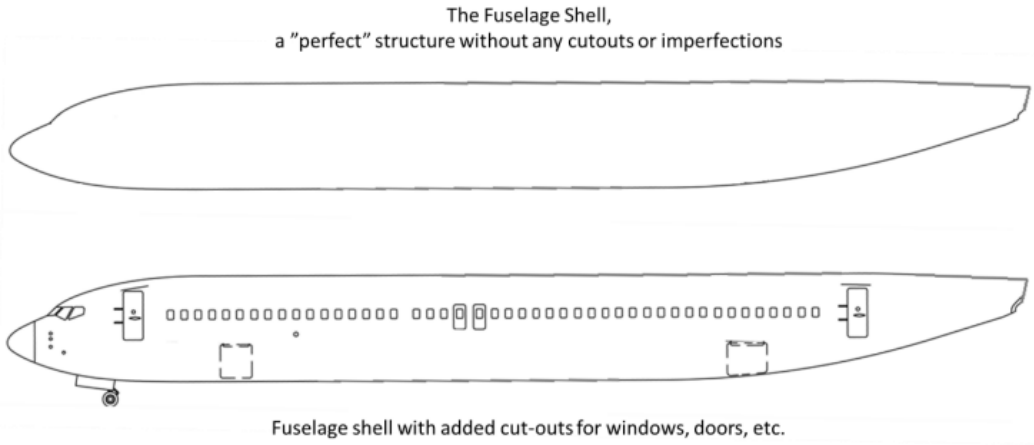

Figure 3.16 - The perfect fuselage structure referred to in the fuselage gross shell weight (top) and a fuselage with cut-outs for windows, doors, etc (bottom) [50].

Equation 18 gives the basic fuselage weight considering the geometry simplifications described above. This simple weight estimation method for Al-alloy fuselages is modified and updated for modern types [46].

$$W_f = k_{wf} \cdot {S_G}^{1.2} \cdot \sqrt{V_D \frac{l_t}{b_f + h_f}} \quad (18)$$

The constant of proportionality is $k_{wf} = 0.23$ with W_f in [kg], V_D in [m/s] and S_G in [m²]. According to Torenbeek [46], to the basic weight given by the previous equation, 8% should be added for pressurisation cabins, 4% for rear fuselage-mounted engines, 7% in case of the main landing gear is attached to the fuselage. Therefore, for our case study, the value of the basic fuselage weight obtained with Equation 11 must be multiplied by *1.08* considering the cabin pressurisation.

Table 3.16 - Basic main fuselage (A320's fuselage) weight calculation.

Constant of proportionality	k_{wf}	0.23
Design dive speed	V_D [m/s]	180
Distance between quarter-chord points of wing root and horizontal tail root	l_t [m]	16.59
Maximum width of fuselage	b_f [m]	3.95
Maximum depth of fuselage	h_f [m]	3.95
Gross shell area	S_G [m²]	421.33
Basic fuselage weight (including 8% penalty due to cabin pressurization)	W_f [kg]	6814.57

The A320 fuselage was drawn following the aircraft's blueprints, whilst the gondola fuselage was sketched regarding its dimension adaptations mentioned before. Thus, the gross shell area from the table above was collected from the CAD software *Catia V5*. However, in case the aircraft's 3D representation is not possible, Torenbeek [46] provides a simple method for the gross shell area calculation of revolution bodies. Once the main and gondola fuselages have near-cylindrical mid-sections they can be considered bodies of revolution. Thus, their gross shell area can be approximately given by Equation 19, if $\lambda_f \geq 4.5$.

$$S_G = \pi \cdot D_f \cdot l_f \cdot \left(1 - \frac{2}{\lambda_f}\right)^{2/3} \cdot \left(1 + \frac{1}{\lambda_f{}^2}\right) \quad (19)$$

Where the fuselage fineness ratio is obtained by Equation 20.

$$\lambda_f = \frac{l_f}{D_f} \quad (20)$$

Table 3.17 - Gross shell area estimation.

Fuselage length	l_f [m]	37.57
Fuselage diameter	D_f [m]	3.95
Fuselage fineness ratio	λ_f	9.51
Gross shell area	S_G [m²]	402.73

Table 3.17 presents the gross shell area result, which is about 4.4% lower than the value obtained with the CAD tool. As the Torenbeek's method is an estimation, the *Catia V5* for S_G was adopted for the basic fuselage weight determination (Table 3.16).

Having the basic fuselage weight, the weight penalties neglected at the beginning can now be addressed. The weight of doors, windows, hatches and enclosures, W_{sct}, is considered by the addition of the actual weight of these items including any operating mechanism (in Table 3.18 is the column named 'Fillings'), and the surround structure weight, i.e., frames, door landing, etc., (in Table 3.18 is the column named 'Surrounds') [46].

Table 3.18 - Weight penalties due to fuselage shell cutouts [46].

		Pressurised	
Weight contribution		Fillings	Surrounds
Passenger and crew doors		$44.2bh\sqrt{\Delta p}$	Front, aft: $22.3\sqrt{A_{ap}}$ Above wing: $29.8\sqrt{A_{ap}}$
Cargo hold doors (belly)		$48.8bh\sqrt{\Delta p}$	Front: $35.7\sqrt{A_{ap}}$ Rear: $50.6\sqrt{A_{ap}}$
Escape hatches		$32.2bh\sqrt{\Delta p}$	$26.8\sqrt{A_{ap}}$
Cockpit window glazing		$4.31 \cdot A_{ws} \cdot \Delta p^{0.25} \cdot \sqrt{b_f V_D}$	$2.8\sqrt{A_{ap}}$
Canopies	Sliding	$41.3 \cdot {A_{ws}}^{0.8} \cdot \Delta p^{0.25}$	$12.5\sqrt{A_{ap}}$
	Hinged	$(41.3 \cdot {A_{ws}}^{0.8} - 17.6) \cdot \Delta p^{0.25}$	
	Fixed	----------	
Windows and ports		$23.9 \cdot A_{ap} \cdot \sqrt{b_f}$	$9.97\sqrt{A_{ap}}$
Equipment bay/access doors, landing gear doors		$22bh$	
Speed brakes		Transport A/C: 10 to 15 kg/m² Jet trainers: 25 to 35 kg/m²	

According to the open literature reference [46], in Table 3.18, the maximum operational pressure differential, Δp, should be used in kg/cm^2 units. For the A320 is around *8.6 psi*, which is equivalent to $0.6046\ kg/cm^2$.

Table 3.19 - Weight penalty values applying the previous table's formulas.

Weight contribution		Number of items	b[m]	h[m]	Fillings [kg]	Surrounds [kg]
Passenger and crew doors		4	1.22	1.8	301.89	132.18
Cargo hold doors	Forward	1	1.82	1.19	82.18	52.54
	Aft	1	1.82	1.19	82.18	74.47
	Bulk	1	0.95	0.77	27.76	43.28
Escape hatches		4	0.5	1.02	51.08	76.56
Cockpit window glazing	Front	2	0.9	1.3	237.13	6.45
	Side	4	0.5	0.6	121.61	6.53
Passenger windows		44	0.3	0.5	313.50	169.90
		Total [kg]			1779.23	

Torenbeek [46] also includes a weight estimate for additional items, considering that for paint, sealing and redux a weight penalty of *1%* to *2%* of gross shell weight (W_G) may be assumed, whilst for production joints in the fuselage of transport aircraft the weight

penalty is about *2%* to *3%*. In both items, the worst-case scenario will be applied, i.e., the upper limits of the percentage penalty will be assumed. Thus, the additional weight items (W_{ai}) will be determined by:

$$W_{ai} = 1.05 \cdot W_G \quad (21)$$

To determined that additional weight items is crucial to estimate the gross weight of the fuselage shell structure (W_G), which is divided into the amounts contributed by the skin, (W_{sk}), stringers (W_{str}) and frames (W_{fr}):

$$W_G = W_{sk} + W_{str} + W_{fr} \quad (22)$$

The gross skin weight (W_{sk}) is the greatest of the values given by Equations 24, 26 and 27:

$$W_{sk} = \max\{W_{sk_1}, W_{sk_2}, W_{sk_3}\} \quad (23)$$

The gross skin weight based on the fuselage slenderness ratio is:

$$W_{sk_1} = constant \cdot k_\lambda \cdot {S_G}^{1.07} \cdot {V_D}^{0.743} \quad (24)$$

where the $constant = 0.05428$ when W_{sk} in [kg], V_D in [m/s] and S_G in [m²]. Allowing for the influence of the fuselage slenderness ratio, the factor k_λ is approximately given by

$$k_\lambda = 0.56 \cdot \left(\frac{l_t}{b_f + h_f}\right)^{3/4} \quad (25)$$

For $l_t/(b_f + h_f)$ up to 2.61, which for the main fuselage is 2.1. The gross skin weight based on cabin pressure, for a constant cabin skin thickness over the complete fuselage shell is:

$$W_{sk_2} = constant \cdot \Delta p \cdot D_f \cdot S_G \cdot \frac{f_{ref}}{f} \quad (26)$$

where the $constant = 1.595$ when W_{sk} in [kg], Δp is in [kg/cm^2] and S_G in [m²]. The Equation 19 represents the skin weight required to resist the cabin pressure operational differential, Δp, based on a mean hoop stress level of $f_{ref} = 843.7\ kg/cm^2$ [46]. The actual value for is $f = 221.4\ kg/cm^2$ [6].

The minimum value of gross skin weight, based on a minimum gauge of *0.8 mm*, is given by:

$$W_{sk_3} = \frac{W_{sk}}{S_G} \cdot S_G \quad (27)$$

where $W_{sk}/S_G = 2.173\ kg/m^2$. It is worth to remember that the gross shell area (S_G) is defined as the area of the entire outer surface of the fuselage with all the apertures faired over and outgrowths removed and faired over also.

The gross stringer and longeron weight can be approximately given by:

$$W_{str} = constant \cdot k_\lambda \cdot {S_G}^{1.45} \cdot {V_D}^{0.39} \cdot {n_{ult}}^{0.316} \quad (28)$$

where the $constant = 0.0117$ when W_{str} in [kg], V_D in [m/s] and S_G in [m²]. The ultimate load factor corresponding to W_{to}, n_{ult}, is *3.75* for the A320 [6] (*1.5* times limit load factor).

According to Torenbeek [46], the gross standard frame weight for other aircrafts than freighters can be approximately given by

$$W_{fr} = \begin{cases} 0.19 \cdot (W_{sk} + W_{str}) & if\ \ W_{sk} + W_{str} > 286\ kg \\ constant \cdot (W_{sk} + W_{str})^{1.13} & if\ \ W_{sk} + W_{str} \leq 286\ kg \end{cases} \quad (29)$$

where the $constant = 0.0911$ when W_{sk} and W_{str} are [kg]. Once calculated every term of Equation 22, it is possible to determine the additional weight items by Equation 21.

For the fuselage flooring, Torenbeek [46] provides typical floor weights for passenger transports of *5 kg/m²*. Then the weight floor (W_{fl}) can be approximately given by:

$$W_{fl} = 5 \cdot A_{fl} \quad (30)$$

The total fuselage weight (W_F) can be estimated adding the weight penalties due to fuselage shell cut-outs (W_{sct}), the additional weight items (W_{ai}), the weight floor (W_{fl}) to the basic fuselage weight (W_f):

$$W_F = W_f + W_{sct} + W_{ai} + W_{fl} \quad (31)$$

All the results for the previous equations addressing the main fuselage weight estimation are summarized in Table 3.20.

Schmidt *et al* [45] documented the *9600 kg* value as the actual A320 fuselage weight. Therefore, the total main fuselage weight estimation (W_F), shown in Table 3.20, differs only *0.41%* from the actual fuselage weight. Having the Torenbeek's method precision verified, it seems reliable to apply it to the gondola fuselage weight estimation, which is simpler than the main fuselage due to its geometry simplifications (has no cutouts for windows or emergency hatches, fewer doors, etc). The wheel bay for the main landing gear and the door to access the LH_2 are the main gondola fuselage apertures to consider for the weight penalties due to fuselage shell cut-outs.

Table 3.20 - Total main fuselage weight estimation.

Factor for the influence of the fuselage slenderness ratio	k_λ	0.977
Mean hoop stress level	f_{ref} [kg/cm²]	843.7
Design hoop stress in fuselage skin in level flight	f [kg/cm²]	221.42
Gross skin weight to gross shell area ratio	W_{sk}/S_G [kg/m²]	2.173
Typical floor weight	W_{fl}/A_{fl} [kg/m²]	5
Fuselage floor area	A_{fl} [m²]	100
Gross skin weight based on the fuselage slenderness ratio	W_{sk_1}[kg]	1616.22
Gross skin weight based on the cabin pressure	W_{sk_2}[kg]	6115.25
Minimum value of gross skin weight	W_{sk_3}[kg]	915.54
Gross skin weight	W_{sk} [kg]	6115.25
Gross stringer and longeron weight	W_{str} [kg]	1730.02
Gross frame weight	W_{fr} [kg]	1490.60
Gross shell weigh	W_G [kg]	9335.87
Additional weight items	W_{ai} [kg]	466.79
Fuselage floor weight	W_{fl} [kg]	500.00
Weight penalties due to fuselage shell cut-outs	W_{sct}[kg]	1779.23
Basic fuselage weight	W_f [kg]	6814.57
Total fuselage weight	W_F [kg]	9560.59

In Section 3.1, the proposed landing gear configuration consists of a main landing gear, mounted in the passenger fuselage and gondola, which will retract sideways into the fuselages and a nose wheel placed behind the cockpit on the inner side of the main fuselage, which will retract sideways into the belly [35]. Thus, following Torenbeek's method for the fuselage weight estimation [46], a 7% penalty over the basic gondola weight (W_f), should be considered because of the main landing gear attachment to the gondola fuselage, besides the 8% due to cabin pressurisation. Therefore, for the gondola airliner, the value of the basic fuselage weight obtained with Equation 18 must be multiplied by *1.15*. The distance between quarter-chord points of the wing root and horizontal tail root, l_t, for the gondola was assumed to be 75% of the main fuselage l_t parameter, maintaining the proportion between the main fuselage length and the gondola's (about 75% also). This assumption was made once the gondola fuselage had no horizontal tail. The gondola's gross shell area from the table below was collected from the model built using the CAD software *Catia V5*. The basic gondola fuselage weight estimation is presented in Table 3.21.

The weight penalties due to fuselage shell cut-outs (W_{sct}) only count with a contribution of belly door (*8 m* by *3.6 m*) to allow the 7.3 m lengthened LH_2 tanks remotion. The weight penalties due to fuselage shell cut-outs are presented in Table 3.22.

Table 3.21 - Basic gondola fuselage weight calculation.

Constant of proportionality	k_{wf}	0.23
Design dive speed	V_D [m/s]	180
Distance between quarter-chord points of wing root and horizontal tail root	l_t [m]	12.36
Maximum width of fuselage	b_f [m]	3.95
Maximum depth of fuselage	h_f [m]	3.95
Gross shell area	S_G [m²]	335.62
Basic fuselage weight (including 8% penalty due to cabin pressurization and 7% due to the main landing gear attachment to the fuselage)	W_f [kg]	4146.14

Table 3.22 - Weight penalty values due to LH_2 tanks access doors apertures.

Weight contribution	Number of items	b[m]	h[m]	Fillings [kg]	Surrounds [kg]
LH_2 tanks access door	1	8	3.6	1092.81	271.55
	Fillings and surrounds - W_{sct} [kg]			1364.36	

The LH_2 tanks take almost the gondola's diameter due to the fuel's storage requirements discussed before. Therefore, the total gondola fuselage weight discards the weight floor (W_{fl}) term, once there is no floor dividing the fuselage lengthwise. Table 3.23 summarises all the intermediate parameters calculated according to Torenbeek's weight estimation method previously described [46] and consequently the total gondola weight.

Table 3.23 - Total gondola fuselage weight estimation.

Factor for the influence of the fuselage slenderness ratio	k_λ	0.784
Mean hoop stress level	f_{ref} [kg/cm²]	843.7
Design hoop stress in fuselage skin in level flight	f [kg/cm²]	221.42
Gross skin weight to gross shell area ratio	W_{sk}/S_G [kg/m²]	2.173
Gross skin weight based on the fuselage slenderness ratio	W_{sk_1}[kg]	1016.36
Gross skin weight based on the cabin pressure	W_{sk_2}[kg]	4871.27
Minimum value of gross skin weight	W_{sk_3}[kg]	729.30
Gross skin weight	W_{sk} [kg]	4871.27
Gross stringer and longeron weight	W_{str} [kg]	1244.03
Gross frame weight	W_{fr} [kg]	1161.91
Gross shell weigh	W_G [kg]	7277.21
Additional weight items	W_{ai} [kg]	363.86
Weight penalties due to fuselage shell cut-outs	W_{sct}[kg]	1364.36
Basic fuselage weight	W_f [kg]	4146.14
Total (gondola) fuselage weight	W_F [kg]	6496.29

The total gondola weight is about *67.7%* of the main fuselage (A320's fuselage) actual weight. This value seems to be reliable once the gondola has about *75%* of the A320

fuselage length, without a dividing interior floor. However, the gondola’s actual weight might be higher than the estimated in Table 3.23, because the fixing mechanisms of the liquid hydrogen tanks to the fuselage probably have a considerable mass. Besides that, the centre part of the gondola’s belly is a suggestion for the LH_2 tank access door location, taking advantage of the larger diameter circular section. This door location introduces a substantial complexity for the wing/fuselage connection since the wing main spar and other structural elements passing through the gondola might no longer be a feasible structural arrangement. For the case that LH_2 tanks are fixed aft and forward of the gondola, the central-mounted access door is compatible with the main wing structure passing through the fuselage: the door can be placed in the lower part of the fuselage (belly), being used only for the interior access (and so it can have smaller dimensions than those assumed for the weight penalties due to the fuselage cutout) and the wing main spar can cross the fuselage in the upper part (next to the fuselage crown). On the other hand, if the LH_2 tanks are removable, which could simplify the maintenance procedures and reduce the turnaround duration, a bearing system might be installed, resulting in additional fuselage weight and structural complexity. This storage layout implies the tanks' displacement to the central section of the gondola for their remotion, thus putting away the wing spar crossing through the fuselage. These structural layouts should be addressed for a more detailed and accurate gondola weight estimation. Regardless of the implemented arrangement, it will add weight to the gondola weight shown in Table 3.23. Thus, the total gondola weight will get closer to the main fuselage weight.

Since the weight estimation of the gondola, central wing, LH_2 and its storage tanks is completed, the gondola airliner longitudinal weight distribution can be computed. Similarly to the other components, the methodology for the gondola fuselage segmentation follows the same line of thought as applied to the A320 longitudinal weight distribution: dividing the fuselage length into $0.2m$ intervals and dividing its total weight by the number of intervals. Remember that the gondola has its nose section at the $H\text{-}arm = 5.8\ m$. Removing the fuel weight distribution anteriorly made along the wing chord (the conventional A320 wings house the fuel) and adding the gondola’s extra components segmentation to the previously mentioned final table where all the components’ mass segmentation was summed for each x location (for each $H\text{-}arm$, $0.2m$ apart from the previous and the next $H\text{-}arm$, starting in the main fuselage nose section, $H\text{-}arm = 2.54\ m$). Thus, we have a mass distribution $[kg/m]$ value for each interval. Representing that mass distribution values according to the x position, results in the gondola airliner longitudinal weight distribution, represented in Figure 3.17, where the A320 longitudinal weight distribution is also shown for comparison purposes.

As shown in Figure 3.17, the A320 and the gondola airliner's longitudinal weight distribution is quite identical. However, there are some sections of the graph where the lines move away from each other. From around $H\text{-}arm = 8.3\ m$ to $H\text{-}arm = 15.6\ m$ the gondola airliner line is above the A320's due to the weight of the gondola fuselage, the forward LH_2 tank and the fuel itself. This pattern is repeated from around $H\text{-}arm = 23.6\ m$ to $H\text{-}arm = 30.9\ m$ because of the aft LH_2 tank.

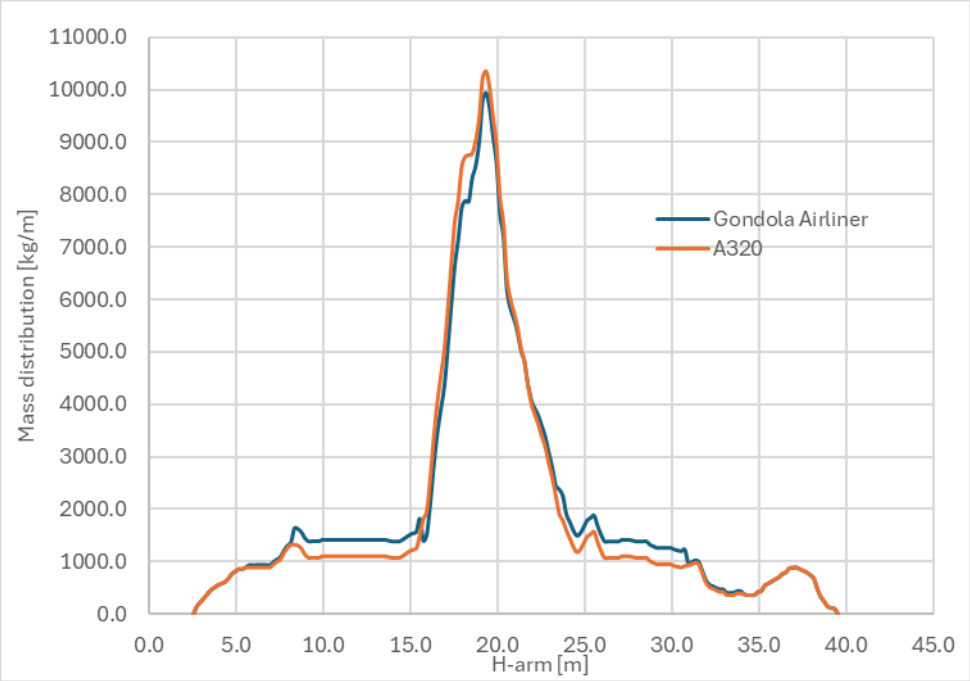

Figure 3.17 - Comparison between the A320 and gondola airliner longitudinal weight distribution.

On the other hand, in the central part of the weight distribution plot, the gondola airliner line is below the A320's, instead of above as expected, since the gondola concept results from adding extra components to the A320's configuration. This might be explained by the fact that the A320's fuel is removed from the wings, and there are no LH_2 tanks in that longitudinal position. Therefore, the central wing mass and the mass of the middle part of the gondola fuselage are compensated by the wing's fuel remotion.

Since it was assumed that the gondola airliner configuration had the A320's structure as a base, adding only the gondola fuselage, LH_2 tanks and the central wing to the conventional aircraft, the gondola aircraft weight can be calculated by following the next steps:

- subtract the A320's fuel weight considered for its longitudinal weight distribution (it was the maximum capacity [6], corresponding to a fuel mass of *19088 kg*) to A320 total weight determined after its longitudinal weight distribution (73

tonnes);

- add the liquid hydrogen mass (*9940 kg*);
- sum the LH_2 tanks weight (*9940 kg*, assuming a 50% gravimetric efficiency);
- add the estimated weight of the gondola fuselage (*6496.29 kg*);
- sum the estimated weight of the central wing (*4855.49 kg*).

The gondola airliner weight then comes *85143.78 kg*, which represents a *16.6%* increase relative to the A320 used for the longitudinal weight distribution study. This percentage might increase if the gravimetric efficiency of LH_2 tanks is lower than the 50% assumed. Considering the hydrogen mass needed, *9940 kg*, if the gravimetric efficiency of the tanks is *30%*, their weight increases to *23193.3 kg*, which is around *2.33* times the weight utilised. Since the gondola airliner has a higher weight, its landing gear system also needs to be sized, instead of considered the same as the A320, which can add some mass to the estimated value of the gondola airliner weight. The horizontal tail and the vertical tail might also be heavier than assumed because, if the A320's wing area to horizontal (and vertical) tail area ratio is pretended to be maintained, then the gondola's horizontal (and vertical) tail should be larger since the novel configuration's wing area is *56%* higher than A320.

It is worth noting that a correct weight estimation should many other elements into consideration, such as performance figures, the detailed mission plan, the components' correct dimensions, etc. Once more, this subchapter served as an overview of the gondola's longitudinal weight distribution and consequently the weight increase introduced comparatively to the equivalent A320. A further study should be addressed in an independent work, regarding a detailed gondola's weight estimation.

3.3 LH_2 Gondola airliner and A320 3D Models

3.3.1 A320 with winglets and FTFs

In this sub-section, the A320 is exhibited with winglets and Flap Track Fairings (FTFs). This is worth mentioning because, the next sub-chapter also presents the A320 model but with clean wings, i.e., without any excrescences in the wings (it has only the engines and their pylons). The idea is to perform a future comparison study between the two models to test the influence of winglets and high-lift devices on the aircraft’s performance. This design bifurcation was also applied to the gondola airliner models, so there will be gondola models with and without the referred devices.

The A320’s 3D models were elaborated with the aircraft’s blueprints, using the CAD software *Catia V5*.

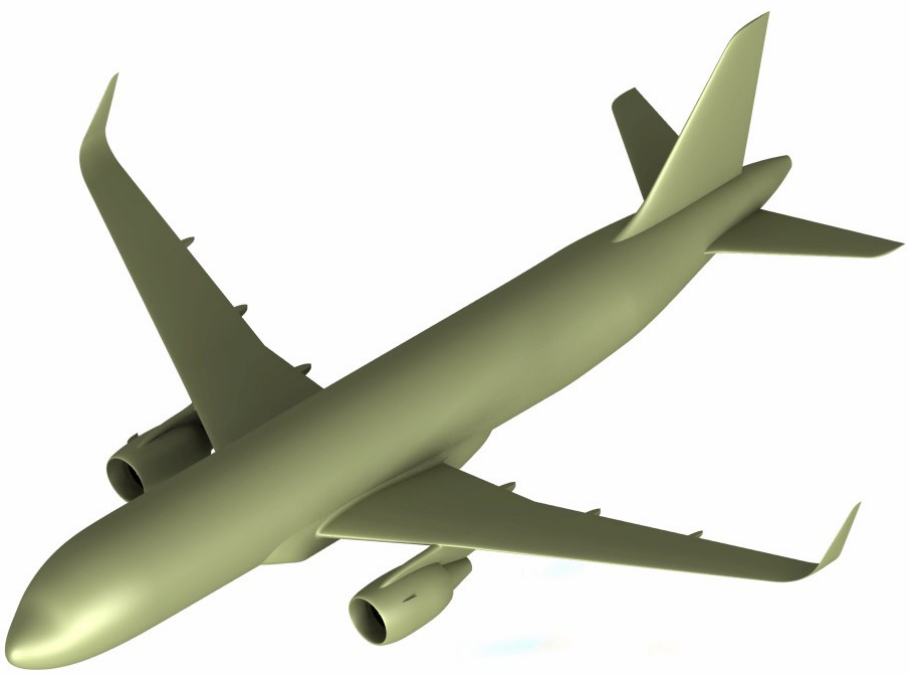

Figure 3.18 - Isometric view of the A320 with winglets and FTFs.

Figure 3.19 - Top view of the A320 with winglets and FTFs.

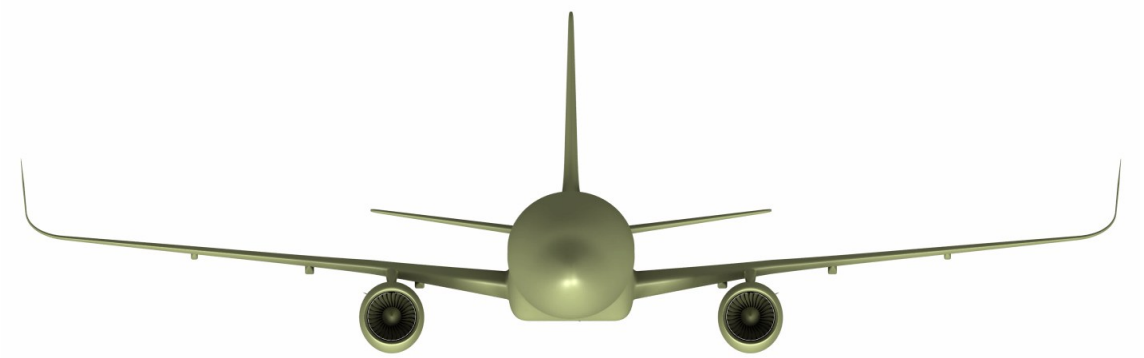

Figure 3.20 - Front view of the A320 with winglets and FTFs.

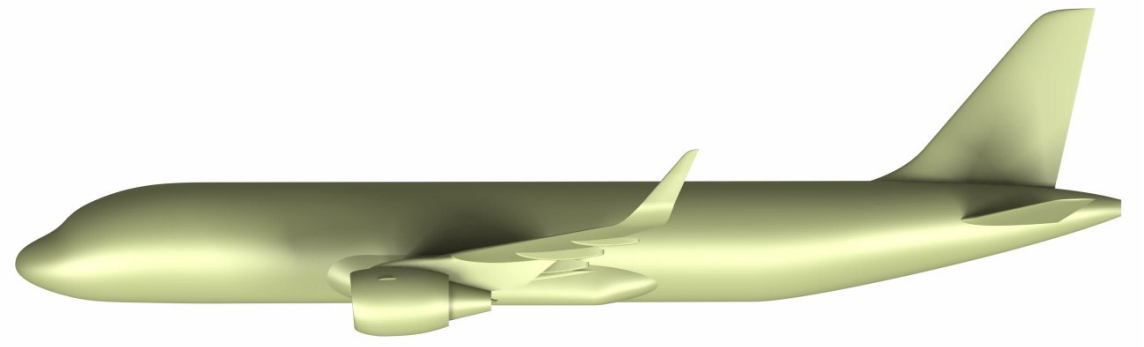

Figure 3.21 - Left view of the A320 with winglets and FTFs.

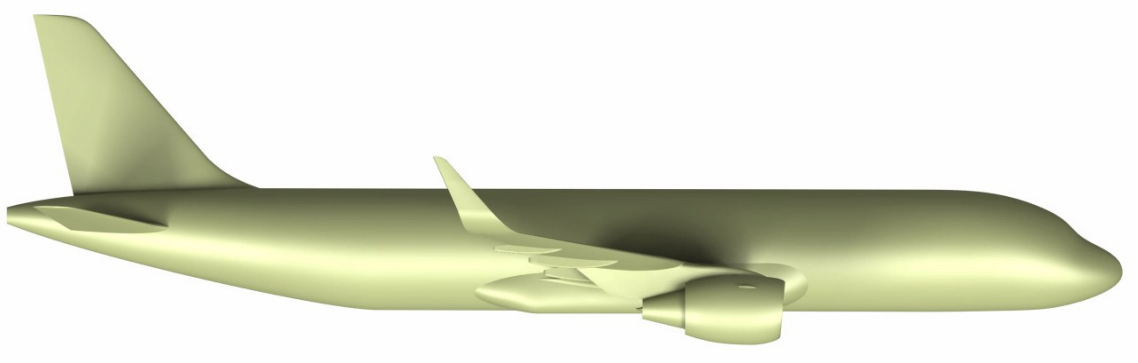

Figure 3.22 - Right view of the A320 with winglets and FTFs.

3.3.2 A320 without winglets and FTFs

As was previously alluded, the A320 model exhibited in the current sub-section has a clean wing configuration, i.e. without winglets and Flap Track Fairings. As the geometry suggests, this wing’s layout is much simpler to execute once it needs only three airfoils placed in key spots of the semi-span (wing root, wing tip and where the tailing edge changes the angle as is noticeable in Figure 3.24) and a vector (*x,y,z*) to place each airfoil correctly in the three-dimensional environment of the *Catia V5* tool, after running an Excel macro.

Figure 3.23 - Isometric view of the A320 without winglets and FTFs.

Figure 3.24 - Top view of the A320 without winglets and FTFs.

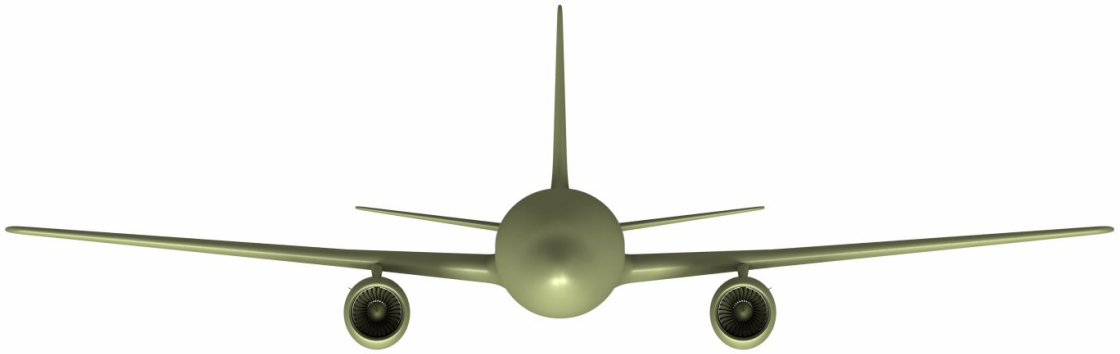

Figure 3.25 - Front view of the A320 without winglets and FTFs.

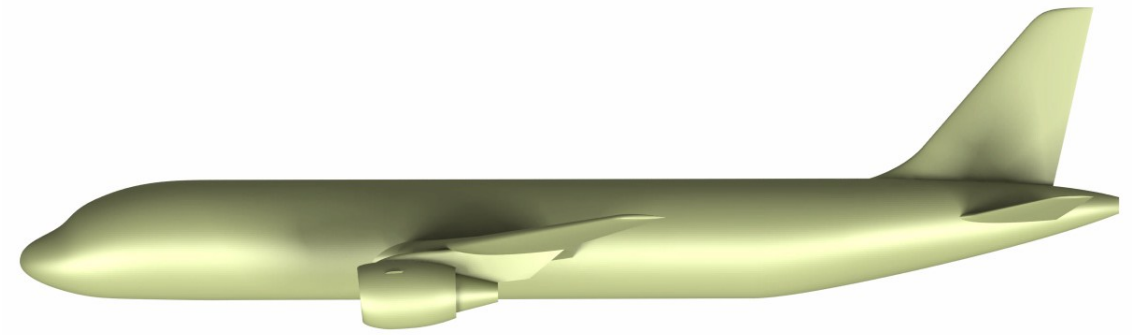

Figure 3.26 - Left view of the A320 without winglets and FTFs.

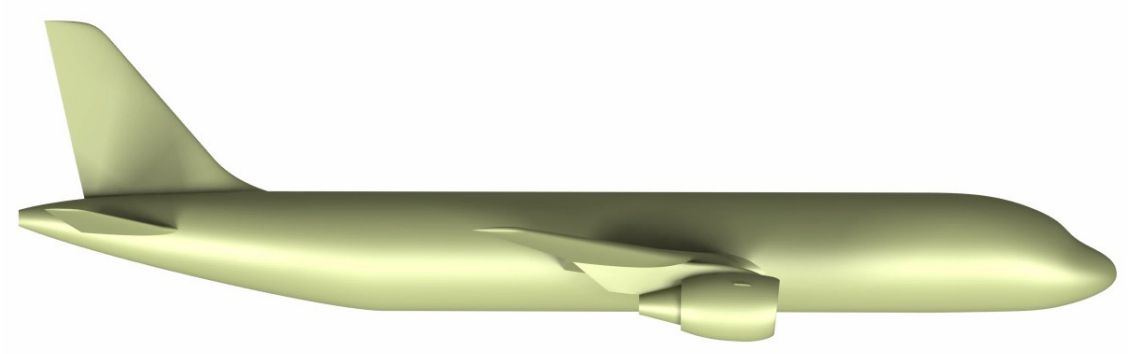

Figure 3.27 - Right view of the A320 without winglets and FTFs.

3.3.3 Gondola airliner with winglets, FTFs and A320’s tail

This sub-section presents the 3D model of the gondola airliner with winglets and FTFs. The main fuselage, tail, engines and outer wings were made following the A320’s geometry. Thus, only the starboard fuselage and the central wing were made freely, i.e., without following a technical drawing. This freedom in executing the gondola’s 3D modelling leads to several readjustments during this phase. For example, this work’s supervisors warn that the first model has a blunt gondola fuselage. Therefore, the gondola’s shape had to be readjusted by narrowing its geometry and sharpening the nose and rear, making it more streamlined.

Figure 3.28 - Isometric view of the gondola airliner with winglets, FTFs and A320’s tail.

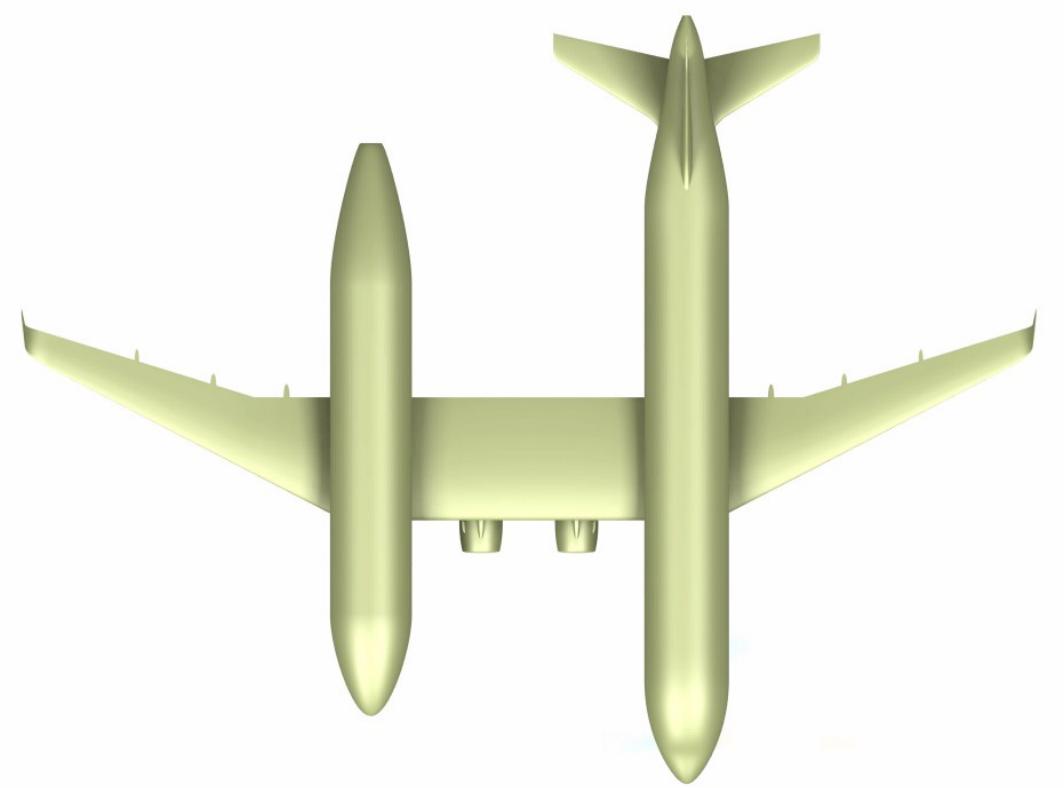

Figure 3.29 - Top view of the gondola airliner with winglets, FTFs and A320’s tail.

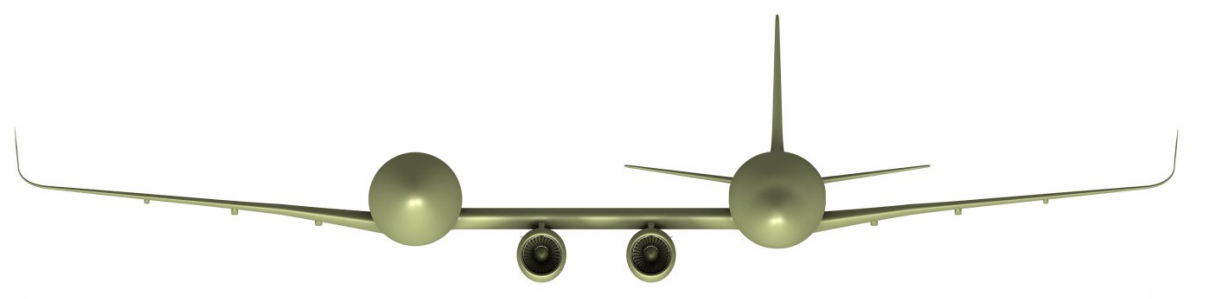

Figure 3.30 - Front view of the gondola airliner with winglets, FTFs and A320’s tail.

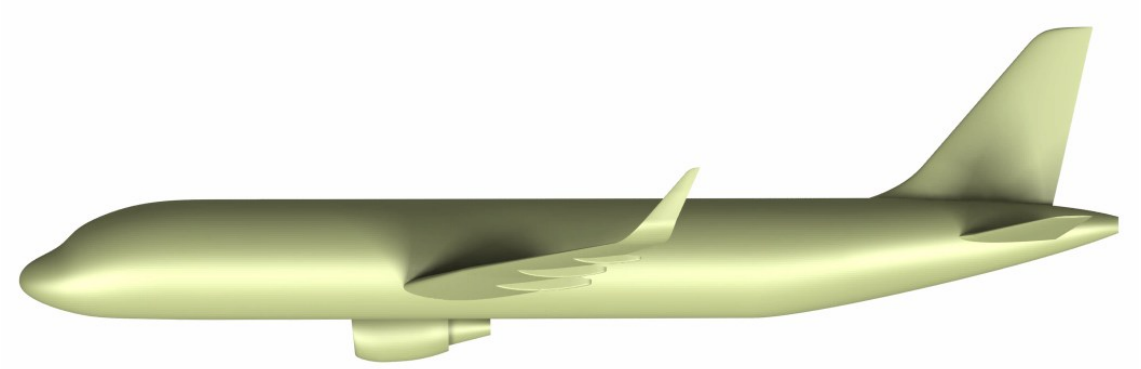

Figure 3.31 - Left view of the gondola airliner with winglets, FTFs and A320’s tail.

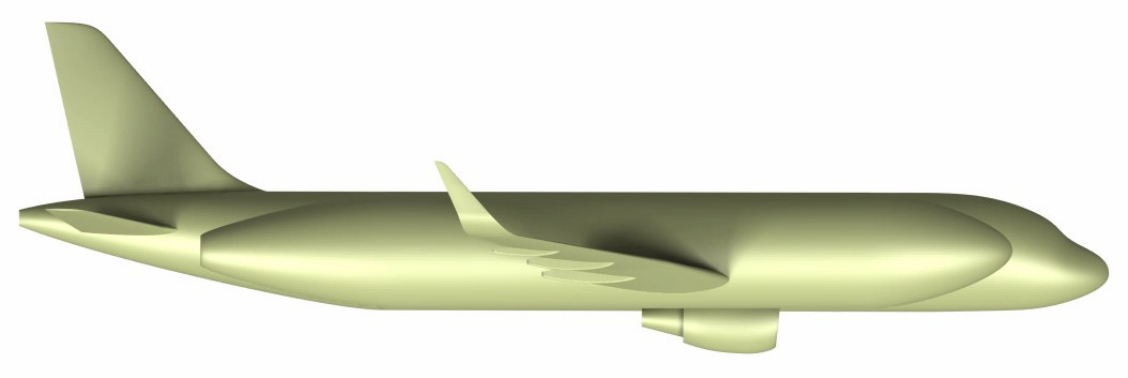

Figure 3.32 - Right view of the gondola airliner with winglets, FTFs and A320’s tail.

3.3.4 Gondola airliner featuring A320’s tail, without winglets and FTFs

Following the pattern of the previous models, this sub-section presents the gondola airliner featuring A320’s tail but without winglets and FTFs. The central wing had to be also adjusted as in the other models shown in this work, regarding the distance between the engines and the fuselages. Once this is not the final design before production, the distance between the engines and the fuselages followed the specifications in A320’s blueprints. Thus, the engines are around *3.8m* apart (considering their centreline), as is the distance between them and the nearest fuselage. The central wingspan is then around *11.4 m*.

Figure 3.33 - Isometric view of gondola airliner featuring A320’s tail without winglets and FTFs.

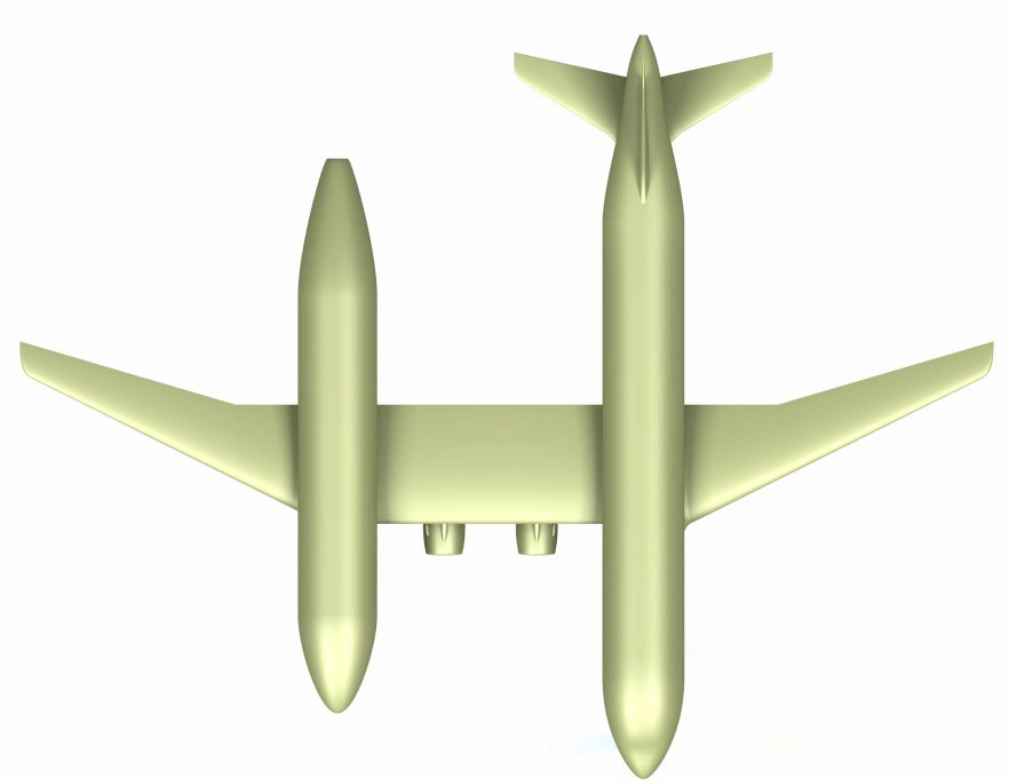

Figure 3.34 - Top view of gondola airliner featuring A320’s tail without winglets and FTFs.

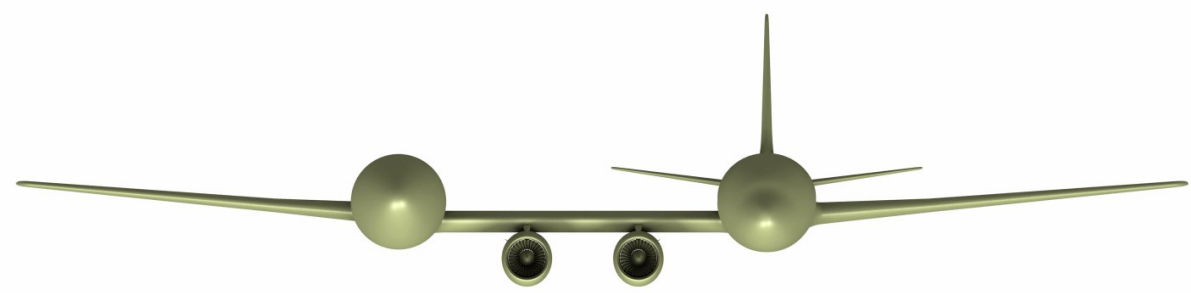

Figure 3.35 - Front view of gondola airliner featuring A320’s tail without winglets and FTFs.

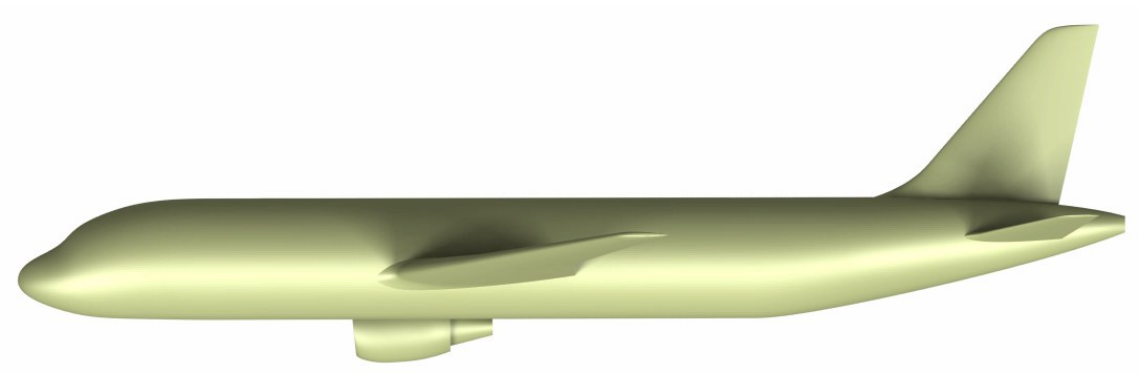

Figure 3.36 - Left view of gondola airliner featuring A320’s tail without winglets and FTFs.

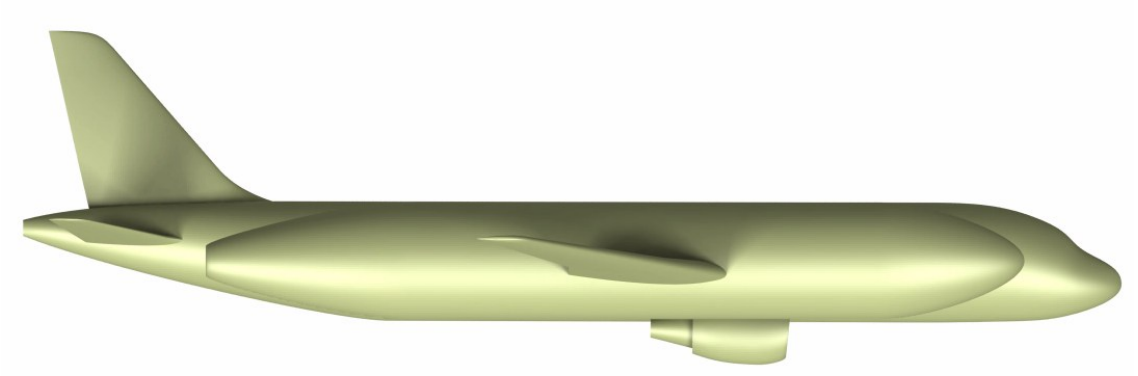

Figure 3.37 - Right view of gondola airliner featuring A320’s tail without winglets and FTFs.

3.3.5 Gondola airliner with winglets, FTFs and a resized tail

Another suggestion for the gondola design is to adjust the tail size so that the wing area to tail area ratio matches that in A320. With the central wing, the wing area from the gondola is about *56%* higher than the A320’s. Therefore, the horizontal and vertical tails’s area were also enlarged by that percentage. As the gondola fuselage is placed on the aircraft starboard, the horizontal stabiliser is specially enlarged on the right side of the main fuselage. The left portion of the horizontal stabiliser was only increased next to its root so that its chord was almost the same as that of the starboard portion.

Figure 3.38 - Isometric view of the gondola airliner with winglets, FTFs and a resized tail.

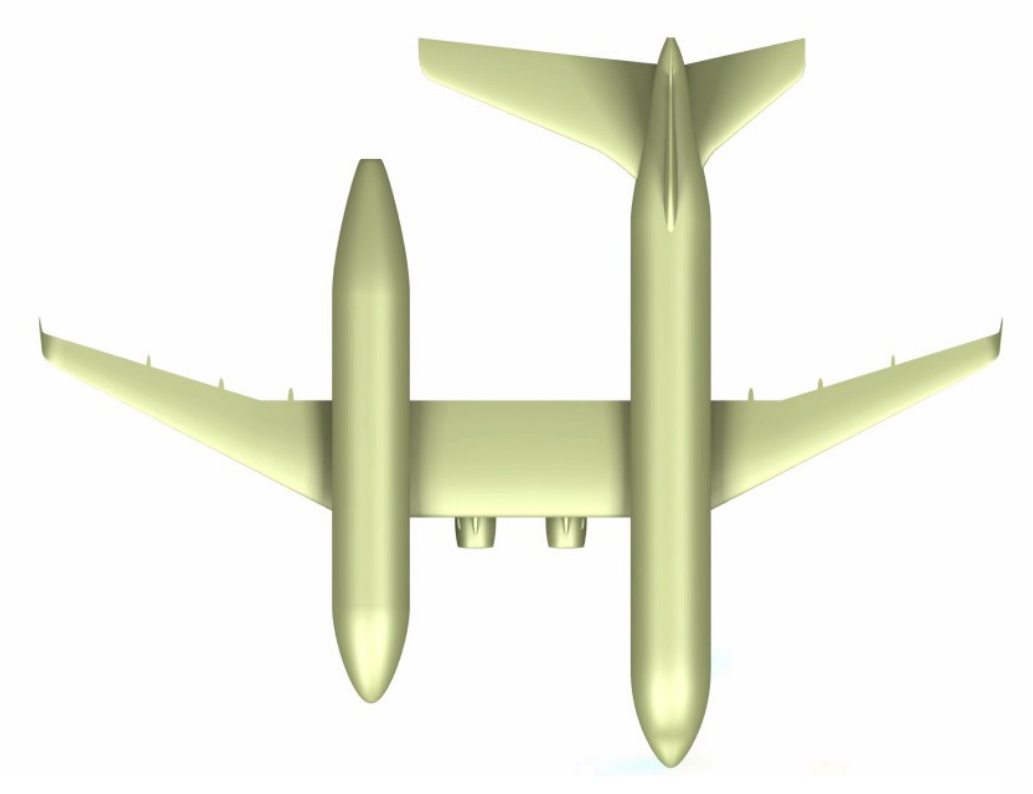

Figure 3.40 - Top view of the gondola airliner with winglets, FTFs and a resized tail.

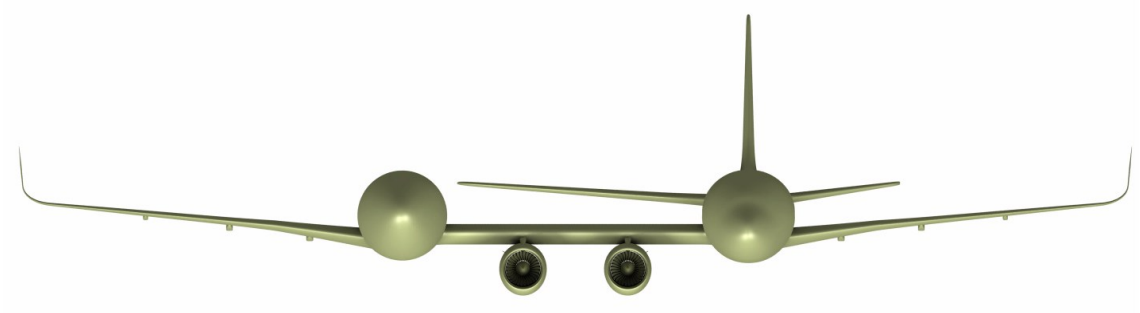

Figure 3.41 - Front view of the gondola airliner with winglets, FTFs and a resized tail.

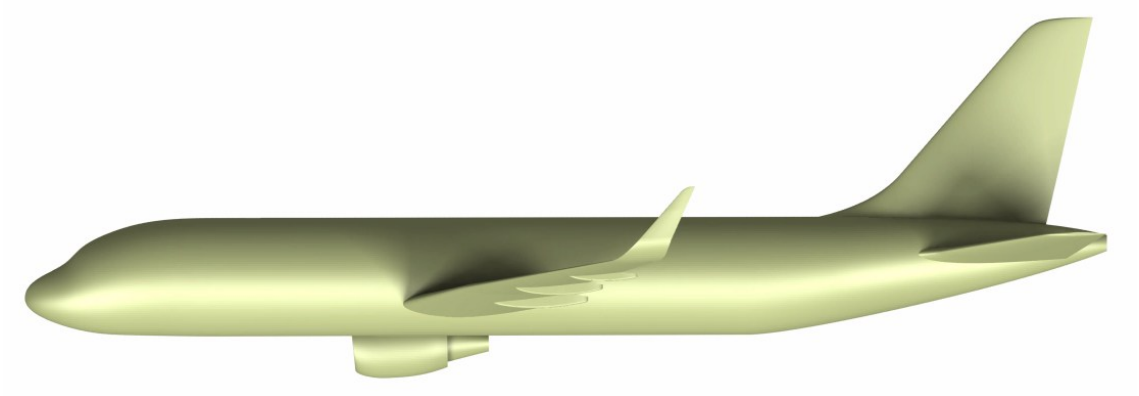

Figure 3.39 - Left view of the gondola airliner with winglets, FTFs and a resized tail.

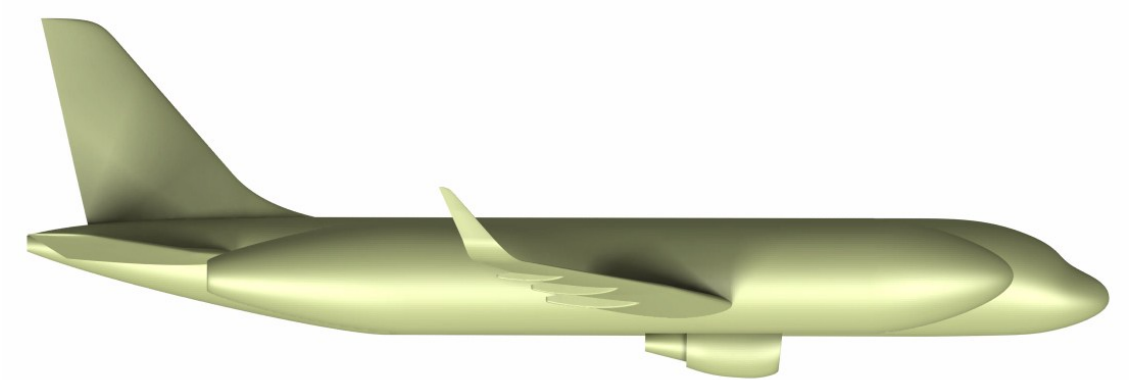

Figure 3.42 - Right view of the gondola airliner with winglets, FTFs and a resized tail.

3.3.6 Gondola airliner featuring a resized tail, without winglets and FTFs

Following the pattern of the previous models, this sub-section presents the gondola airliner with a resized tail but without winglets and FTFs. Figure 3.45, like the other front view images, highlights that the ground clearances are one of the future issues that should be addressed when sizing the gondola’s landing gear. As suggested by Dr Raj, the central wing might be designed with a curvature along the span to prevent accidental contact between engines and the ground.

Figure 3.43 - Isometric view of the gondola airliner featuring a resized tail, without winglets and FTFs.

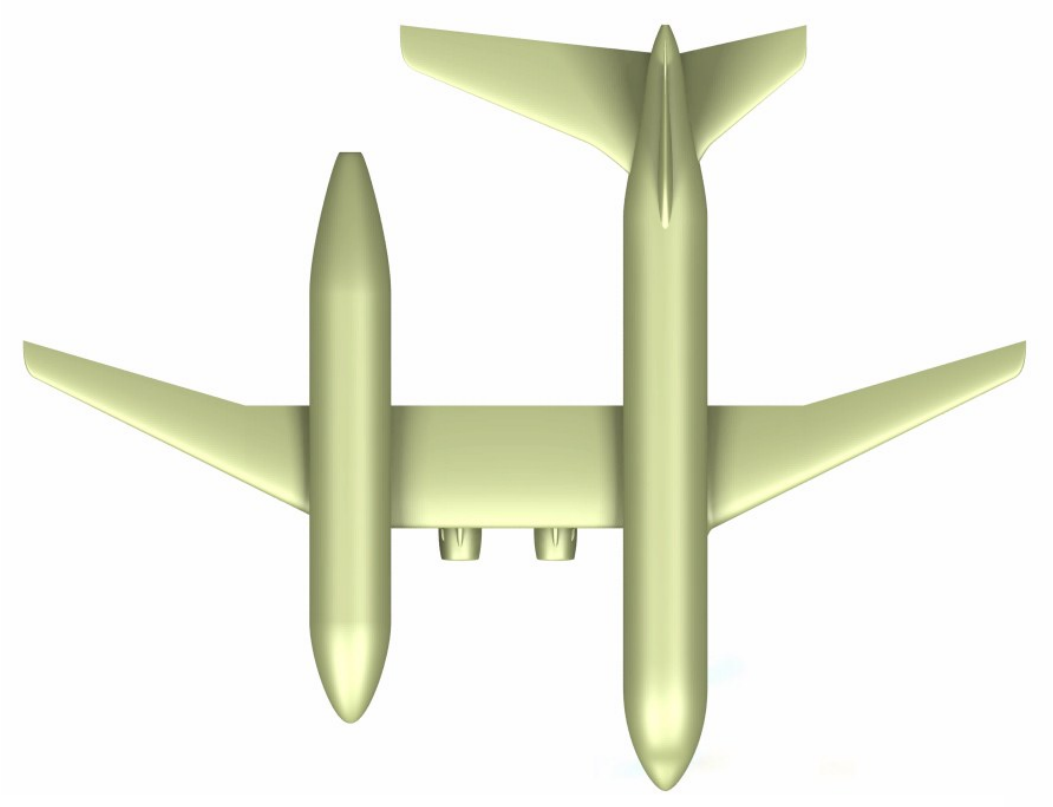

Figure 3.44 - Top view of the gondola airliner featuring a resized tail, without winglets and FTFs

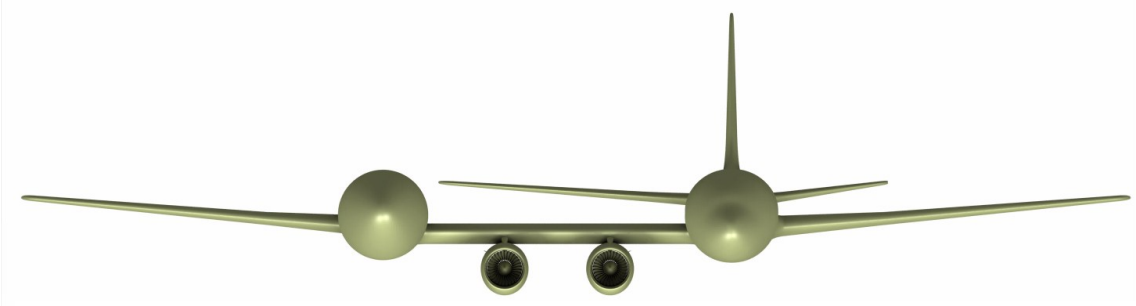

Figure 3.45 - Front view of the gondola airliner featuring a resized tail, without winglets and FTFs.

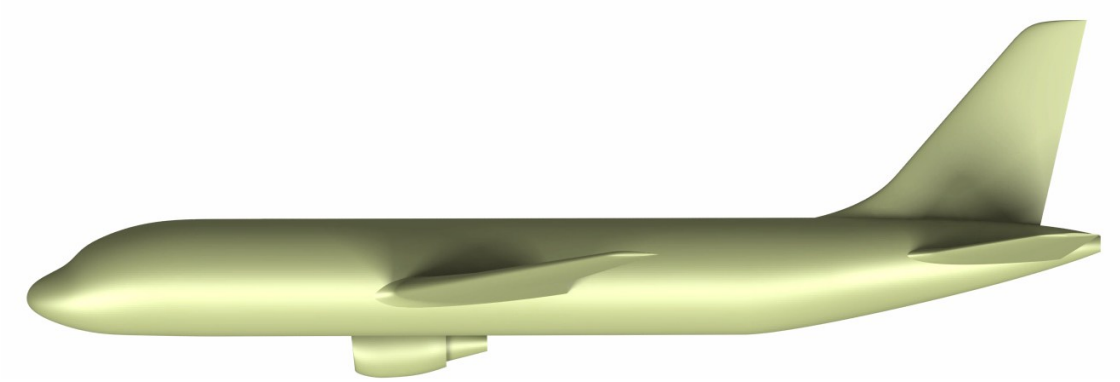

Figure 3.46 - Left view of the gondola airliner featuring a resized tail, without winglets and FTFs.

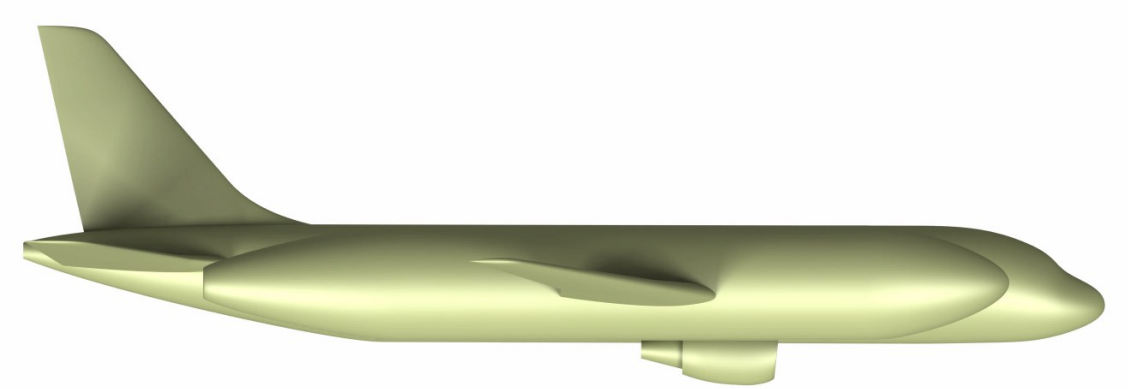

Figure 3.47 – Right view of the gondola airliner featuring a resized tail, without winglets and FTFs.

3.3.7 Gondola airliner with a vertical stabiliser offset

Single-engine tractor aircraft usually have a fin offset to assuage the corkscrew effect. Airplane Flying Handbook [47] describes this phenomenon as the slipstream of a propeller-driven plane that rotates around the aeroplane body (inside the propeller wake) and strikes the left side of the vertical fin, causing the aircraft to yaw slightly. Thus, aircraft designers use a vertical fin offset to counteract this tendency. It is worth mentioning that this spiralling rotation is quite severe and exerts a strong sideward force on the aeroplane’s vertical tail surface at high propeller speeds, i.e., high rotation speeds, and low forward speed (as in take-offs and approaches to power-on stalls) [47]. However, as the forward speed increases the spiral elongates and becomes less effective. Some single-engine aircraft have an engine offset of some degrees on the mount to counter yawing tendencies.

In the gondola airliner case, the twin layout produces a “natural” asymmetry yawing moment, represented in Figure 3.48. Nangia *et al* [4] tested a 4° fin offset to produce a moment in the opposite direction, cancelling the already mentioned “natural” yawing moment. A determined lateral-directional stability condition is generally accomplished by a coordinated motion of rolling and yawing moments. The rolling moment balance can be performed with aileron deflection and wing twist [4].

Figure 3.48 and Figure 3.49 have a thin red line to help visualise the vertical tail offset. Dr Raj Nangia suggested implementing only a 2° offset. Figure 3.48 also shows the “natural” asymmetry yawing moment (represented in the central wing) and the side force generated by the fin offset implementation, which cancels the initial yawing tendency.

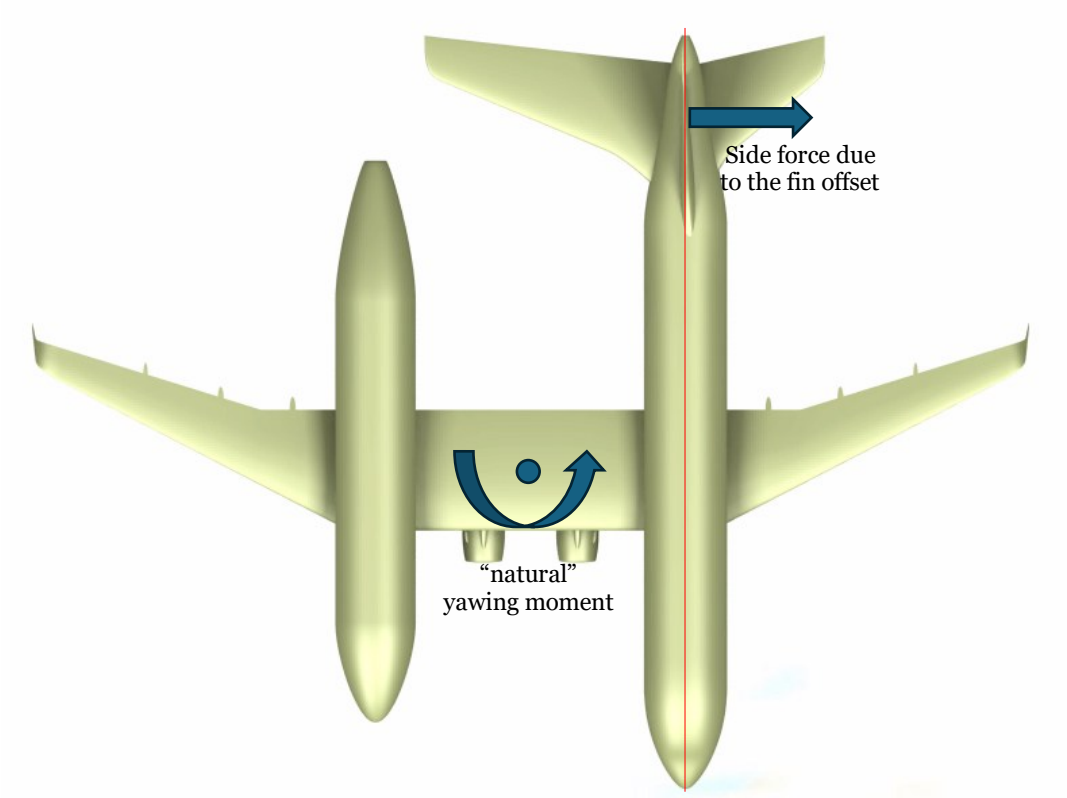

Figure 3.48 - Top view of Gondola airliner with a resized tail, vertical stabiliser offset, winglets and FTFs. The representation of the yawing moment cancellation (dark blue arrows) was adopted from Nangia *et al* [4].

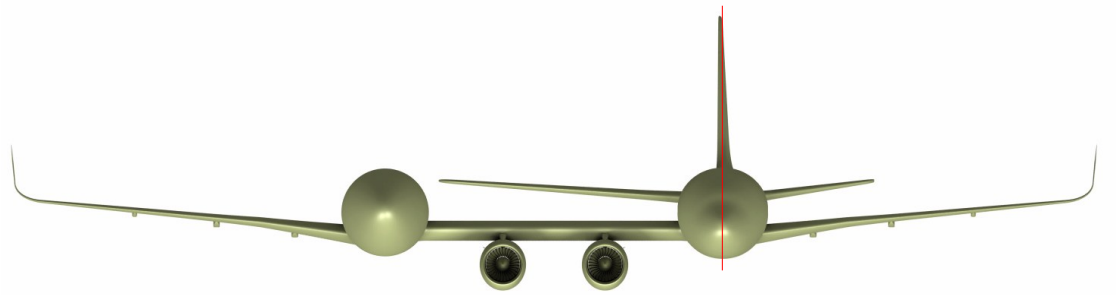

Figure 3.49 - Front view of Gondola airliner with a resized tail, vertical stabiliser offset, winglets and FTFs.

Regarding isometric, left and right views, the visual differences between this 3D model and the one shown in sub-section 3.3.5 are negligible when the vertical fin offset is minimal. Therefore, these 3D model views of the gondola airliner featuring an offset wing were not presented.

4 Conclusions and future work

In the closing chapter of this dissertation, the main emerging conclusions will be presented, some critical points of this work that may require further studies will be suggested, and some future work tasks will be proposed towards developing a certifiable gondola airliner.

The A320's TOW estimation was deeply supported by its weight and balance manual [6]. Therefore, to check the calculations that were being made in Excel, the H-arms of the design weights (Table 4.1) were calculated.

Table 4.1 - Desing weights' value and their CG's H-arm.

Weight Nomenclature	Weight [kg]	*H-arm* [m]	%RC
MEW	38254	18.80	23.70
OEW	43364	19.00	28.51
TOW	76738	18.93	27.00

The MEW's values matched the manufacturer's, which was expected once this weight definition accounts for the fixed component's mass, such as the aircraft's structure, power plant, systems, furnishings and integral equipment items. As the OEW depends on MEW and Operator's items list, the %RC differs from the value shown in the weighing report included in A320's manual [6], fixed at $\%RC = 28.60$. However, that difference can be negligible due to magnitude. For TOW determination, the cargo weight and its arrangement (location) in the cargo hold were adjusted so that certified CG limits and MTOW were respected. In fact, the TOW determined (Table 4.1) was below the MTOW fixed at 77 tonnes in the weight and balance manual [6]. The TOW's location in terms of the reference chord percentage was about 27%, respecting the CG limits established for an A320 operating around the MTOW, as shown in the A320 CG envelope (Appendix 1), validating the weight results and their location. Once the A320 weighing and balance values were according to its weight and balance manual [6], the mass of the aircraft's components and its location were utilised to calculate the longitudinal weight distribution.

The fuel cell discretisation, regarding the fuel weight distribution, was the part of this calculation process most likely to raise some incongruity because of the geometric simplifications adopted in the fuel cell representation. However, as shown in Table 3.14, using these approximations, the total capacity obtained for the inner cell was 6927.68 l,

about 0.04% higher than the capacity indicated in the A320 manual [6], fixed at 6925 l. Applying the same approximations to the centre tank and outer cells, the total capacity obtained was 23865 l, about 0.02% higher than the usable fuel capacity indicated in the A320 manual, listed as 23860 l. Once this difference has a minute magnitude, the methodology adopted for the fuel tank segmentation seems reliable and accurate.

The main irregularities in the A320's longitudinal weight distribution (Figure 3.11) must be explained. The first graph "bump" (H-arm between *7.5m* and *9.0m*) is mainly due to the aircraft's nose gear. The second and most expressive peak of the plot starts is located between *15.0m* and around *24.0m*. This graph region concentrates the contribution of the aircraft's heaviest groups such as the block fuel (housed in the wings), the propulsion system (engines, pumps, filters, valves, vent lines, etc), the wings structure and the main landing gear. Then, there is a much smaller peak caused by the intentional cargo arrangement near that region to obtain the referred TOW's location in terms of the reference chord percentage. In the final portion of the graph, there is a concavity followed by a peak. That plot hollow is caused because the passengers' seats, cabin hatracks and cargo hold end around this region and the fuselage structure tapers. The terminal peak is due to the weight of the vertical and horizontal tails.

Using the mass distribution values calculated for the A320, the total mass of the aircraft is around 73 tonnes, which is plausible, given that the MTOW is 77 tonnes. The difference between the aircraft mass obtained with this method and the mass calculated in the aircraft weighing and balance process (76.74 tonnes) is explained by the fact that some operators' items do not have their x location indicated in the A320 weight and balance manual [6], i.e., it is unknown where they start and where they finish along the x-axis. Instead, they only have the H-arm indicated concerning their centre of mass. However, the longitudinal mass distribution graph reliability is endorsed by Liu [38] who, based on established FE models of A320 and using the program HyperMesh, measured the longitudinal mass distribution section by section, resulting in mass per unit length quite similar to Figure 3.11.

Completed the A320 longitudinal weight distribution, we moved forward into the gondola's one. Once the detailed weight analysis is not the main goal of this work, the gondola longitudinal weight distribution was mightily based on the A320, using every component's weight and location from the previous calculations, except the new components added to the conventional aircraft (the central wing and the gondola fuselage that houses the LH_2). Thus, for the gondola aircraft weight distribution, it is necessary to estimate the central wing, gondola, tanks and LH_2 weights for an equivalent mission of A320.

Breguet’s Range equation (Equation 11) was applied for the LH_2 weight estimation, which comes to be around 10 tonnes (140 m^3) for the flight considered. Then, it was assumed the fuel tanks weigh as much as the LH_2 (*9940 kg*) by using a conservative value of 50% for the tanks’ gravimetric efficiency. The fuel is housed in two separate tanks, which introduce a redundancy to the power supply system and provides an easiest structural connection of the central wing, gondola fuselage and right wing, once the gap separating the tanks permits the wing main spar and other structural elements passing through the gondola.

For the gondola fuselage weight estimation, Torenbeek’s method was applied and the total main fuselage weight (A320’s fuselage) makes up about *9560.6 kg* (Table 3.20), which differs only 0.41% from the actual A320 fuselage weight (*9600 kg*) documented by Schmidt *et al* [45].

Taking advantage of familiarisation with this method, it was also used for the gondola fuselage weight estimation. For the starboard fuselage, the volume of calculations is smaller than the main fuselage, once there are not as many shell cutouts and therefore weight penalties to account for. The total gondola fuselage weight also discarded the weight floor, once there is no floor dividing the fuselage lengthwise. The total gondola weight (Table 3.23) is about *6496.29kg*, which is 67.7% of the main fuselage (A320’s fuselage) actual weight. This value seems to be reliable, once the gondola has about 75% of the A320 fuselage length, without a dividing interior floor. However, the gondola's actual weight might be higher than the estimated in Table 3.23, because the fixing mechanisms of the liquid hydrogen tanks to the fuselage probably have a considerable mass. Besides that, the centre part of the gondola’s belly is a suggestion for the LH_2 tank access door location, taking advantage of the larger diameter circular section. This door location introduces a substantial complexity for the wing/fuselage connection since the wing main spar and other structural elements passing through the gondola might no longer be a feasible structural arrangement. For the case that LH_2 tanks are fixed aft and forward of the gondola, the central-mounted access door is compatible with the main wing structure passing through the fuselage: the door can be placed in the lower part of the fuselage (belly), being used only for the interior access (and so it can have smaller dimensions than those assumed for the weight penalties due to the fuselage cutout) and the wing main spar can cross the fuselage in the upper part (next to the fuselage crown). On the other hand, if the LH_2 tanks are removable, which could simplify the maintenance procedures and reduce the turnaround duration, a bearing system might be installed, resulting in additional fuselage weight and structural complexity. This storage layout implies the tanks' displacement to the central section of the gondola for their remotion,

thus putting away the wing spar crossing through the fuselage. These structural layouts should be addressed for a more detailed and accurate gondola weight estimation. Regardless of the implemented arrangement, it will add weight to the gondola weight shown in Table 3.23. Thus, the total gondola weight will get closer to the main fuselage weight.

With the gondola airliner weight estimate, the longitudinal weight distribution proceeded (Figure 3.17). Despite the gondola concept being heavier than the equivalent A320, we conclude that their longitudinal weight distribution is quite identical. However, there are some sections of the graph where the lines move away from each other. From around $H\text{-}arm = 8.3\ m$ to $H\text{-}arm = 15.6\ m$ the gondola airliner line is above the A320's due to the weight of the gondola fuselage, the forward LH_2 tank and the fuel itself. This pattern is repeated from around $H\text{-}arm = 23.6\ m$ to $H\text{-}arm = 30.9\ m$ because of the aft LH_2 tank. On the other hand, in the central part of the weight distribution plot, the gondola airliner line is below the A320's, instead of above as expected, since the gondola concept results from adding extra components to the A320's configuration. This might be explained by the fact that the A320's fuel is removed from the wings, and there are no LH_2 tanks in that longitudinal position. Therefore, the central wing mass and the mass of the middle part of the gondola fuselage are compensated by the wing's fuel remotion. The fact that the longitudinal weight distribution of the two aircraft is quite identical, suggests that the longitudinal variation of the aircraft CG due to payload and fuel variations are similar.

The estimated gondola airliner weight was about 85143.78 kg, which represents a 16.6% increase relative to the A320 used for the longitudinal weight distribution study. This percentage might increase if the gravimetric efficiency of LH_2 tanks is lower than the 50% assumed. Considering the hydrogen mass needed, 9940 kg, if the gravimetric efficiency of the tanks is 30%, their weight increases to 23193.3 kg, which is around 2.33 times the weight utilised. Since the gondola airliner has a higher weight, its landing gear system also needs to be sized, instead of considered the same as the A320, which can add some mass to the estimated value of the gondola airliner weight. The horizontal tail and the vertical tail might also be heavier than assumed because, if the A320's wing area to horizontal (and vertical) tail area ratio is pretended to be maintained, then the gondola's horizontal (and vertical) tail should be larger since the novel configuration's wing area is 56% higher than A320. It might be also necessary to implement a new set of engines, more powerful, which has the chance to be heavier than the A320's. Regardless of these weight changes, the 16.6 percentage seems to be a reliable value, considering Dr Raj Nangia's insights, during one of the meetings held periodically, and also because of his

article presented in the ICAS 2022 [41], where for a *2950 nm* range the LH_2 aircraft is around 15% heavier than the conventional model. However, as the range increases the WFB/MTOW ratio also increases [43], nothing the obvious need for a larger WFB (more fuel). Despite LH_2 being a lighter fuel, it has a lower energy density and thus requires more tankage volume. So, bigger ranges obviously demand larger tankage volume that increase more rapidly for LH_2 aircraft than the conventional aircraft tankage volume. During this work execution, we also concluded that LH_2 tanks are one of the main accountable for the gondola airliner's weight penalties so, for a given range the LH_2 aircraft will be increasingly heavier than the equivalent conventional aircraft. Thus, achieving long ranges with LH_2 aircraft is more difficult.

Regarding the 3D models shown in the previous section, there are no concrete conclusions but rather suggestions for future use. Therefore, as a final remark of this work, the following tasks are proposed as a future work:

- CFD comparison between the 3D models presented, studying the influence of winglets, interference of the central wing in the airflow around the empennages, aerodynamic differences of having a gondola airliner featuring an A320's tail or resized one (as presented in this work);
- Create and compare other gondola airliner configurations, introducing a dihedral angle, sweep angle or both in the central wing of the aircraft;
- Study gondola airliner stability considering the A320's tail configuration or the resized version;
- Manufacture a small-scale model of the gondola aircraft, perform flight tests and register the experimental data to compare with the theoretical stability results;
- Study gondola airliner aeroelastic behaviour;
- Perform a parametric study regarding several tank layouts, i.e., position inside gondola fuselage, number of tanks, gondola fuselage position along the span, etc.

Aiming for the net-zero emissions requires a technology development, which in aviation founds a particular hindrance regarding the certification and crashworthiness directives fulfilment. The LH_2 gondola concept appears as feasible alternative to help achieving the environmental goals. However, design a novel configuration involves the conceptual design, the preliminary design and the detail design, which usually take years with several professional teams working in cooperation. For all of this, the work developed throughout this document seems to be like a grain of sand in the Sahara. Besides, for each new concept that I researched during the preparation of this work, many new ones emerged before my eyes, which is why the phrase uttered by Isaac Newton was specifically chosen to open this dissertation.

5 Bibliography

[1] E. J. Adler and J. R. R. A. Martins, “Hydrogen-powered aircraft: Fundamental concepts, key technologies, and environmental impacts,” *Progress in Aerospace Sciences*, vol. 141, 2023, doi: https://doi.org/10.1016/j.paerosci.2023.100922.

[2] T. Yusaf *et al.*, “Sustainable hydrogen energy in aviation - A narrative review,” *International Journal of Hydrogen Energy*, vol. 52, no. 1026–1045, 2024, doi: https://doi.org/10.1016/j.ijhydene.2023.02.086.

[3] R. Spencer, “Certification considerations for the configuration of a hydrogen-fuelled aeroplane,” *The Aeronautical Journal*, vol. 127, pp. 213–231, 2023, doi: 10.1017/aer.2022.79.

[4] R. Nangia, L. Hyde, and J. Cooper, “Developing Certifiable Liquid Hydrogen ‘Gondola’ Airliner, Design Innovations & Challenges,” in *Aerospace Europe Conference 2023*, 2023, p. 11.

[5] ACI, “Global passenger traffic expected to recover by 2024 and reach 9.4 billion passengers.” Accessed: Mar. 15, 2024. [Online]. Available: https://aci.aero/2023/09/27/global-passenger-traffic-expected-to-recover-by-2024-and-reach-9-4-billion-passengers/

[6] Airbus, *Weight and Balance*. 1988.

[7] Eurostat, “Passenger mobility statistics.” Accessed: Mar. 15, 2024. [Online]. Available: https://ec.europa.eu/eurostat/statistics-explained/index.php?title=Passenger_mobility_statistics

[8] C. Bergero, G. Gosnell, and D. et al. Gielen, “Pathways to net-zero emissions from aviation,” *Nat Sustain*, vol. 6, no. 404–414, 2023, doi: https://doi.org/10.1038/s41893-022-01046-9.

[9] G. Quaresma, L. B. Magalhães, A. F. Ferreira, and A. Silva, “E-Kerosene Potential for Commercial Aviation Decarbonization,” *ICAS Proceedings*, pp. 1–13, 2024.

[10] I. Abrantes, A. F. Ferreira, A. Silva, and M. Costa, “Sustainable aviation fuels and imminent technologies - CO2 emissions evolution towards 2050,” *Journal of Cleaner Production*, vol. 313, no. February 2021, doi: 10.1016/j.jclepro.2021.127937.

[11] IATA, "Fact Sheet: Liquid hydrogen as a potential lowcarbon fuel for aviation," 2019. [Online]. Available: https://www.iata.org/contentassets/d13875e9ed784f75bac90f000760e998/fact_sheet7-hydrogen-fact-sheet_072020.pdf

[12] S. Tiwari, M. J. Pekris, and J. J. Doherty, "A review of liquid hydrogen aircraft and propulsion technologies," *International Journal of Hydrogen Energy*, vol. 57, no. 1174–1196, 2024.

[13] "Clean Sky 2 Joint Undertaking and Fuel Cells and Hydrogen 2 Joint Undertaking, Hydrogen-powered aviation: A fact-based study of hydrogen technology, economics, and climate impact by 2050," 2020. doi: http://dx.doi.org/10.2843/471510.

[14] A. Contreras, S. Yiğit, K. Özay, and T. N. Veziroğlu, "Hydrogen as aviation fuel: a comparison with hydrocarbon fuels," *International Journal of Hydrogen Energy*, vol. 22, no. 10–11, pp. 1053–1060, 1997.

[15] R. Falkenstein-Smith, "The equivalence ratio concept in fire safety science," *Fire Safety Journal*, vol. 141, no. August, p. 103919, 2023, doi: 10.1016/j.firesaf.2023.103919.

[16] B. Khandelwal, A. Karakurt, P. R. Sekaran, V. Sethi, and R. Singh, "Hydrogen powered aircraft : The future of air transport," *Progress in Aerospace Sciences*, vol. 60, pp. 45–59, 2013, doi: http://dx.doi.org/10.1016/j.paerosci. 2012.12.002.

[17] C. Marek, T. Smith, and K. Kundu, "Low Emission Hydrogen Combustors for Gas Turbines Using Lean Direct Injection," in *41st AIAA/ASME/SAE/ASEE Joint Propulsion Conference & Exhibit*, 2005. doi: http://dx.doi.org/10.2514/6.2005-3776.

[18] G. Dahl and F. Suttrop, "Engine control and low-NOx combustion for hydrogen fuelled aircraft gas turbines," *International Journal of Hydrogen Energy*, vol. 23, no. 8, pp. 695–704, 1998, doi: http://dx.doi.org/10.1016/S0360-3199(97)00115-8.

[19] G. Corchero and J. L. Montañés, "An approach to the use of hydrogen for commercial aircraft engines," *Journal of Aerospace Engineering*, vol. 219, no. 1, pp. 35–44, 2005, doi: http://dx.doi.org/10.1243/095441005X9139.

[20] D. Verstraete, "The potential of liquid hydrogen for long range aircraft propulsion," Cranfield University, 2009.

[21] D. Verstraete, "Long range transport aircraft using hydrogen fuel," *International Journal of Hydrogen Energy*, vol. 38, no. 14824–14831, 2013, doi: http://dx.doi.org/10.1016/j.ijhydene.2013.09.021.

[22] "Liquid Hydrogen Fuelled Aircraft – System Analysis," 2003.

[23] G. Onorato, P. Proesmans, and M. M. F. Hoogreef, "Assessment of hydrogen transport aircraft," *CEAS Aeronautical Journal*, vol. 13, pp. 813–845, 2022, doi: https://doi.org/10.1007/s13272-022-00601-6.

[24] D. Pinto, "Hydrogen aircraft conceptual design and life cycle assessment," 2022.

[25] G. D. Brewer, R. Morris, R. Lange, and J. Moore, "Study of the application of hydrogen fuel to long-range subsonic transport aircraft," 1975.

[26] A. Gomez and H. Smith, "Liquid hydrogen fuel tanks for commercial aviation: Structural sizing and stress analysis," *Aerospace Science and Technologie*, vol. 95, 2019, doi: https://doi. org/10.1016/j.ast.2019.105438.

[27] G. D. Brewer, *Hydrogen aircraft technology*. 1991.

[28] T. Y. Druot, N. Peteilh, P. Roches, and N. Monrolin, "Hydrogen Powered Airplanes, an exploration of possible architectures leveraging boundary layer ingestion and hybridization," in *AIAA SCITECH 2022 Forum*, 2022. doi: https://doi.org/10.2514/6.2022-1025.

[29] D. Debney *et al*, "Zero-carbon emission aircraft concepts", Aerospace Technology Institute (UK) 2022.

[30] D. Verstraete, "On the energy efficiency of hydrogen-fuelled transport aircraft," *International Journal of Hydrogen Energy*, vol. 40, no. 7388–7394, 2015, doi: http://dx.doi.org/10.1016/j.ijhydene.2015.04.055.

[31] D. Verstraete, "Hydrogen fuel tanks for subsonic transport aircraft," *International Journal of Hydrogen Energy*, vol. 35, no. 11085–11098, 2010, doi: 10.1016/j.ijhydene.2010.06.060.

[32] EASA, “Certification Specifications and for Large Aeroplanes CS-25 amendment 26,” in *The European Union Aviation Safety Agency*, Cologne, 2020.

[33] D. Scholz, “Design of Hydrogen Passenger Aircraft –How much ‘Zero-Emission’ is Possible?,” 2020. doi: https://doi.org/10.5281/zenodo.4301103.

[34] K. Seeckt, W. Heinze, and D. Scholz, “Hydrogen powered freighter aircraft – the final results of the green freighter project,” in *27th International Congress of the Aeronautical Sciences*, 2010. [Online]. Available: https://www.fzt.haw-hamburg.de/pers/Scholz/GF/GF_Paper_ICAS_10-09-19.pdf

[35] R. K. Nangia and L. Hyde, “A twin-fuselage liquid hydrogen airliner, design with foresight towards certification,” in *RAeS Alternative Propulsion Conference*, London, 2021.

[36] E. Torenbeek, *Advanced Aircraft Design*. Wiley, 2013.

[37] J. W. Moore, E. P. Craven, B. T. Farmer, J. F. Honrath, R. E. Stephens, and R. T. Meyer, “Multibody Aircraft Study,” 1982.

[38] X. Liu, H. Wu, Y. G. Qu, Z. Y. Xu, J. H. Sheng, and Q. Fang, “Safety assessment of Generation Ⅲ nuclear power plant buildings subjected to commercial aircraft crash Part I: FE model establishment and validations,” *Nuclear Engineering and Technology*, vol. 52, no. 2, pp. 381–396, 2020, doi: 10.1016/j.net.2019.07.014.

[39] R. M. Ajaj, M. I. Friswell, D. Smith, and A. T. Isikveren, “A conceptual wing-box weight estimation model for transport aircraft,” *Aeronautical Journal*, vol. 117, no. 1191, pp. 533–551, 2013, doi: 10.1017/S0001924000008174.

[40] Y. Ma, J. Yan, and A. Elham, “Initial weight estimation of twin-fuselage configuration in aircraft conceptual design,” *Proceedings of the Institution of Mechanical Engineers, Part G: Journal of Aerospace Engineering*, vol. 237, no. 1, pp. 130–140, 2023, doi: 10.1177/09544100221095370.

[41] R. K. Nangia and L. Hyde, “Arriving at certifiable novel airliner using liquid hydrogen & efficiency metrics,” in *33rd congress of the International Council of the Aeronautical Sciences*, pp. 1–10.

[42] R. Radovitzky, “Breguet Range Equation.” pp. 2–12.

[43] R. K. Nangia, “Efficiency parameters for modern commercial aircraft,” *Aeronautical Journal*, vol. 110, no. 1110, pp. 495–510, 2006, doi: 10.1017/S0001924000001391.

[44] R. K. Nangia, “Highly efficient civil aviation, now via operations-AAR & challenges,” in *2018 Aviation Technology, Integration, and Operations Conference*, 2018. doi: 10.2514/6.2018-3591.

[45] K. Schmidt and R. Vos, “A semi-analytical weight estimation method for oval fuselages in conventional and novel aircraft,” *52nd Aerospace Sciences Meeting*, no. January, pp. 1–20, 2014, doi: 10.2514/6.2014-0026.

[46] E. Torenbeek, *Synthesis of Subsonic Airplane Design*. 1982.

[47] A. T. S. B. Flight Standards Service, *Airplane Flying Handbook*. 2004.

[48] A. Westenberger, “LH2 as Alternative Fuel for Aeronautics – Study on Aircraft Concepts,” 2007.

[49] “TUPOLEV.” Accessed: Apr. 18, 2024. [Online]. Available: https://tupolev.ru/en/

[50] L. Franzén, E. Magnusson, I. Staack, and C. Jouannet, “Weight Penalty Methods for Conceptual Aircraft Design,” 2018.

Appendix 1 – A320 CG Envelope